Synthesis of Metal Oxide, Core-Shell Nanoparticles, Their Surface Modifications and Applications

Thesis Submitted to AcSIR for the Award of
the Degree of
DOCTOR OF PHILOSOPHY
In Chemical Sciences

By

Pravin Narayan Shinde
Registration Number: 10CC11A26041

Under the guidance of

Dr. B. L. V. PRASAD

CSIR-National Chemical Laboratory
Dr. Homi Bhabha Road, Pune-411008

CERTIFICATE

This is to certify that the work incorporated in this Ph.D. thesis titled **"Synthesis of Metal Oxide, Core-Shell Nanoparticles, Their Surface Modifications and Applications"** submitted by **Mr. Pravin Narayan Shinde** to the Academy of Scientific and Innovative Research (AcSIR) in fulfillment of the requirements for the award of Degree of **Doctor of Philosophy**, in **Chemical Sciences**, embodies original research work under my supervision. We further certify that this work has not been submitted to any other university or institution in part or full for any other degree or diploma. Research material obtained from other sources has been duly acknowledged in the thesis. Any text, illustration, table etc., used in the thesis from other sources, has been duly cited and acknowledged.

Mr. Pravin Narayan Shinde

(Student)

B. L. V. Prasad

(Supervisor)

DECLARATION

I, **Pravin Narayan Shinde**, hereby declare that the work described in this thesis titled **"Synthesis of Metal Oxide, Core-Shell Nanoparticles, Their Surface Modifications and Applications"** was carried out by me for the degree of **Doctor of Philosophy** in **Chemical Sciences** under the guidance and supervision of Dr. B. L. V. Prasad, Physical and Materials Chemistry Division, CSIR-National Chemical Laboratory, Pune, India. I confirm that this work was done by me in a candidature for a research degree at this institute. This work is original and no part of this thesis has been submitted for a degree or diploma at this institution or any other institution. The interpretation put forth are based on my literature survey of the original articles and all the sources have been duly acknowledged in this thesis.

Date: 25th March 2019   Mr. Pravin Narayan Shinde

Place: Pune   (Student)

ACKNOWLEDGEMENTS

Table of Content

List of Tables

List of Schemes

List of abbreviations

NP	Nano particles
DDS	Drug delivery systems
EPR	Enhanced permeation and retention
MDR	Multidrug resistance
SPR	Surface plasmon resonance
RES	Reticuloendothelial system
QD	Quantum dots
β-CD	β-Cyclodextrin
GSH	Glutathione
NGO	Nano graphene oxide
PEG	Polyethylene glycol
GO	Graphene oxide
MSN	Mesoporous silica nano particles
MRI	Magnetic resonance imaging
SPION	Superparamagnnetic iron oxide nanoparticles
AzPTS	Azidopropyl triethoxysilane
HMDS	Hexamethyl disilazane
R6G	Rhodamine 6G
MB 17	Mordant black 17
TEOS	Tetra Ethyl Ortho-Silicate
CTAB	Cetyl/Hexadecyl trimethyl ammonium bromide
NR	Nile red
CA	Calcein
PXRD	Powder X-ray diffraction
FT-IR	Fourier transform infra-red
CP-MAS	Cross polarization magic angle spinning
TGA	Thermo gravimetric analysis
NMR	Nuclear magnetic resonance
TEM	Transmission electron microscopy
BJH	Barrett-Joyner-Halenda
BET	Brunauer–Emmett–Teller
PL	Photo-luminescence

UV-Vis	Ultra violet –visible
TMS	trimethyl silyl
EDTA	Ethylenediamine tetraacetic acid
THPTA	3-hydroxypropyltriazolylmethyl amine
THF	tetrahydrofuran
TEG	triethylene glycol
PA	Propargyl alcohol
DCM	Dichloro methane
DMSO	Dimethyl sulphoxide
LCMS	Liquid chromatography-mass spectrometry
RPM	Rotations per minute
PBS	Phosphate buffer saline
PET	Positron emission tomography
CT	Computed tomography
BBB	Blood brain barrier
NSF	Nephrogenic system fibrosis
DMEM	Dulbeco's modified eagles media
FBS	Fetal bovine serum
VSM	Vibrating sample magnetometer
SQUID	Super conducting quantum interface device
AAS	Atomic absorption spectroscopy
ZFC	Zero field cooled
FC	Field cooled
CPMG	Carr-Purcell-Meiboom-Gill
COF	Covalent organic frameworks
MOF	Metal organic frameworks

Chapter I

Introduction

1.1 Introduction

Last two decades has seen a tremendous development in the area of nano science and technology. Manipulation of matter at nano scale can generate materials which possess emphatically different properties compared to their bulk form[1]. This happens predominantly because of very high surface to volume ratio and quantum confinement effects in nano materials[2]. Here, the surface of the nanomaterials plays an important role and greatly influence their characteristic properties and their applications. Some of the celebrated examples of such materials are carbon nano tubes[3], fullerenes[4], semi-conductor quantum dots[5], graphene[6], gold nanoparticles[7] etc. These nanomaterials have significantly impacted various areas of science and technology like catalysis[8], sorption[9] and separation[10], biotechnology[11], photonics[12], solar energy[13], electronics[14], energy storage[15], medicine[16]; sensors[17] so on and so forth.

It is believed that the most impactful contribution of nano science would be in the area of nano biotechnology[18] and nano medicine[19]. The most important developments have been made particularly in Drug Delivery Systems (DDS)[20]. Drug delivery consists of systems and methodologies to safely transport a therapeutic agent to a desired site in the body to enhance its therapeutic effect while reducing its side-effects. The important aspect of this is the mode of administration of the drug[21]. Figure 1.1 schematically describes classic routes of drug administration. The major non-invasive ways of drug administration are peroral, topical and transmucosal (which includes ocular, nasal, buccal/sublingual, vaginal and rectal)[22]. In case, the above routes are not effective intravenous injections are used to deliver the drug directly in to the blood stream. Transdermal patches can also deliver drugs below skin in a controlled way[23]. The drug after being absorbed in blood reaches its site of action by systemic circulation. In many cases e.g. antineoplastic agents; the systemic circulation causes the drug action at non intended sites resulting in toxicity and side-effects. For this reason targeted delivery becomes necessary.

1.2 Nanomedicine

Nano medicine includes formulations, coatings; delivery vehicles, imaging agents based on nanomaterials. It also includes tissue engineering and biomedical devices based on nanotechnology. Our focus is mainly on theranostic materials, i.e. therapy and diagnostics combined.
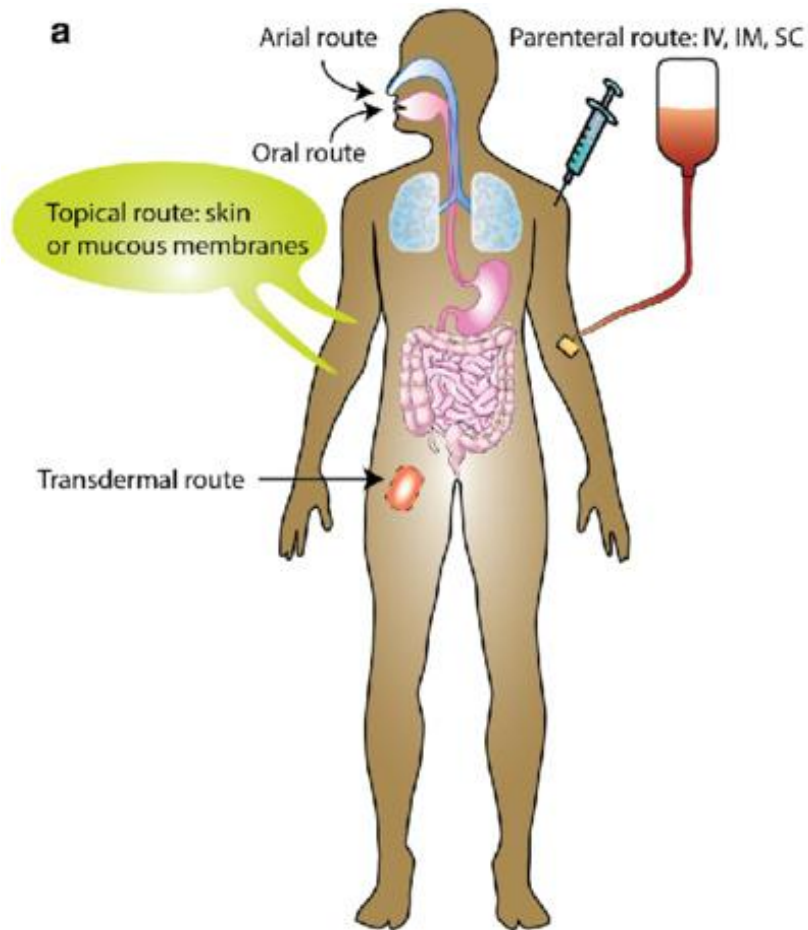
Figure 1.1 Different methods of conventional drug administration. Reproduced with permission of SPINGERNATURE from reference 22
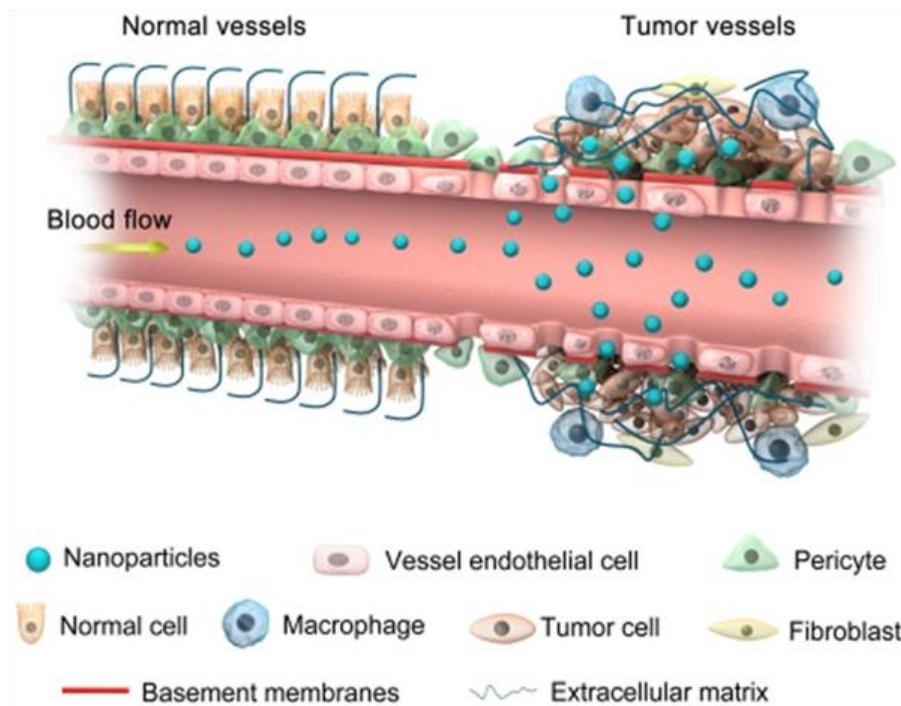
Figure 1.2 Enhanced Permeation and retention (EPR) effect reproduced from reference 24

1.3 Nanotheranostics

Initially nanoparticle based independent platforms were designed for imaging or delivery. But combination of diagnostic and therapy has recently become a phenomenon. Synthesis of a single multifunctional hybrid nano system which can perform both detection and deliver therapeutic agents with high efficiency has attracted interests from a lot of researchers. One of the early attempts for making a theranostic system is Iodine-131 therapy for detection and treatment of thyroid cancer. With theranostic system it is possible to monitor the effect of drug efficacy and response of treatment in real time. Recent developments in nano biomedicine have furthered the capability to make multifunctional nanoparticles that combine diagnosis, targeting and therapeutic functions in a single nano platform. Even in the individual functions; it is possible to incorporate plurality. Thus, a nano theranostic can perform multiple tasks like multimodal imaging and multi-drug delivery increasing overall ac curacy and effectiveness of treatment. The prominent expectations from a theranostic system are biocompatibility, high dispersion stability in aqueous systems, high cargo capacity, ease of functionalization (for specific targeting), tumour site accumulation and high circulation time. The typical components of a theranostic system are: carrier, drug/therapeutic agent, stimuli responsive release mechanism, targeting probe and an imaging probe.
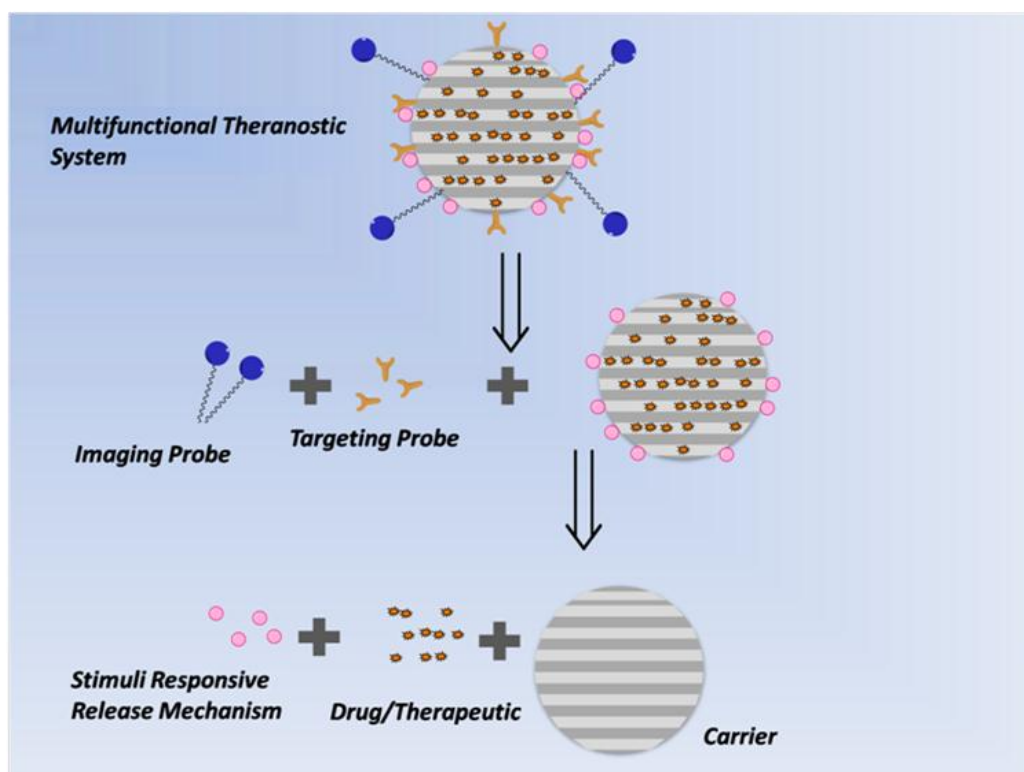
Scheme 1.1 Retro-synthesis of a Multifunctional theranostic system

A simple retro analysis of nano theranostic is shown in scheme 1.1. A typical multifunctional theranostic system would consist of five components- a) targeting probe b) Imaging probe c) stimuli responsive probe d) drug/therapeutic agent and e) carrier. We will be focusing on two major components of these, namely imaging and carrier.

1.3.2 Nano diagnostic systems

Diagnosis is the first and essential step of treatment for any disease condition. This helps to identify, ascertain, asses and monitor the disease condition of patients. Traditional way of diagnosis involved study of medical history, physical inspection of patients for symptoms and pathological tests. The diagnostic methods may involve *in vivo* or *in vitro* approaches. The common example of former is an X-ray scan or MRI image. The *in vitro* tests involve collection of physiological sample from patient and performing various analyses in lab such as urine/blood sugar detection or microbial culture. Nanoparticles have also been employed to diagnose a disease condition recently[24]. Nanoparticles with their inherent properties e.g. luminescence, surface plasmon resonance (SPR) have been proved as potential diagnosis vectors. Figure 1.3 shows some examples of such kind. Some commonly used nanomaterials for diagnosis includes Au NP, semiconducting quantum dots (QD) and magnetic NPs. Among all these magnetic resonance imaging (MRI) is very well practiced contemporory technique. Here, a strong magnetic field is applied to polarize hydrogen nuclie. They are then exposed to a radiofrequency pulse which excites them to higher degenerate state and subsequently undergo relaxation. The T1/T2 relaxation time of the protons (usually of water) in tissue is measured. The diffrence in relaxivity generates a contrast in the image. There are two major pathways of relaxation viz. spin-spin relaxation and spin-lattice relaxation. The commonly used contrast agent today are manily based on paramagnetic gadolinium (Gd) complexes which decreases the T1 relaxivity. Inorganic nanoparticles and especially superparamagnnetic iron oxide nanoparticles (SPION) other are recently been studied for their applications in MRI contrast[25]. Their biocompatibility and aquous stability has major role in increasing interest of many researchers. Heyon and co-workers has done a notable work in this regard[26-27]. They have synthesized uniform particles, coated them with silica and other ligands to increase their bioavailability and stability[28].
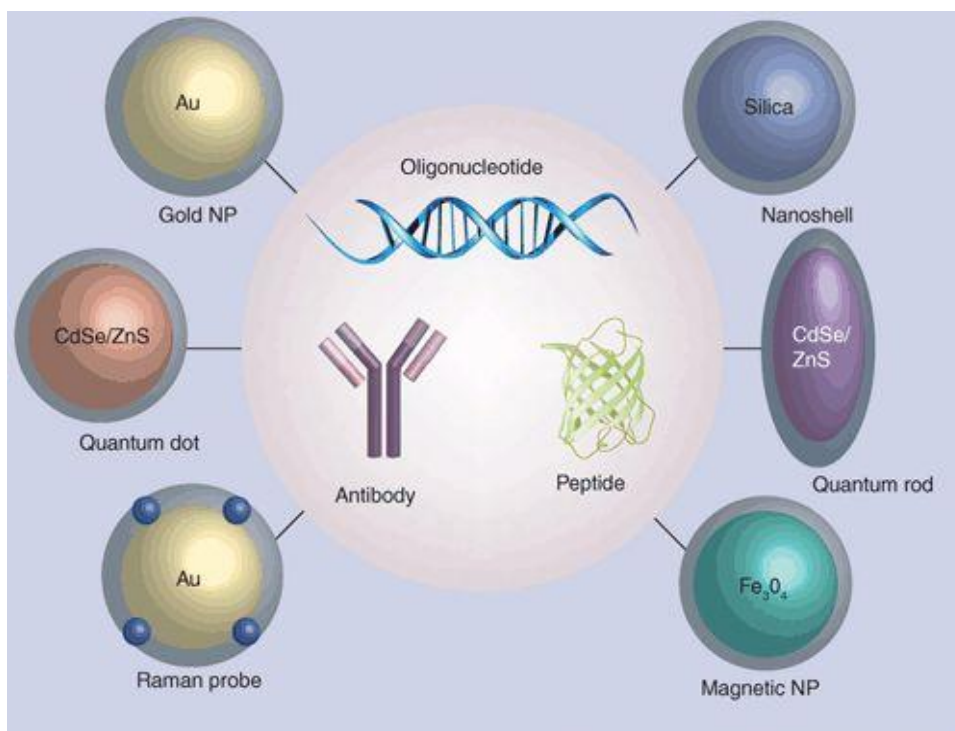
Figure 1.3 various NP based systems used for diagnosis applications
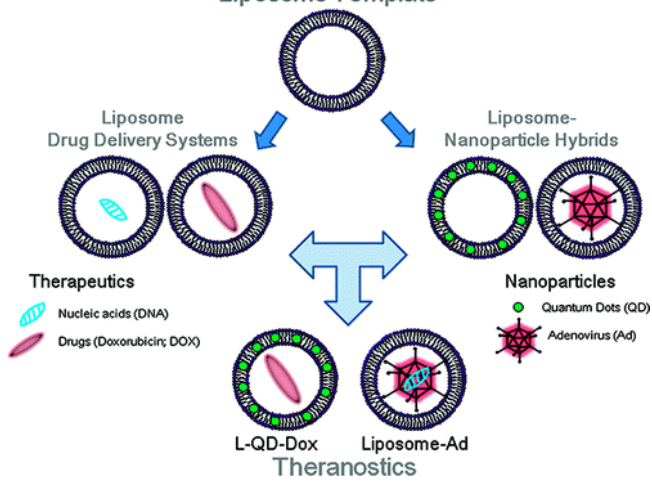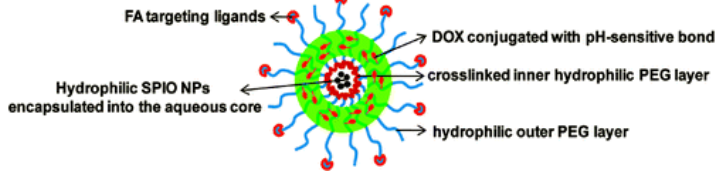
1.3.2 Nanoparticle Delivery Systems

Nanoparticles have very high surface area which can be used to load drugs. Due to small size they generally show high stability in dispersions compared to macro particles. This means the particles do not settle in given dispersion resulting in longer shelf life. The stable particle also results in longer circulation time in body. Nanoparticles of size < 100 nm can accumulate at tumour site by enhanced permeation and retention (EPR) effect thus enables passive targeting for delivery of anticancer agents[29]. The EPR effect can be understood as represented in the figure 1.2. Because of its rapid growth the tumour environment generally develops very poor vasculature. The vessal endothelial cells are loosely packed creating pores of size ~100 nm. So, the particles of size lower than this can easily escape from blood flow and never returns back dues to lack of vasculation in the tumour. This results in accumulation of NPs at the tumour site. Nanoparticles unlike molecules can enter into a cell by multiple pathways. Nanoparticle based drug delivery systems are considered to gain capability of avoiding multidrug resistance (MDR)[30], which has become a serious problem in traditional therapy[31]. The toxicity and biocompatibility of material is major concern and needs to be considered

seriously while designing a NP based DDS[32-33]. The method of conjugation of drug on NP determines the release mechanism and kinetics.

1.3 Carriers

Table 1.1 Different types of carriers used in drug delivery

Sr. No.	Carrier Type	Example/Scheme	Reference
1	Liposome		Al-Jamal et.al. *Accounts of Chemical Research* **2011,** 44, (10), 1094-1104.
2	Polymeric vesicles		Tanner et.al. *Accounts of Chemical Research* **2011,** 44, (10), 1039-1049.

3	Metal Nanoparticles		Heo et.al. *Biomaterials* **2012,** 33, (3), 856-866.
4	Carbon nanomaterials		Sun et.al. *Nano Research* **2008,** 1, (3), 203-212.
5	Mesoporous Silica		Slowing et. al. *Advanced Drug Delivery Reviews* **2008,** 60, (11), 1278-1288.

The carrier in drug delivery systems can be a liposome, polymeric vesicle, hydrogels, carbon/graphitic material, metal nanoparticle or porous silica nanoparticles. A list of examples has been summarized in Table 1.1. In case of metal nanoparticles it is the surface

on which the drug is loaded either by covalent bond or physisorption. In that case the loading capacity is solely dependent on surface area of the particles. The drugs along with vehicles can be targeted either actively by attaching targeting group e.g. an antibody or passively by enhanced permeation and retention (EPR) effect.

Metal nanoparticles such as gold and silver have been used to load a variety of drugs. Gold nanoparticles have been extensively studied systems in general. The easy surface decoration of gold with various surface groups such as thiol, amine and carboxylic acids makes it a preferred choice. One such example of Au NP based drug delivery system is by Heo et.al. Wherein, they decorated Au NP surface with β-cyclodextrin(β-CD) which would later act as a pocket for paclitaxel drug[34]. When these β-CDs decorated Au NPs were incubated with the drug, it gets bound to NP surface by formation of inclusion complex with β-CD. The NP surface was also decorated by attaching PEG ligands for anti-fouling and chemically conjugated biotin molecules for specific targeting towards cancer cells. It is reported that the drug gets released by the action of Glutathione (GSH) enzymes in intra-cellular environment.

Carbon based materials have also been widely explored as carrier systems for drugs. Fullerenes,[35] carbon nanotubes,[36] graphene and graphene oxide[37] are being the prominent examples. One such example is shown in the above table is by Sun and co-workers. Here, they have synthesized nano graphene oxide (NGO) which is intrinsically fluorescent and can be used for imaging[37]. The NGO was further functionalized with PEG to improve its water dispersibility and also decorated with antibodies for targeting. The anticancer drug doxorubicin was loaded by π-π interactions. The high surface area for loading drug and intrinsic photoluminescence has been utilized for imaging and delivery. Amongst the different carbon based materials graphene has attracted tremendous interest from researchers working in multiple areas. The extraordinary properties of the material such as very high surface area, electrical and thermal conductivity as well as high mechanical strength makes it promising candidate for many applications. Being the single sheet of carbon atoms, it is considered as a 2-D material. Sun et.al. used graphene oxide (GO) to load Doxorubicin where it binds to the graphene surface majorly through π-π interactions. In this particular example, graphene oxide was functionalized by star like polyethylene glycol (PEG) and antibody probe for specific targeting. As the GO exhibit photoluminescence, it was easily tracked for imaging purpose.

The porous particles such as mesoporous silica nanoparticles (MSN), on the other hand have additional advantages in that these materials are characterized with two surfaces i.e. outer surface and pore surface[38]. In this context, one of the most attractive features of these MSNs is that while the inner pore can be filled with cargo molecules, the pore mouth can be capped with a blocking unit, thus protecting the cargo from exposure to external environment. After removal of the blocking cap, the cargo may get released by diffusion[39]. In case of MSN, there are various other advantages that foster their use in drug delivery systems. The high surface area, ease of synthesis of silica in various morphologies and sizes[40], tunable pore sizes and geometries, plethora of tools available for chemical modification of its surface[41] and biocompatibility[42-43] are some of the advantages of these classes of materials. Mesoporous silica has pore sizes in the range of 2-50 nm and various types of mesoporous silica such as MCM-41[44], SBA-15[45], KIT-6[46], and KCC-1[47] etc. have been synthesized. Among these MCM-41 type silica nanoparticles also known as mesoporous silica nanoparticles (MSN) are more common. It is then becomes a very attractive feature since these pores could be utilized for loading additional cargo. In a recent example, Rahmani et.al. have used large pore MSN as delivery vector for Pepstatin A which is a non cell-penetrating peptide drug effective in breast cancer[48]. In another example, Gounania et.al. have shown that MSN can be used to carry multiple antibiotics such as polymyxin B and vancomycin to provide synergistic effect and improved biocompatibility[49]. In some reports hollow mesoporous silica nanoparticles have been designed. In one such case, Moghaddam et.al. have synthesized hollow MSN by selective etching of stober silica with sodium carbonate[50]. Before the etching an outer shell of mesoporous silica was synthesized which was used for loading Doxorubicin. The outer mesoporous shell which is composed of glutathione sensitive disulphide linkages undergoes redox degradation in presence of tumour environment to release doxorubicin. The system could effectively release ~60% of dox in 14 days. Furthermore, once the desired cargo loaded inside the pores they can be blocked by using various strategies[51]. This gives huge advantages over other materials in terms of controlling the release. Li et.al. have prepared hollow MSN structures for drug delivery using CaCO3 as sacrificial template[52]. The hollow cavity was loaded with fluorouracil anticancer drug and the pores were capped by hydrotalcite sheets by layer by layer assembly method. These sheets act as pH responsive gatekeepers for controlled release. Similarly, more complex designs have been attempted to incorporate multifunctionality in these carriers. One of the common approaches is to make core-shell architectures to incorporate other NPs which have magnetic or photo luminescent properties.

Ullah et al. have designed a proof-of-concept delivery vehicle which can release drug with heat trigger[53]. The core of the system consists of SPION NP coated with MSN shell. The drug maytasin is loaded in MSN and the whole system is entrapped in macrophages. After subjecting this system to alternating magnetic field (AMF) the SPION produced heat which kills the macrophages and the thermally labile linker is cleaved which triggers the release of drug which in turn causes killing of tumour cells in 3 D co-cultures. Li et.al. have designed a more complex dual functional Janus system based on MSN by anisotropic island nucleation and growth of ordered silica mesostructures[54]. This system can be triggered by heat and IR light due to up-conversion nanoparticle (UCNP) core imbedded in it. In another example of heat triggered delivery vehicle, Rafael R. Castillo has developed a thermo-responsive controlled release vehicle based on MSN[55]. Here they have used a diels-alder adduct as temperature labile group which is connected to AuNP caps. The unique characteristic of this design is the AuNP cap can be used as easy functionalization platform for targeting ligands; in this particular case biotin. Liu et. al. have fabricated a core-shell structured nanoparticles system for the treatment of prostate cancer[56]. In this work they have used mesoporous silica nanoparticles as drug carrier for doxorubicin and $CaCO_3$ as pH sensitive gatekeeper which gets dissolved at lower pH around malignant tumour environment. The whole system can be wrapped in cancer cell membrane which improved its colloidal stability as well as capacity to accumulate at tumour site. Due to amorphous nature and hydrogen bonding ability of surface silanol groups MSN can be easily blended with many polymers to create multifunctional hybrid materials. Asefa and co-workers has used hydrophobic functionalized MSN to load dexamethasone drug. The particles were then encapsulated in polymers such as PVA & PAA which were then subjected to solid state thermally activated condensation to form polymer/silica aerogel[57]. The silica was also functionalized by quaternary ammonium species to impart anti-bacterial activity. The aerogel functioned as carrier for prolonged and sustainable drug release In another example, Zhou et. al. functionalized the MSN with two different moieties viz. PEI-PLL copolymer and RGD peptide[58]. This bifunctional system used to carry osteogenic DNA and Dexamethasone drug to enhance the osteogenic differentiation.

Due to these advantages MSN have been widely explored for the applications in drug delivery systems. The drug can be loaded on outer surface by physisorption as well as by chemical conjugation. For later the specific surface modification of the nanoparticle has to be carried out. In case of physisorption the drug molecules gets adsorbed on particle surface by van der Waal's forces, hydrogen bonding or electrostatic interactions. In case of drug loading

in the pores, earlier reports were focussed on pristine porous silica particles without any surface modifications. Very recently attempts to improve the drug loading by different types of surface modifications of MSN have been attempted[59]. In most of the cases it has been found that the electrostatic attraction between drug molecule and the surface functional group attached on silica wall has been utilized[60]. For example, amine functionalized MSN can be loaded with carboxylic acid containing drug molecule as vice versa. Interesting thing to note here is the pH of solution during incubation plays important role in adsorption as well as release. However, it is very easy to realize that loading of drug molecules which lack acidic/basic functional groups in their structure needs different strategy of functionalization. Use this very orthodox principle inevitably limits its scope. It is very unlikely to have these complimentary functional groups in the drug and carrier for most times. So we acknowledge a need to revisit functionalization strategies of carriers itself. It has to be modified in such a way that its utility is not limited for drugs with a certain class of functional groups.

Since mesoporous silica has pores in each particle; it is characterized with extraordinarily high surface area. In fact, the high surface area of mesoporous silica is due to larger contribution from the internal pore structure. It is then becomes a very attractive feature since these pores could be utilized for loading additional cargo. Furthermore, once the desired cargo loaded inside the pores they can be blocked by using various strategies. This gives huge advantages over other materials in terms of controlling the release.

1.4 Statement of the problem:

1. After going through the published literature in a careful and systematic way; we realized that the loading of drugs by functionalizing pores of MSN has not been demonstrated. The specific functionalization which is useful to adsorb drug molecules independent of their functional groups is necessary. The functionalization should increase the loading capacity of the drug on to the carrier.

2. The carrier stability in the aqueous medium should be higher to have higher systemic circulation times as well as shelf life. So the carrier should be appropriately functionalized on outer surface.

3. Incorporation of appropriate surface modification for theranostic application in the above carrier should be demonstrated.

1.5 Scope of this thesis:

Here we tried to address following issues

1. First we tried to design a carrier based on mesoporous silica nanoparticles (MSN) which is tailored for adsorbing hydrophobic drugs. This has been achieved by selectively functionalizing inner pore surface of these MSN particles by hydrophobic functionality. The outer surface of these carriers was functionalized with a polar group, helps to give dispersion stability in aqueous medium. The hydrophobic inner surface helps to load higher amounts of hydrophobic drug.

2. Here we tried to understand the effect of tailoring the outer surface functionality. We demonstrate that by changing the size of outer surface ligands can affect the uptake as well as release of drugs loaded in a mesoporous system. Here we also demonstrate the two different drug loading methods and their advantages and shortcomings.

3. Lastly, we incorporate the second theranostic element; magnetic core in these amphifunctional mesoporous silica shell. We demonstrate the usefulness of this multifunctional system for drug delivery as well as MRI contrast agent.

1.6 References

(1)   Klabunde, K. J.; Richards, R. *Nanoscale Materials in Chemistry*; Wiley Online Library, New York, 2001; Vol. 1035.

(2)   Roduner, E. *Chem. Soc. Rev.* **2006**, *35*, 583.

(3)   Iijima, S.; Ichihashi, T. *Nature* **1993**, *363*, 603.

(4)   Taylor, R.; Hare, J. P.; Abdul-Sada, A. a. K.; Kroto, H. W. *Chem. Commun.* **1990**, 1423.

(5)   Alivisatos, A. P. *Science* **1996**, *271*, 933.

(6)   Geim, A. K.; Novoselov, K. S. *Nat. Mater.* **2007**, *6*, 183.

(7)   Brust, M.; Walker, M.; Bethell, D.; Schiffrin, D. J.; Whyman, R. *Chem. Commun.* **1994**, 801.

(8)   Haruta, M.; Date, M. *Appl. Catal., A* **2001**, *222*, 427.

(9)   Patil, S.; Sandberg, A.; Heckert, E.; Self, W.; Seal, S. *Biomaterials* **2007**, *28*, 4600.

(10)   Gu, H.; Xu, K.; Xu, C.; Xu, B. *Chem. Commun.* **2006**, 941.

(11)   Cao; Jin, R.; Mirkin, C. A. *J. Am. Chem. Soc.* **2001**, *123*, 7961.

(12)   Loo, C.; Lin, A.; Hirsch, L.; Lee, M.-H.; Barton, J.; Halas, N.; West, J.; Drezek, R. *Technol Cancer Res Treat.* **2004**, *3*, 33.

(13)   Baxter, J. B.; Aydil, E. S. *Appl. Phys. Lett.* **2005**, *86*, 053114.

(14)   Li, Y.; Wu, Y.; Ong, B. S. *J. Am. Chem. Soc.* **2005**, *127*, 3266.

(15)   Poizot, P.; Laruelle, S.; Grugeon, S.; Dupont, L.; Tarascon, J. *Nature* **2000**, *407*, 496.

(16)   Giljohann, D. A.; Seferos, D. S.; Daniel, W. L.; Massich, M. D.; Patel, P. C.; Mirkin, C. A. *Angew. Chem. Int. Ed.* **2010**, *49*, 3280.

(17)   Howes, P. D.; Chandrawati, R.; Stevens, M. M. *Science* **2014**, *346*, 1247390.

(18)   Whitesides, G. M. *Nat. Biotechnol.* **2003**, *21*, 1161.

(19)   Wicki, A.; Witzigmann, D.; Balasubramanian, V.; Huwyler, J. *J. Control. Release* **2015**, *200*, 138.

(20)   De Jong, W. H.; Borm, P. J. *Int. J. Nanomed* **2008**, *3*, 133.

(21)   Langer, R. *Science* **1990**, *249*, 1527.

(22)   Bose, T.; Latawiec, D.; Mondal, P. P.; Mandal, S. *J. Nanoparticle Res.* **2014**, *16*, 2527.

(23)   Prausnitz, M. R.; Langer, R. *Nat. Biotechnol.* **2008**, *26*, 1261.

(24)   Yezhelyev, M.; Yacoub, R.; O'Regan, R. *Nanomedicine* **2009**, *4*.

(25)   Na, H. B.; Song, I. C.; Hyeon, T. *Adv. Mater.* **2009**, *21*, 2133.

(26)   Kim, J.; Kim, H. S.; Lee, N.; Kim, T.; Kim, H.; Yu, T.; Song, I. C.; Moon, W. K.; Hyeon, T. *Angew. Chem. Int. Ed.* **2008**, *47*, 8438.

(27)   Xie, H.; Zhu, Y.; Jiang, W.; Zhou, Q.; Yang, H.; Gu, N.; Zhang, Y.; Xu, H.; Xu, H.; Yang, X. *Biomaterials* **2011**, *32*, 495.

(28)   Kim, B. H.; Lee, N.; Kim, H.; An, K.; Park, Y. I.; Choi, Y.; Shin, K.; Lee, Y.; Kwon, S. G.; Na, H. B.; Park, J.-G.; Ahn, T.-Y.; Kim, Y.-W.; Moon, W. K.; Choi, S. H.; Hyeon, T. *J. Am. Chem. Soc.* **2011**, *133*, 12624.

(29)   Abdalla, A. M. E.; Xiao, L.; Ullah, M. W.; Yu, M.; Ouyang, C.; Yang, G. *Theranostics* **2018**, *8*, 533.

(30)   Wang, F.; Wang, Y.-C.; Dou, S.; Xiong, M.-H.; Sun, T.-M.; Wang, J. *ACS Nano* **2011**, *5*, 3679.

(31)   Perez, F.; Hujer, A. M.; Hujer, K. M.; Decker, B. K.; Rather, P. N.; Bonomo, R. A. *Antimicrob. Agents Chemother.* **2007**, *51*, 3471.

(32)   Oberdörster, G. *J. Intern. Med.* **2010**, *267*, 89.

(33)   Lam, P.-L.; Wong, W.-Y.; Bian, Z.; Chui, C.-H.; Gambari, R. *Nanomedicine* **2017**, *12*, 357.

(34)   Heo, D. N.; Yang, D. H.; Moon, H.-J.; Lee, J. B.; Bae, M. S.; Lee, S. C.; Lee, W. J.; Sun, I.-C.; Kwon, I. K. *Biomaterials* **2012**, *33*, 856.

(35)   Shi, J.; Zhang, H.; Wang, L.; Li, L.; Wang, H.; Wang, Z.; Li, Z.; Chen, C.; Hou, L.; Zhang, C.; Zhang, Z. *Biomaterials* **2013**, *34*, 251.

(36)   Pastorin, G.; Wu, W.; Wieckowski, S.; Briand, J.-P.; Kostarelos, K.; Prato, M.; Bianco, A. *Chem. Commun.* **2006**, 1182.

(37)   Sun, X.; Liu, Z.; Welsher, K.; Robinson, J. T.; Goodwin, A.; Zaric, S.; Dai, H. *Nano Res.* **2008**, *1*, 203.

(38)   Vinu, A.; Hossain, K. Z.; Ariga, K. *J. Nanosci. Nanotech.* **2005**, *5*, 347.

(39)   Slowing, I. I.; Vivero-Escoto, J. L.; Wu, C.-W.; Lin, V. S. Y. *Adv. Drug Deliv. Rev.* **2008**, *60*, 1278.

(40)   Rosenholm, J. M.; Sahlgren, C.; Linden, M. *Nanoscale* **2010**, *2*, 1870.

(41)   Moeller, K.; Bein, T. *Chem. Mater.* **2017**, *29*, 371.

(42)   Tarn, D.; Ashley, C. E.; Xue, M.; Carnes, E. C.; Zink, J. I.; Brinker, C. J. *Acc. Chem. Res.* **2013**, *46*, 792.

(43)   Fangqiong, T.; Linlin, L.; Dong, C. *Adv. Mater.* **2012**, *24*, 1504.

(44)   Slowing, I. I.; Trewyn, B. G.; Giri, S.; Lin, V. Y. *Adv. Funct. Mater.* **2007**, *17*, 1225.

(45)   Vavsari, V. F.; Ziarani, G. M.; Badiei, A. *RSC Adv.* **2015**, *5*, 91686.

(46)   Ayad, M. M.; Salahuddin, N. A.; El-Nasr, A. A.; Torad, N. L. *Micropor. Mesopor. Mater.* **2016**, *229*, 166.

(47)   Huang, X.; Tao, Z.; Praskavich, J. C.; Goswami, A.; Al-Sharab, J. F.; Minko, T.; Polshettiwar, V.; Asefa, T. *Langmuir* **2014**, *30*, 10886.

(48)   Rahmani, S.; Budimir, J.; Sejalon, M.; Daurat, M.; Aggad, D.; Vives, E.; Raehm, L.; Garcia, M.; Lichon, L.; Gary-Bobo, M. *Molecules* **2019**, *24*, 332.

(49)   Gounani, Z.; Asadollahi, M. A.; Pedersen, J. N.; Lyngsø, J.; Pedersen, J. S.; Arpanaei, A.; Meyer, R. L. *Colloids Surf. B* **2019**, *175*, 498.

(50)   Moghaddam, S. P. H.; Yazdimamaghani, M.; Ghandehari, H. *J. Control. Release* **2018**, *282*, 62.

(51)   Slowing, I. I.; Vivero-Escoto, J. L.; Wu, C.-W.; Lin, V. S. Y. *Adv. Drug Delivery Rev.* **2008**, *60*, 1278.

(52)   Jin, L.; Huang, Q.-J.; Zeng, H.-Y.; Du, J.-Z.; Xu, S.; Chen, C.-R. *Micropor. Mesopor. Mater.* **2019**, *274*, 304.

(53)   Ullah, S.; Seidel, K.; Türkkan, S.; Warwas, D. P.; Dubich, T.; Rohde, M.; Hauser, H.; Behrens, P.; Kirschning, A.; Köster, M. *J. Control. Release* **2019**, *294*, 327.

(54)   Li, X.; Zhou, L.; Wei, Y.; El-Toni, A. M.; Zhang, F.; Zhao, D. *J. Am. Chem. Soc.* **2014**, *136*, 15086.

(55)   Castillo, R. R.; Hernández-Escobar, D.; Gómez-Graña, S.; Vallet-Regí, M. *Chem. Eur. J.* **2018**, *24*, 6992.

(56)   Liu, C.-M.; Chen, G.-B.; Chen, H.-H.; Zhang, J.-B.; Li, H.-Z.; Sheng, M.-X.;
         Weng, W.-B.; Guo, S.-M. *Colloids Surf. B* **2019**, *175*, 477.

(57)   Follmann, H. D.; Oliveira, O. N.; Lazarin-Bidóia, D.; Nakamura, C. V.;
         Huang, X.; Asefa, T.; Silva, R. *Nanoscale* **2018**, *10*, 1704.

(58)   Zhou, X.; Zhang, Q.; Chen, L.; Nie, W.; Wang, W.; Wang, H.; Mo, X.; He, C.
         ACS Biomater. Sci. Eng. **2019**, 5, 710.

(59)   Yang, P.; Gai, S.; Lin, J. *Chem. Soc. Rev.* **2012**, *41*, 3679.

(60)   Manzano, M.; Aina, V.; Areán, C. O.; Balas, F.; Cauda, V.; Colilla, M.;
         Delgado, M. R.; Vallet-Regí, M. *Chem. Eng. J.* **2008**, *137*, 30.

Chapter II

Design and Synthesis of Amphi-functional Mesoporous Silica Nanoparticles

2.1 Introduction

Drug delivery consists of systems and methodologies to safely transport a therapeutic agent to a desired site in the body to enhance its therapeutic effect while reducing the side-effects. The important aspect of this is the mode of administration of the drug[1]. The major non-invasive ways of drug administration are peroral, topical and transmucosal (which includes ocular, nasal, buccal/sublingual, vaginal and rectal). In case, the above routes are not effective, intravenous injections are used to deliver the drug directly into the blood stream. Transdermal patches can also deliver drugs below skin in controlled way[2]. In general, the drug after being absorbed in blood reaches its site of action by systemic circulation. In many cases e.g. antineoplastic agents; the systemic circulation causes the drug action in non intended sites resulting in toxicity and side-effects. For this reason targeted delivery becomes necessary. Targeted delivery involves the delivery of drugs along with vehicles to the site of action either actively by attaching targeting group e.g. an antibody or passively by processes such as enhanced permeation and retention (EPR) effect[3].

The list of carriers being used in drug delivery systems consist liposomes[4], polymeric vesicles[5-6], hydrogels, carbon/graphitic materials[7-8], metal nanoparticles[9] or porous silica nanoparticles[10]. Amongst these in case of metal nanoparticles it is the surface on which the drug is loaded either by covalent bond or physisorption[11]. In that case the loading capacity is solely dependent on surface area of the particles. In many of the other systems the drug is encapsulated inside the vehicle. The porous particles such as mesoporous silica nanoparticles (MSN), on the other hand have an added advantage,[12] in the sense that these materials possess two surfaces, namely, an outer surface and the pores. Here apart from the outer surface, the inner pore also can be filled with cargo molecules. A most attractive consequence of loading the drug inside a pore is, protecting the drug from exposure to external environment if the pore is capped with a blocking unit. It is also possible then to release the drug in a controlled fashion or by simple diffusion by removing this cap [13]. In case of MSN, there are various other advantages that foster their use in drug delivery systems. The MSN are very easy to synthesize[14], their morphologies and pore sizes can be tuned easily in a wide range[15], silica surface offers variety of post-synthesis functionalization possibilities[16] and the material is biocompatible[17-18].

Due to these advantages, MSN have been widely explored for the applications in drug delivery systems. From the above discussion it also becomes clear that the drug can be loaded

on MSN surface or inside the pores by physisorption[19] as well as by chemical conjugation[20]. In case of physisorption the drug molecules gets adsorbed on particle surface by van der Waal's force, hydrogen bonding or electrostatic interactions[21]. While most of the earlier efforts, where MSN were used as vehicles; they were employed without any surface modifications. In several other reports where to improve the drug loading, surface modifications of MSN has been attempted[22]. However, in most of these cases the electrostatic attraction between drug molecule and the surface functional group attached on silica wall has been utilized for drug loading purpose[23]. For example, amine functionalized MSN have been loaded with carboxylic acid containing drug molecule and vice versa[24]. It is important to note here that the pH of solution during incubation plays an important role in adsorption as well as release[25]. Thus it becomes clear that for loading of drug molecules those lack acidic/basic functional groups in their structures; we need different strategy of surface functionalization. Our literature search indicated that such approaches are lacking in the available literature.

2.2 Statement of the problem:

1. Would it be possible to develop a specific functionalization strategy that allows the loading of drug molecules independent of their functional groups? We reasoned that such functionalization would increase the loading capacity of the drug on to the carrier.

2. We also wanted to develop a strategy where the carrier stability in the aqueous medium would be higher that allows higher systemic circulation time as well as shelf life. For this the carrier should be appropriately functionalized on outer surface.

So firstly we decided to address this issue by imparting selective functionalization to the MSNs. We realized that for this the outer surface should have a polar functionality so that the carrier particles will be highly stable in the aqueous dispersion. This will give them high systemic stability as well as shelf life. On the other hand, we also wanted to increase the loading capacity of the drug without having concerns about its functional groups. We envisaged that this will benefit in reducing the dosage size for patients. To make this a reality, the adsorption process has to be different than acid-base interactions that were exploited in previous examples[26]. We envisioned that most of the drug molecules have hydrophobic part in their chemical structure as either an aromatic/polycyclic ring or aliphatic chain. If we can generate hydrophobicity on the pore surface of the mesoporous silica, we could adsorb various drugs by hydrophobic-hydrophobic interactions. So combining the above two

strategies, we aimed to synthesize an amphi-functional MSN system where the pores are hydrophobic while the outer surface is hydrophilic.
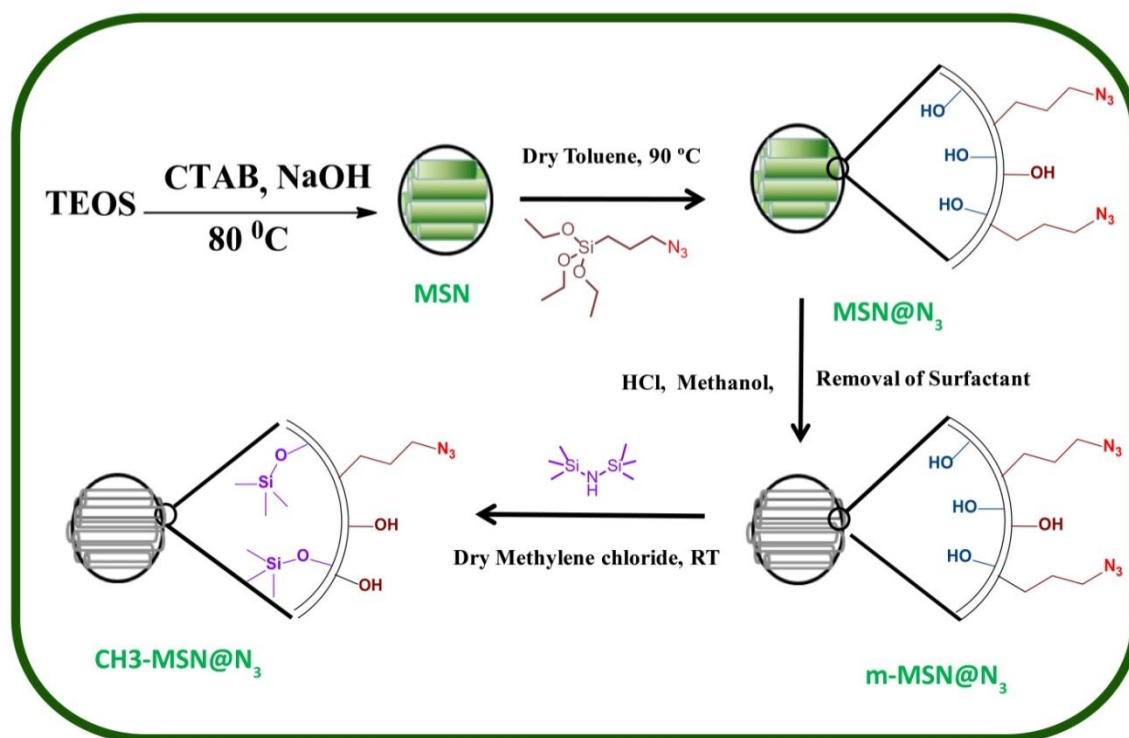
Scheme 2.1: Synthesis of amphi-functional silica nanoparticles by stepwise chemical modification

Accordingly, we present in this chapter our strategy and results of the preparation of amphi-functional MSNs in a stepwise manner. Our strategy involved the modification of the outer surfaces of particles with azidopropyl triethoxysilane (AzPTS) groups while the pores were still occupied with surfactant template which was used during synthesis. This results in the predominant functionalization of particle surface with azide groups. The polar mesomeric structures possible for the azide group make them sufficiently polar. This azide functionalization allows MSN to disperse well in water. In addition, they are also chemically inactive towards the reagents used in subsequent functionalization. But, these can be utilized in a "click reaction" with an alkyne[27-28]. So the azide groups act as platform to tune surface chemistry with a desired functional moiety if needed. Finally, the small size of azidopropyl groups does not hinder adsorption of chemical entities into the pores of MSN. All these properties make them unique in comparison to other surface functionalized MSNs with polar groups such as carboxylic acid, amines or ethylene glycol. The surfactant template was then removed by acidic methanol extraction without affecting the azide functionalization. The

opened pore walls having fresh silanols were then treated with hexamethyldisilazane (HMDS) to transform them into hydrophobic trimethylsilyl functionalities. The polar azide surface helps to disperse the particles in aqueous medium while the hydrophobic pockets/pores can be utilized to load the drug. Another important aspect that we kept in view while developing the amphi-functional MSNs is to be able to load the drug by simple incubation of the molecule with the MSNs. To prove our concept in a clear manner we have used dyes instead of drugs because it would be easy to characterize the process using simple analytical techniques like UV-Vis and fluorescence spectroscopy. It may be noted that most of the drugs and dyes have similar molecular structures. Also to prove the effectiveness of our strategy, we have used the amphi-functional MSNs for separating relatively more hydrophobic dyes from a mixture of dyes in water. Accordingly, we have chosen Calcein, Rhodamine 6G (R6G) and Mordant black 17 (MB17) as model dyes. The chemical structures of these dyes have been shown in figure 2.1.The material selectively removed the relatively more hydrophobic dyes R6G and MB17 when they were present as a mixture along with calcein in water. The adsorbed dye could be recovered from the pores by simple washing with ethanol. These adsorbents have shown excellent recyclability up to 10 cycles. To the best of our knowledge, this is first ever report that demonstrate the construction of an amphi functional MSN which can absorb a dye/drug based on hydrophobic interactions. This eliminates the necessity for pre-treatment of effluent for maintaining favourable conditions for adsorption e.g. pH as required in some of the previous reports.
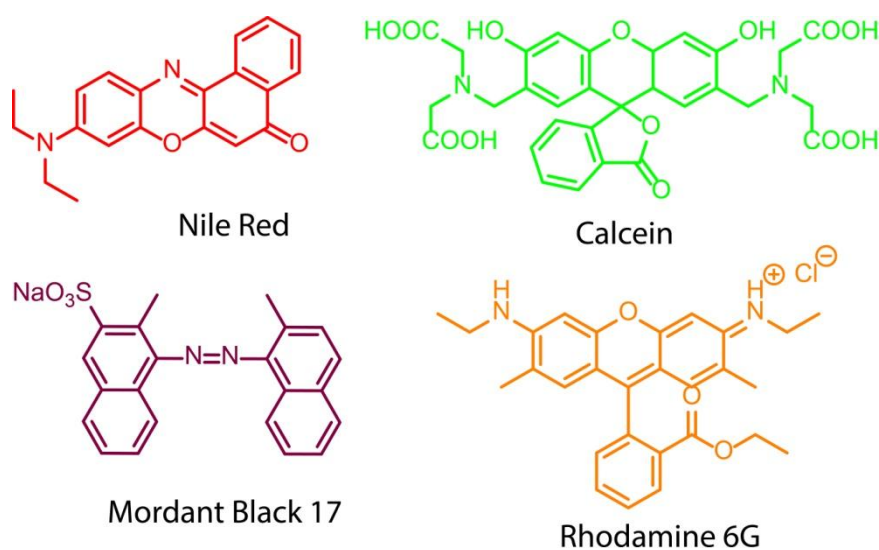
Figure 2.1: Chemical structures of different dyes used

2.3 Experimental Section

2.3.1 Materials:

Tetra Ethyl Ortho-Silicate (TEOS), sodium hydroxide, hexadecyl trimethyl ammonium bromide (CTAB), 3-chloropropyl triethoxy silane, hexamethyl disilazane (HMDS), Nile red (NR), Rhodamine 6G (R6G) and Calcein were purchased from Sigma Aldrich. Mordant Black 17 was purchased from TCI chemicals. Sodium azide, ethanol, methanol, dry toluene, dry dichloro methane, dimethyl formamide and concentrated hydrochloric acid were obtained from Merck India. All of them were used without further purification. 3-Azidopropyl triethoxy silane, and Sodium dithio carbamate was prepared as reported before. Milli Q water was used for all experiments. All manipulations were performed in open atmosphere until otherwise mentioned.

2.3.2 Synthesis:

2.3.2.1 Synthesis of selectively functionalized MSN

Scheme 2.1 briefly illustrates the methodology used for synthesis of selectively functionalized mesoporous silica nanoparticles. 1.0 g of CTAB (0.0027 mol) was dissolved in 480 mL of water in a jacketed reaction flask and heated to 80 °C with constant stirring using overhead stirrer for 30 minutes. 3.5 mL of 2M NaOH was added into above mixture followed by drop wise addition of 5.0 mL of TEOS (0.0223 mol). The reaction was stirred for 2 hours at 80 °C after which it was immediately filtered through Whatman no. 1 filter paper and washed with copious amount of water to remove excess alkali (till filtrate became neutral to litmus). Finally the product was washed with 100 mL of ethanol and aged at 80 °C for 12 hours. This sample termed as MSN. Yield 1.8 g.

To graft azide groups on the surface; 1.5 g dried powder of MSN particles were taken in a two neck round bottom flask and dispersed in anhydrous toluene under inert atmosphere of argon. The reaction mixture was heated at 80 °C before addition of 0.75 mL (0.0030 mol) of 3-azidipropyl triethoxy silane (AzPTS). Reaction was stopped after 12 hours and cooled to room temperature. Product was washed by centrifugation at 20000 rpm for 20 min to remove unreacted AzPTS. The supernatant was discarded and precipitate was dispersed in ethanol by sonication and centrifuged again. This cycle was repeated for three times. The product at this stage was labelled as MSN@N$_3$. This product was then dispersed in 100 mL methanol and acidified with 2 mL of concentrated HCl. Azide grafted particles were refluxed in methanol for 6 hours to remove CTAB after which it was centrifuged at 20000 rpm for 20 min and the supernatant containing acidic methanol was discarded. It was again dispersed in 100 mL fresh methanol and refluxed for another 24 hours. It was then subjected to centrifuge and purified

by washing for three times as mentioned above. Finally the precipitate was dried in vacuum oven at 80 °C. Yield 0.850 g. This sample was labelled as m-MSN@N$_3$.

For functionalization of mesoporous pores by hydrophobic functionality; 0.5 g of m-MSN@N$_3$ was dispersed in 50 mL of anhydrous dichloro methane under dry and inert atmosphere. 0.150 mL (0.0012 mol) of hexamethyl disilazane (HMDS) was injected while stirring at room temperature. After 24 hours of reaction, the product was isolated by centrifugation at 20000 rpm for 20 minutes and washed with ethanol (50 mL) three times similar to previous experiment. Finally, the precipitate was dried in a vacuum oven for 12 hrs @ 80 °C. The material was labelled as CH$_3$-MSN@N$_3$, yield 0.430 g.

2.3.2.2 Demonstration of hydrophobic compartments in MSN by encapsulation of Nile Red

In 0.5 mL of particle dispersions (2 mg.mL^{-1}) of silica particles in Millipore water, 10 µl Nile red solution (2.3 mg.mL^{-1}) in ethanol was added. The mixture was then incubated on a rotospin spinning at 25 rpm at room temperature for 3 hours. 0.1 mL of aliquot was diluted to 1.0 mL with water and used to measure photoluminescence by exciting at 530 nm using 5nm slit widths for both excitation and emission. The intensity at 645 nm was used to compare quantitative uptake of dye in particles.

2.3.2.3 Uptake of water soluble dyes in functionalized MSN

Various water soluble dyes, such as Calcein (CA), Rhodamine 6G (R6G) and Mordant Black 17 (MB17) were chosen for the study. 20.0 mg.mL^{-1} stock solution of silica particles was prepared after vigorous shaking of the functionalized particles (CH$_3$-MSN@N$_3$) with water followed by sonication. Aliquots of various concentrations of initial stock solutions of dyes were added in micro centrifuge tubes to make final volume of 0.5 mL. Final concentration before incubation for particle was 10 mg.mL^{-1}. The dye concentrations were 0.01, 0.05, 0.1, 0.2, 0.5 & 1.0 mM. The tubes were rotated on rotospin at 25 rpm for 6 hours for mixing and equilibrating at room temperature. The supernatants were taken out after centrifugation at 20000 RPM for 10 minutes and analyzed by UV-Vis spectrometer. The adsorption capacities were calculated from the isotherms using formula,

$$q_t = \frac{(C_0 - C_e)V}{W} \qquad\qquad 2.1$$

Where, q_t is adsorption capacity (mmol.g^{-1}), C_0 and C_e are initial and equilibrium concentration (mmol.dm^{-3}) of dyes after sorption respectively, V is volume of solution (dm^3) and W is mass of sorbent (g).

2.3.2.4 Selective separation of dye from dual dye mixture

The experiments were carried out with procedure very similar as mentioned above. Only change was instead of one dye, an equimolar mixture of dyes having final concentration 0.05 mM of each was used. After centrifugation the UV-Vis spectra of supernatant solutions were recorded after appropriate dilutions.

2.3.2.5 Reusability of MSN cargo

The reusability of the functionalized silica materials were studied with R6G dye. The dye encapsulation experiment was performed with incubation with 0.1 mM of R6G with 10 mg per mL CH$_3$-MSN@N$_3$ particles for 6 hours at ambient temperature. The procedure for incubation and measurement was similar as above. After taking out the supernatant the precipitate with adsorbed dye was mixed with 1 mL of ethanol and sonicated for 10 minutes followed by centrifugation. The supernatant ethanol was removed. The precipitate was subjected to ethanol (1 mL) washings for two times and subsequently washed with 1 mL of Milli Q water. Finally, it was dispersed again in Milli Q water and used for next adsorption cycle. % Removal was calculated as,

$$\%\text{Removal} = \frac{(C_0 - C_e)}{C_0} \times 100 \qquad\qquad 2.2$$

2.4 Physicochemical Characterizations

FTIR spectra were obtained on Perkin Elmer Spectrum Two spectrophotometer in 4000-400 cm^{-1} range with a resolution of 4 cm^{-1}. The sample were thoroughly mixed with dried KBr (0.5 % wt/wt) and pressed into 13 mm diameter pellets at a pressure of 8 ton.cm^{-2}. UV-Visible spectra were recorded on a Carry 300 Conc UV-Visible spectrophotometer in quartz cuvette having path length of 10 mm. Photoluminescence was measured on a Carry eclipse fluorescence spectrophotometer with excitation and emission slit widths of 5 nm. Photoluminescence was measured in a quartz cuvette with path length of 10 nm at a resolution of 1 nm. Powder X-ray diffraction of all the mesoporous samples was carried out in a PANalytical X″pert Pro diffractometer with a proportional counter detector for low angle experiments. An X″celerator solid state detector was employed in the low angle experiments. The radiation source was Cu Kα (1.5418 Å) with a Ni filter and the data collection was

carried out with a flat holder in Bragg–Brentano geometry (0.5 to 10°; 0.2° min^{-1}). TEM images were taken on a FEI Technai T20 operating at a voltage of 200 kV. The samples were prepared by dispersing a 0.1 mg.mL^{-1} of nanoparticles in ethanol by sonication. The dispersion was drop casted on a carbon coated copper grid of 400 mesh and allowed to dry in air. Thermo gravimetric analysis (TGA) of the silica nanoparticles was carried out using a TA Instrument SDT Q600 analyzer between ambient and 800 °C in nitrogen atmosphere (flow 100 mL.min^{-1}) at a heating rate of 10 °C.min^{-1}. All samples were dried under vacuum at 60 °C overnight prior to the analysis. ^{29}Si and ^{13}C Cross Polarization Magic Angle Spinning (CPMAS) NMR experiments were carried out on a Bruker AVANCE 300 wide bore spectrometer equipped with a superconducting magnet with a field of 7.1Tesla. The RF-powers were 50 kHz and 60 kHz while contact times were 6ms and 3ms for the ^{29}Si and ^{13}C CPMAS experiments. All the chemical shifts were referenced to TMS. Nitrogen adsorption and desorption studies were carried out using Quadrasorb *SI* instrument. Before the nitrogen adsorption measurement, the samples were degassed overnight under vacuum using FloVac Degasser at 80 °C. Multi point BET surface area was obtained from adsorption isotherm from P/P0 0.01-0.1. Pore size distributions were calculated from adsorption isotherm using the BJH method.

2.5 Results and Discussion:

Our strategy for the preparation of amphi-functional MSNs involves stepwise functionalization as shown in Scheme 2.1. The MSNs were synthesized by previously reported procedure[29]. In the next step,the azide groups were covalently grafted on the particle surface using AzPTS. As the CTAB surfactant is still trapped in the pores of MSN particles, AzPTS gets preferentially attached on the outer surface to give the material designated as MSN@N$_3$ in Scheme 2.1. The surfactant was then removed by refluxing this material with HCl in methanol to obtain silica with free pores which will be referred to as m-MSN@N$_3$. This method was used instead of removing surfactant by commonly used calcination as the latter can lead to the removal of all the organic surface functionalities like propyl azide. After CTAB removal the exposed silanol groups in the pores were available for functionalization with hexamethyldisilazane (HMDS). Accordingly, the MSN@N$_3$ particles were then treated with HMDS where it preferentially reacts with free silanol groups in the pores[30]. This sequential functionalization strategy ultimately afforded CH$_3$-MSN@N$_3$ with hydrophilic surface and hydrophobic pores in the same particle. The material was thoroughly characterized with transmission electron microscopy (TEM), powder X-ray diffraction

(PXRD), FT-IR absorption spectroscopy, thermo gravimetric analysis (TGA) and cross polarization magic angle spinning (CP-MAS)solid state NMR.
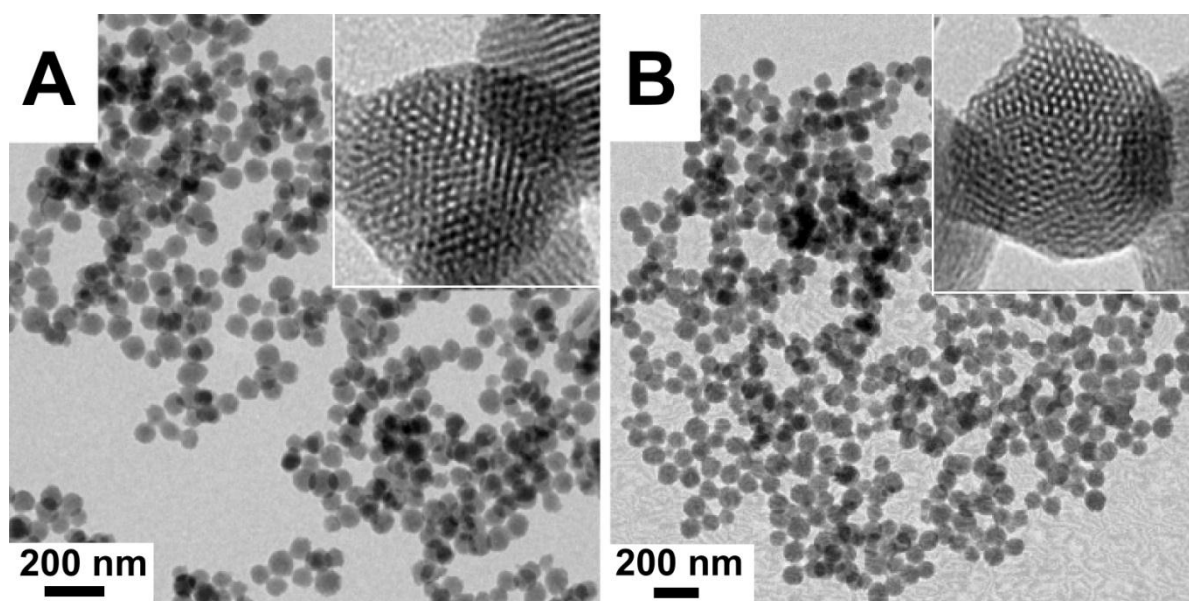
Figure 2.2 TEM images of A) as synthesized MSN and B) CH$_3$-MSN@N$_3$. Inset shows high resolution images.

To check the size, morphology and porosity of synthesized materials we carried out TEM analysis of samples. The TEM images revealed that as-synthesized MSN particles are spherical and porous with an average size of 80 nm. This is very useful size range as EPR effect is prominent below 100 nm. Presence of one dimensional ordered pores in these particles can be clearly seen in high resolution image (Figure 2.2 A, inset). The pore size measured from TEM for these particles was 1.3 nm. The size, morphology and pore structure were intact after the sequential functionalization (Fig.2.2 B). Retention of pore structure was also confirmed by low angle PXRD patterns of MSN (Fig.2.3 A) at various stages of functionalization. The characteristic (100) diffraction at 2θ = 2.2 º was observed for all samples[31]. Surface area and pore structure of the materials were analyzed by nitrogen adsorption studies (Figure 2.3 C and D). Both control and sample materials (i.e. m-MSN@N$_3$ and CH$_3$-MSN@N$_3$) showed type-IV adsorption isotherm characteristic for mesoporous materials[29]. The BET surface area of CH$_3$-MSN@N$_3$ decreased from 1117 m^2/g of m-MSN@N$_3$ to 987 m^2/g. The pore sizes were calculated from BJH method and shows very narrow size distribution. Mean pore size for m-MSN@N$_3$ and CH$_3$-MSN@N$_3$ are 3.14 & 3.07 nm. The pore volumes were also very similar in both samples i.e. 1.01and 0.99 cc/g for

m-MSN@N$_3$ and CH$_3$-MSN@N$_3$ respectively. These results confirm that the pore structure remained intact even after sequential functionalization.
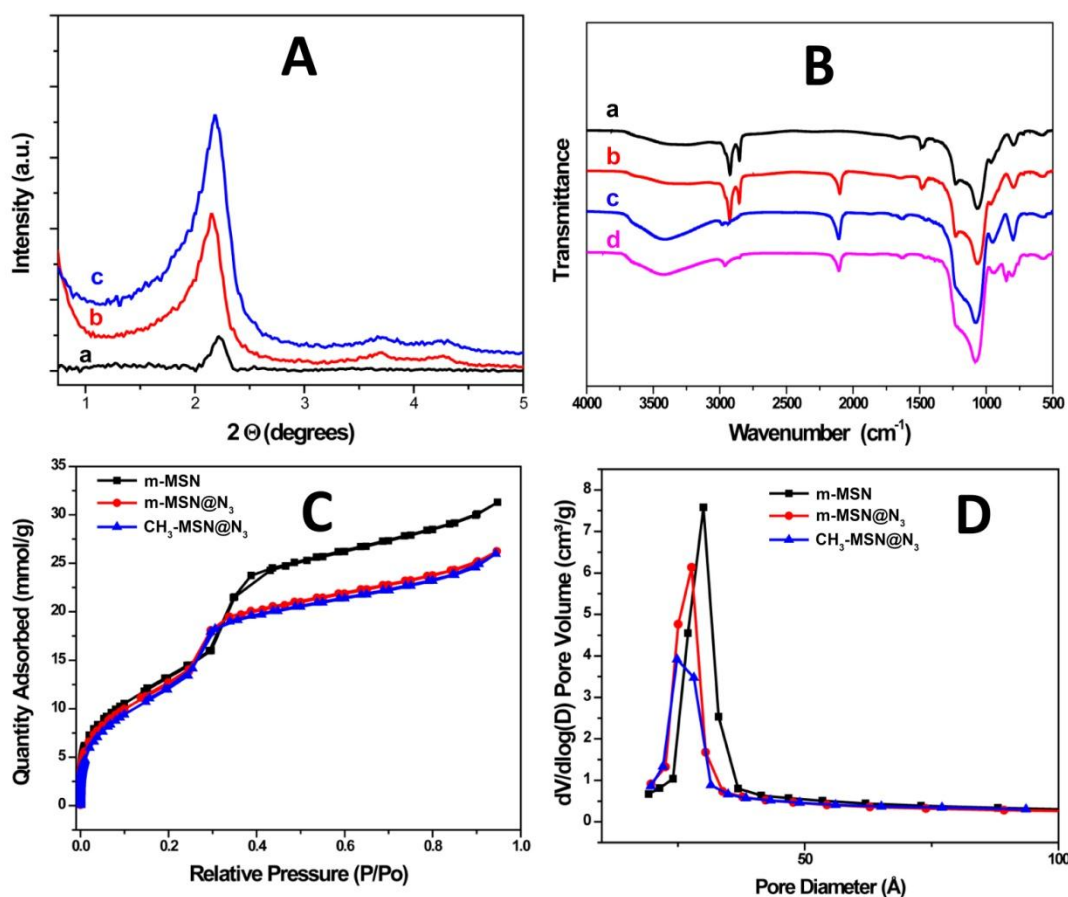
Figure 2.3 A) Low angle powder X-ray Diffraction pattern of various functionalized silica samples a) m-MSN b) m-MSN@N$_3$ c) CH$_3$-MSN@N$_3$ B) FT-IR spectrum of functionalized silica samples a) MSN b) MSN@N$_3$ c) m-MSN@N$_3$ d)CH$_3$-MSN@N$_3$ C) Surface analysis of functionalized silica by nitrogen adsorption-desorption A) Isotherms @77 K D) BJH pore size distribution

To check the covalent attachment of various functional groups with MSN, FTIR analysis was done. Figure 2.3 B shows FT-IR spectroscopy of functionalized silica at various stages. All samples show the characteristics of extended silica networks at 795, 945, 1075 and 1215 cm^{-1}. Notably, after treatment of AzPTS the silica samples have shown a strong absorption peak at 2100 cm^{-1} which is characteristic stretching vibration of organic azide groups. This suggests successful incorporation of azide groups into MSNs. This peak remains intact after further functionalization confirming the existence of azidopropyl groups in functionalized MSNs. There was no apparent reduction in the relative intensity of the azide peak after

extraction of the surfactant which suggests that the process is devoid of any ramifications on prior functionality. The stepwise functionalization was further confirmed and quantified by TGA measurements (Figure 2.4). Three stage weight losses have been observed in the regions–ambient to 130 °C, 200 to 400 °C and 400 to 650 °C. These can be correlated with the loss of surface adsorbed moisture, surfactant/propyl azide moieties and loss of trimethylsilyl functionality respectively[32]. The as synthesized MSNs were treated with a similar protocol to remove the surfactant and the product was labelled as m-MSN. This was used as the background to calculate the weight loss from only silica due to condensation of silanol groups. This m-MSN sample shows 2.87% and 3.08% weight losses in 200–400 °C and 400–650 °C regions respectively. These values were subtracted as background from functionalized MSNs for calculating the weight losses in these regions. After grafting of azidopropyl and removal of surfactant, m-MSN@N_3 showed 5.21% weight loss from 200 to 400 °C which can be attributed to only azidopropyl groups present on the surface. This corresponds to grafting of 0.27 mmol g^{-1} of azidopropyl groups. The sample after hydrophobization with HMDS i.e. CH_3-MSN@N_3 has shown a weight loss of 13.64% in the temperature range of 400– 650 °C. This can be attributed to the trimethylsilyl groups from the sample. After background correction, the grafting density of trimethylsilyl groups was found to be 1.42 mmol g^{-1}. After grafting of trimethylsilyl groups the surface adsorbed moisture was totally absent as seen from the TGA curve of CH_3-MSN@N_3, which does not show any weight loss up to 130 °C unlike the samples without hydrophobic functionality. The conclusive evidence of functionalization was provided by solid state NMR by the Cross Polarization Magic Angle Spinning (CP-MAS) technique. Figure 2.5 (I and II) show ^{29}Si and ^{13}C NMR spectra of solid samples respectively. The ^{13}C spectrum shows peaks at 6.42, 20.21, and 51.54 ppm corresponding to C1, C2 and C3 of the azidopropyl moiety[27]. In the case of the HMDS treated sample, one extra signal was observed in the shielded region at 2.59 ppm which can be assigned to the trimethylsilyl carbons. Trimethylsilyl functionalization of silica was also proved by ^{29}Si NMR. For only the HMDS treated sample a ^{29}Si signal at 12.71 ppm was observed which can be assigned to Si–$(CH3)3$. For both HMDS treated and control samples ^{29}Si signals were observed at 110.99, 102.24 and 93.25 ppm for Q4, Q3 and Q2 sites of Si in the SiO_2 network. Peaks at 67.41 and 59.20 ppm are assigned to R–Si–(O)3– and R–Si–OH–(O)2 respectively. The spectra were deconvoluted by fitting with the Gaussian function in Origin Pro 8.5 Software. The areas under the peak were used to quantify different Q species of silicon (Table 2.1). There was a decrease of 1.38 and 0.02% of Q3 and Q2 sites

respectively after treatment of HMDS with concomitant 1.4% increase in Q4 sites. These results suggest that the majority of HMDS functionalization occurs at Q3 sites.
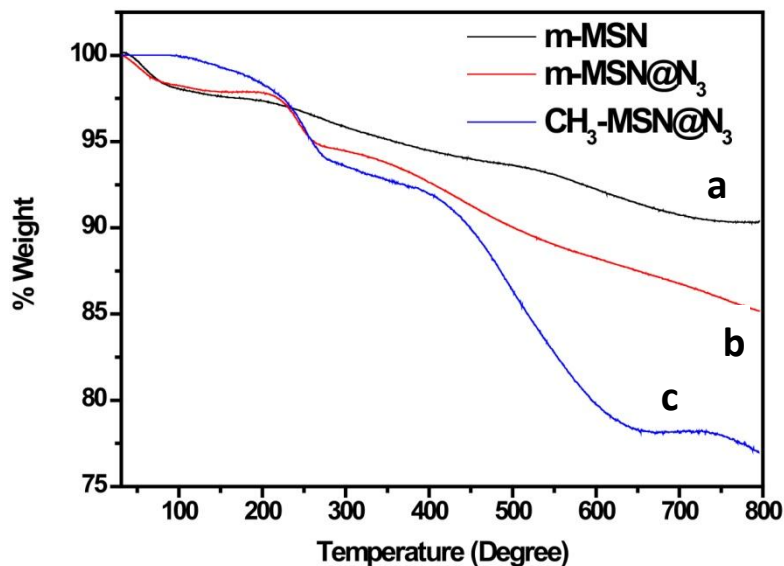
Figure 2.4 Thermo gravimetric analysis of silica samples performed under Nitrogen atmosphere. a) m-MSN b) m-MSN@N₃ c)CH₃-MSN@N₃
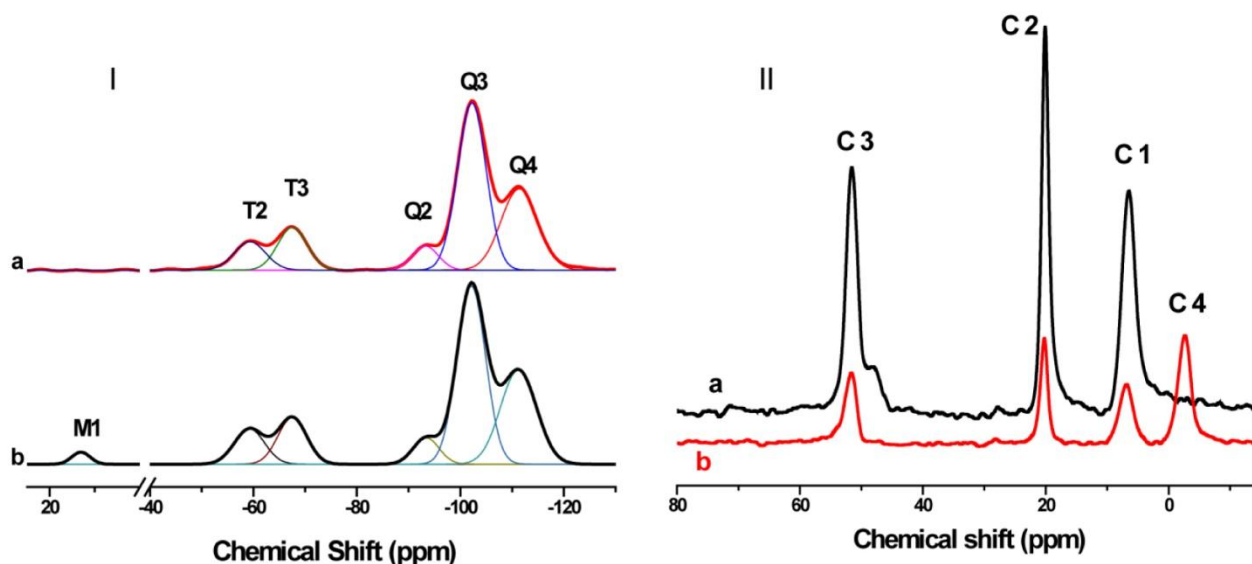
Figure 2.5 CP-MAS solid state NMR Spectra I) ^{29}Si nuclei with deconvulated peak fits and II) ^{13}C nuclei of a) m-MSN@N₃ and b) CH₃-MSN@N₃ respectively.

Table 2.1: Quantitative analysis of different types of Si species before and after functionalization with HMDS as deduced from ^{29}Si CP-MAS spectra

Sample Name	% of different Silicon Species			Change in % of different Silicon Species after Functionalization		
	Q4	Q3	Q2	Q4	Q3	Q2
m-MSN@N3	35.52	57.0	7.48	-	-	-
CH3-MSN@N3	36.92	55.62	7.46	+1.40	-1.38	-0.02
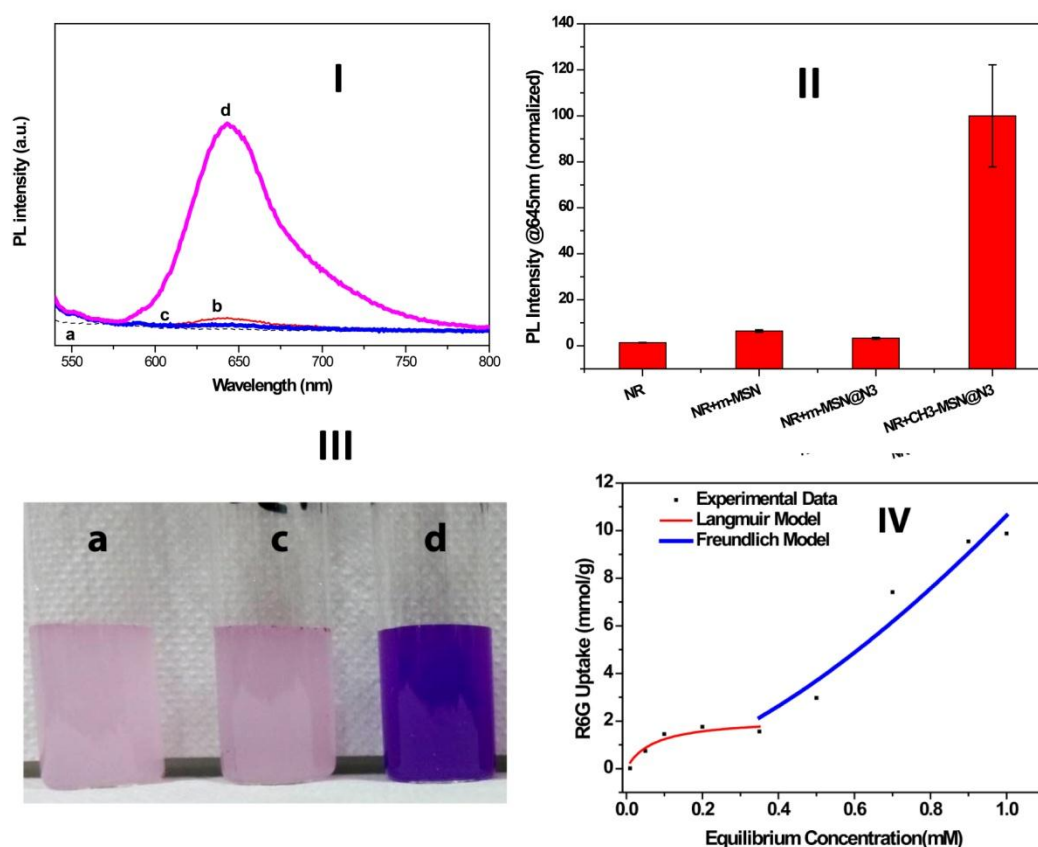
Figure 2.6 (I) PL spectra after incubating the hydrophobic dye with different MSN particles prepared (curve a) NR in water (curve b) NR in water incubated with m-MSN (curve c) NR in water incubated with m-MSN@N3 (curve d) NR in water incubated with CH3-MSN@N3 (II) Quantitative estimation of dispersing ability of different particles based on PL intensity (II) The actual photographs of the dye in water with different MSN particles (a) Pure dye in water, (c) NR in water incubated with m-

MSN@N$_3$ and (d) NR in water incubated with CH$_3$-MSN@N$_3$ (IV) Adsorption isotherm for R6G along with Langmuir & Freundlich models.

To ascertain the presence of hydrophobic compartments within the synthesized material it was tested by encapsulation of hydrophobic dye Nile Red (NR) as cargo. Figure 2.6 I a and 2.6 I b shows the emission spectra of NR in water without and with addition of pristine MSN respectively. Samples were excited at 530 nm and emission intensity at 633 nm was used for quantitative analysis. This dye when mixed with water undergoes severe aggregation. Consequently, NR in water showed negligible PL emission (Figure 2.6 I a). When the control sample i.e. with m-MSN@N$_3$ was added to this NR dispersed in water the PL emission intensity slightly increased (Figure 2.6 I, c). We attribute this to the non-specific adsorption of NR on m-MSN@N$_3$ particle surface. Quite gratifyingly, a dramatic increase in PL intensity was observed for the CH$_3$-MSN@N$_3$ particles (Figure 2.6 I, d) which suggested the substantial enhancement of NR dispersibility (without aggregation) in water. CH$_3$-MSN@N$_3$ assisted dispersion of NR can be further visualized by naked eyes (figure 2.6 III). Dye dispersing ability of CH$_3$-MSN@N$_3$ can be explained on the basis of the presence of hydrophobic pockets within pores which can sequester the hydrophobic NR into them and hence enhance their dispersion. This is akin to the addition of a "solvent" miscible with water and in which NR can dissolve. Furthermore, we have tried to quantify the hydrophobicity present in the material on Reichard's scale using solvatochromic property of NR[33]. The dye was incubated with functionalized particles (CH$_3$-MSN@N$_3$) as mentioned in the above experiment and the sample was centrifuged out of solution with encapsulated dye. The powder was dried and solid state UV-Vis spectrum was recorded. It shows absorption maxima at 547 nm corresponding to the transition energy of 52.27 kcal mol^{-1}. This closely matched to NR's transition energy when dissolved in 1-propanol.

After establishing the presence of hydrophobic compartments in CH$_3$-MSN@N$_3$ particles, we proceeded to study the adsorption capacity of the material using R6G. This dye has better solubility in water as compared to NR. Isotherms were obtained by measuring the uptake of R6G while varying the initial concentration of dye solution at room temperature. The contact time was 6 hours for all experiments. Figure 2.6 IV shows the experimental data as well as theoretical fitting using models for Langmuir and Freundlich. The data indicate that R6G shows very high adsorption capacity of 9.88 mmol/g with a two step adsorption isotherm feature[34]. We tried to fit the data into two sets with both Langmuir and Freundlich adsorption models. The first set in which R6G concentration is varied from 0.01 mM to 0.35mM fits

more closely with Langmuir adsorption model ($R^2 =0.868$) suggesting monolayer adsorption. But, at higher concentrations the adsorption follows Freundlich model of multilayer adsorption.
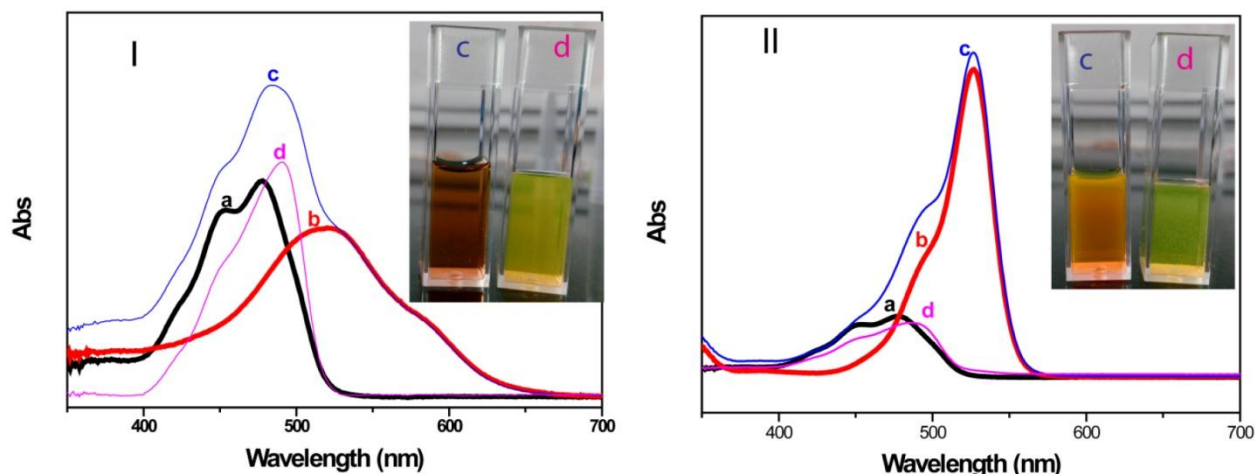
Figure 2.7 UV-Visible spectra for separation dual dye mixtures I) R6G & CA B) MB17 & CA. The photographs shown in insets are c) dye mixture and d) supernatant after incubating with CH₃-MSN@N₃ particles respectively.

Finally to prove the amphi functional nature of the CH3-MSN@N3 particles we tested their capability to separate the dyes from a mixture. Here again we used dyes that have appreciable solubility in water. If the uptake is driven by hydrophobic-hydrophobic interactions then our amphi functional MSN should be able to show more uptake of a relatively more hydrophobic dye from a mixture of two dyes. The dyes selected for the study were Rhodamine 6G (R6G) and Mordant Black 17 (MB17). These belong to cationic and anionic forms respectively. R6G and MB17 are soluble in water as well as few other polar solvents. For comparison, we also mixed these with a highly hydrophilic dye calcein (CA). In the actual experiment, CA was individually mixed with R6G and MB17 and the resultant mixtures were incubated with functionalized particles for 6 hours. The particles were then separated by centrifugation. Figure 2.7 (I and II) show the UV-Vis absorption results of these separation experiments. It may be noticed that in the both cases after centrifugation, supernatant was mostly composed of CA. This indicates that the R6G and MB17 were preferentially and completely separated from their respective binary mixtures with CA. We wish to emphasize that CA is highly

hydrophilic to the extent that it only dissolves in water unlike R6G and MB17 which are soluble in less polar solvents like ethanol as well. We deduce that both R6G and MB17 get preferentially partitioned into the pores of CH_3-MSN@N_3 particles due to the strong hydrophobic interactions. Hydrophobic molecules when put into water undergo aggregation due to the stronger mutual attraction between them and also their poor solvation by water due to many reasons including entropic considerations[35]. On the other hand in case of non-polar solvents, the solvation energy becomes much higher than intermolecular cohesive energy hence making them dissolved. Consequently, such molecules partition into hydrophobic pores of different materials like carbon[36] and also cavities of coacervates of assembled polymers[37]. The methylated silica surface in the present case offers favourable environment leading to the loading of the dye into the pores of the particles. We also carried out an interesting experiment where the CH_3- MSN@N_3 particles were incubated with the mixture of NR with R6G or MB17. In this case the results hint that NR (the more hydrophobic dye) is more selectively sequestered into the CH_3- MSN@N_3 particles. We hasten to add here that these results are only qualitative and we could not determine the extent of sequestration in this case due to experimental issues. Nevertheless, our results allow us to conclude that there is a clear distinction between the material presented here from other materials where dye separation was mainly achieved by specific binding with either metal or electrostatic interactions[24,38-40].
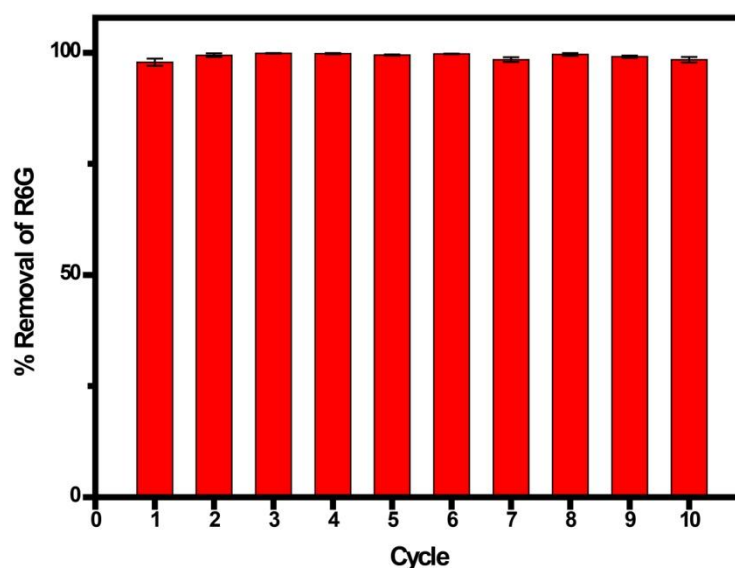
Figure 2.8 Quantitative data for recycling of adsorbent (CH_3-MSN@N_3) for removing R6G dye from water

This kind of material can also be used in water purifiying applications as well. Moreover, for use in such practical applications, the recyclability of the sorbent material is of paramount importance. Thus we tested the same for the removal of R6G from a 0.1 mM solution in water. The sorbent has shown 99% removal of the dye which was consistent for 10 minimum consecutive cycles (Figure 2.8). Most importantly, in the present case the recovery of the adsorbed dye and the regeneration of the sorbent are very easy as they only require a simple washing with ethanol. The washings can be collected and processed to retrieve the adsorbed moiety.

2.6 Summary and Conclusion:

In conclusion, amphi-functional mesoporous silica nanoparticles were synthesized by stepwise chemical modification approach. This has hydrophobically functionalized pores by TMS groups and hydrophillically functionalized outer surface with azide groups. The presence of hydrophobic pockets created by trimethylsilyl groups inside the pores has been indirectly demonstrated by NR encapsulation. The wide applicability of this strategy is proven with various dyes (cationic and anionic). This selectively functionalized silica material can specifically adsorb and remove a dye from binary mixtures depending predominantly upon the hydrophobic-hydrophobic interactions between adsorbate and adsorbent. Thus, in this chapter we have successfully demonstrated the importance and effect of appropriate surface functionalization. This material and strategy has been used to build the advanced theranostic system in the later parts of this thesis.

2.7 References

(1)   Langer, R. *Science* **1990**, *249*, 1527.

(2)   Prausnitz, M. R.; Langer, R. *Nat. Biotechnol.* **2008**, *26*, 1261.

(3)   Abdalla, A. M.; Xiao, L.; Ullah, M. W.; Yu, M.; Ouyang, C.; Yang, G. *Theranostics* **2018**, *8*, 533.

(4)   Al-Jamal, W. T.; Kostarelos, K. *Acc. Chem. Res.* **2011**, *44*, 1094.

(5)   Kashyap, S.; Jayakannan, M. *J. Mater. Chem. B* **2015**, *3*, 1957.

(6)   Kashyap, S.; Singh, N.; Surnar, B.; Jayakannan, M. *Biomacromolecules* **2016**, *17*, 384.

(7)   Sun, X.; Liu, Z.; Welsher, K.; Robinson, J. T.; Goodwin, A.; Zaric, S.; Dai, H. *Nano Res.* **2008**, *1*, 203.

(8)   Cale, D. F.; Mallinath, H.; King, S. B.; Suzy, V. T.; Ravi, S. *Nanomedicine* **2015**, *10*, 2481.

(9)   Ghosh, P.; Han, G.; De, M.; Kim, C. K.; Rotello, V. M. *Adv. Drug Deliv. Rev.* **2008**, *60*, 1307.

(10)   Slowing, I. I.; Trewyn, B. G.; Giri, S.; Lin, V. Y. *Adv. Funct. Mater.* **2007**, *17*, 1225.

(11)   Brown, S. D.; Nativo, P.; Smith, J.-A.; Stirling, D.; Edwards, P. R.; Venugopal, B.; Flint, D. J.; Plumb, J. A.; Graham, D.; Wheate, N. J. *J. Am. Chem. Soc.* **2010**, *132*, 4678.

(12)   Vinu, A.; Hossain, K. Z.; Ariga, K. *J. Nanosci. Nanotech.* **2005**, *5*, 347.

(13)   Slowing, I. I.; Vivero-Escoto, J. L.; Wu, C.-W.; Lin, V. S. Y. *Adv. Drug Deliv. Rev.* **2008**, *60*, 1278.

(14)   Li, Z.; Barnes, J. C.; Bosoy, A.; Stoddart, J. F.; Zink, J. I. *Chem. Soc. Rev.* **2012**, *41*, 2590.

(15)   Rosenholm, J. M.; Sahlgren, C.; Linden, M. *Nanoscale* **2010**, *2*, 1870.

(16)   Moeller, K.; Bein, T. *Chem. Mater.* **2017**, *29*, 371.

(17)   Tarn, D.; Ashley, C. E.; Xue, M.; Carnes, E. C.; Zink, J. I.; Brinker, C. J. *Acc. Chem. Res.* **2013**, *46*, 792.

(18)   Fangqiong, T.; Linlin, L.; Dong, C. *Adv. Mater.* **2012**, *24*, 1504.

(19)   Szegedi, A.; Popova, M.; Goshev, I.; Mihály, J. *J. Solid State Chem.* **2011**, *184*, 1201.

(20)   M., R. J.; Emilia, P.; Tabe, B. E. L.; E., E. J.; Cecilia, S.; Mika, L. *Small* **2010**, *6*, 1234.

(21)   Song, S. W.; Hidajat, K.; Kawi, S. *Langmuir* **2005**, *21*, 9568.

(22)   Kim, M. S.; Jeon, J. B.; Chang, J. Y. *Microporous and Mesoporous Mater.* **2013**, *172*, 118.

(23)   Chia-Hung, L.; Leu-Wei, L.; Chung-Yuan, M.; Chung-Shi, Y. *Adv. Funct. Mater.* **2008**, *18*, 3283.

(24)   Ho, K. Y.; McKay, G.; Yeung, K. L. *Langmuir* **2003**, *19*, 3019.

(25)   Sarkar, C.; Bora, C.; Dolui, S. K. *Ind. Eng. Chem. Res.* **2014**, *53*, 16148.

(26)   Jie, L.; Monty, L.; I., Z. J.; Fuyuhiko, T. *Small* **2007**, *3*, 1341.

(27)   Malvi, B.; Sarkar, B. R.; Pati, D.; Mathew, R.; Ajithkumar, T. G.; Gupta, S. S. *J. Mater. Chem.* **2009**, *19*, 1409.

(28)   Kar, M.; Vijayakumar, P. S.; Prasad, B. L. V.; Gupta, S. S. *Langmuir* **2010**, *26*, 5772.

(29)   Ganai, A. K.; Kumari, S.; Sharma, K. P.; Panda, C.; Kumaraswamy, G.; Gupta, S. S. *Chem. Commun.* **2012**, *48*, 5292.

(30)   Suratwala, T. I.; Hanna, M. L.; Miller, E. L.; Whitman, P. K.; Thomas, I. M.; Ehrmann, P. R.; Maxwell, R. S.; Burnham, A. K. *J. Non-Cryst. Solids* **2003**, *316*, 349.

(31)   Gusev, V. Y.; Feng, X.; Bu, Z.; Haller, G. L.; O'Brien, J. A. *J. Phys. Chem.* **1996**, *100*, 1985.

(32)   Popat, A.; Ross, B. P.; Liu, J.; Jambhrunkar, S.; Kleitz, F.; Qiao, S. Z. *Angew. Chem. Int. Ed.* **2012**, *51*, 12486.

(33)   Reichardt, C. *Chem. Rev.* **1994**, *94*, 2319.

(34)   Rouquerol, F.; Rouquerol, J.; Sing, K. *Adsorption by Powders & Porous   Solids*; Academic Press, London, **1999**.

(35)   Israelachvili, J. N. *Intermolecular and surface forces*; Academic Press, Burlington, 2011.

(36)   Fang, Y.; Gu, D.; Zou, Y.; Wu, Z.; Li, F.; Che, R.; Deng, Y.; Tu, B.; Zhao, D. *Angew. Chem. Int. Ed.* **2010**, *49*, 7987.

(37)   Zhao, M.; Eghtesadi, S. A.; Dawadi, M. B.; Wang, C.; Huang, S.; Seymore, A. E.; Vogt, B. D.; Modarelli, D. A.; Liu, T.; Zacharia, N. S. *Macromolecules* **2017**, *50*, 3818.

(38)   Karan, C. K.; Bhattacharjee, M. *ACS Appl. Mater. Interfaces* **2016**, *8*, 5526.

(39)   Sasmal, A. K.; Pal, J.; Sahoo, R.; Kartikeya, P.; Dutta, S.; Pal, T. *J. Phys. Chem. C* **2016**, *120*, 21580.

(40)   Zare, K.; Gupta, V. K.; Moradi, O.; Makhlouf, A. S. H.; Sillanpaa, M.; Nadagouda, M. N.; Sadegh, H.; Shahryari-ghoshekandi, R.; Pal, A.; Wang, Z.-j.; Tyagi, I.; Kazemi, M. *J. Nanostruct. Chem.* **2015**, *5*, 227.

Chapter III:

Regulation of Dye/drug Uptake/release by Outer Surface Modification and Molecular Gating

3.1 Introduction

In our quest to design better theranostic system, we have shown how a delivery vehicle can be optimized for drug loading in the previous chapter. In that work we have mainly focused on the functionalization of pores for better loading of the hydrophobic dyes/drugs. In contrast to the earlier reports we have exploited the hydrophobic-hydrophobic attractive forces to load the dye/drug into these pores. Such systems are quite rarely utilized in this area. Our next objective in the direction of making a better theranostic system was to impart the outer surface functionalization to the MSN surface so that it becomes stable in circulation as well as biocompatible. It should be noted that this has to be achieved without jeopardizing the earlier optimized properties. The cargo loaded has to be protected for degradation as well as premature release. In literature, several approaches to make the surface of drug delivery systems, especially those containing the inorganic core, hydrophilic as well as biocompatible have been described[1-2]. Most notable examples include use of peptides[3], carbohydrates[4], proteins[5], antibodies[6], supramolecular complexes[7] as well as other non-biogenic macromolecules[8]. One of the most commonly utilized molecules for such purpose is poly-ethylene glycol (PEG)[9-10]. PEG has been the most preferred choice due to its easy availability in wide range of molecular weights and inexpensiveness. The tail ends of PEG chains can be modified using conventional chemistry to introduce a plethora of functional groups[11-12]. The tenability in the chain length has led its use in synthesis of many biocompatible linker molecules to attach other targeting moieties[13].

In this chapter we have attempted to functionalize the outer surface of the amphi-functional MSN by PEG. Furthermore, we have also tried to rationalize the role of outer surface functionalization on the uptake of drug/dye molecules in this kind of systems. To study that systematically, we decided to modify the outer surface of MSN with various molecules such as of propargyl alcohol and triethylene glycol apart from PEG. These molecules are similar to PEG in functionality but have different chain lengths. This methodology as we reasoned; would allow us to systematically study the effect of molecular size of the surface functionalized moieties on the uptake of various cargos. We also wanted to answer yet another important question here: does the method of loading play any role? For example, Scheme 3.1 shows two different approaches for loading of drug molecules in a vehicle. These can be summarized briefly as loading the drug/dye after the outer surface has been modified (Scheme 3.1 Path A) or loading the drug/dye first and then modifying the outer surface in a desired fashion (Scheme 3.1 Path B). Our literature search indicated that the former one is the

most practiced method[14]. In delivery vehicles like ours the major surface area for loading lies in the pores[15] and we have modified it so that hydrophobic molecules can be loaded into them. In this morphology we speculated the loading the drug/dye after the outer surface functionalization as is being routinely practiced as described in Scheme 3.1 Path A would not result in highest uptake. To ascertain that our contention is true and to ensure higher uptake, we propose a slightly different approach as shown in the scheme 3.1 Path B. In this chapter we tried to load different molecules into amphi-functionalized MSNs by these two different approaches and compare the uptake. We will also try to understand the effect of different surface functional group on uptake as well as release process.
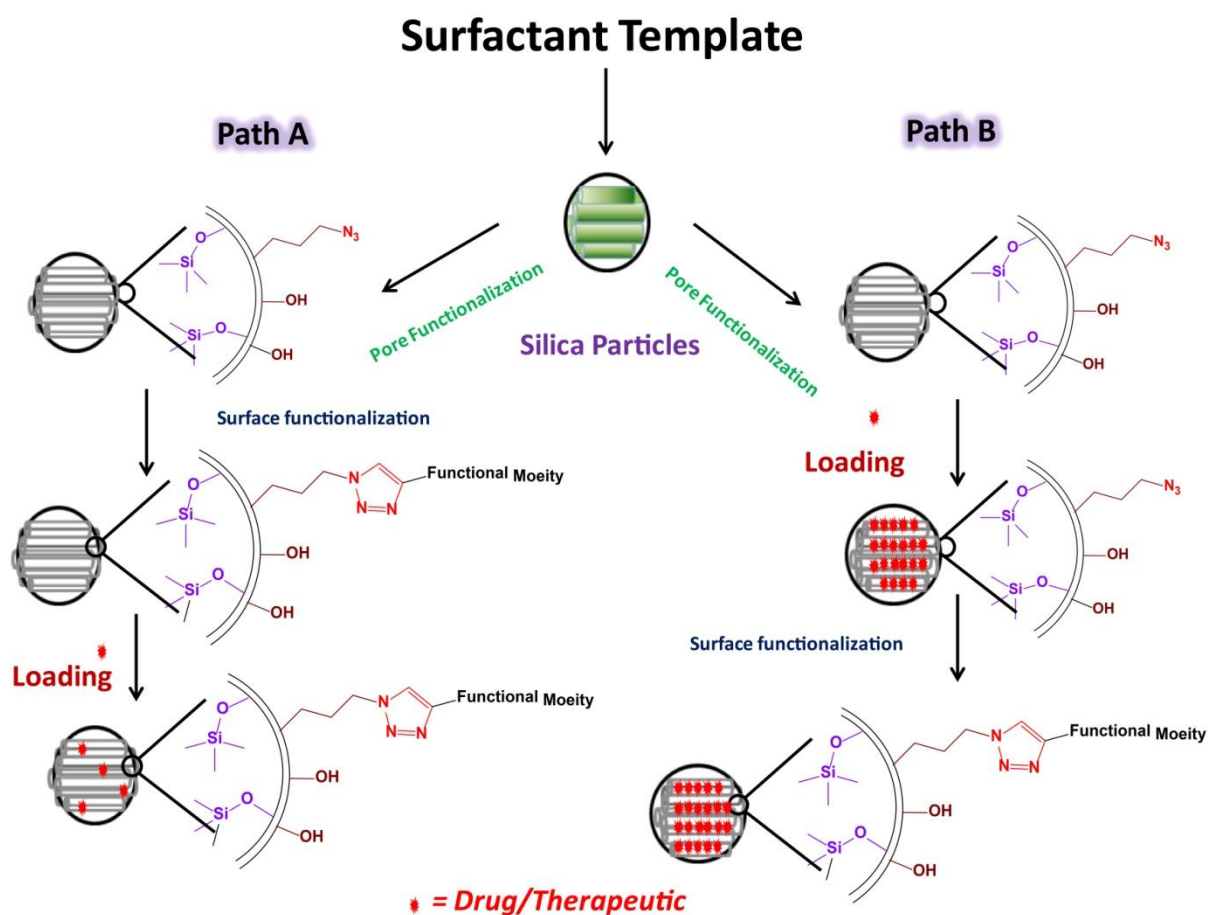
Scheme 3.1 Methods of drug loading conventional vs. our proposed method

3.2 Experimental Section

3.2.1 Materials:

Tetraethyl orthosilicate (TEOS), sodium hydroxide, hexadecyl trimethyl ammonium bromide (CTAB), 3-chloropropyl triethoxy silane, hexamethyl disilazane (HMDS), tert-butyl ammonium bromide, nile red (NR), rhodamine 6G (R6G), propargyl bromide(80%), PEG (2000) monomethyl ether, triethylene glycol monoethyl ether (TEG), sodium hydride (NaH), EDTA-disodium salt and were purchased from sigma aldrich. Sodium azide, ethyl acetate, ethanol, methanol, n-hexane, dry toluene, dry dichloro methane, cupric chloride pentahydrate $(CuCl_2.5H_2O)$ dimethyl sulphoxide and concentrated hydrochloric acid were obtained from Merck India. Sodium ascorbate and propargyl alcohol were purchased from fluka. All of them were used without further purification. Azidopropyl triethoxysilane (AzPTS)[16] and tris (3-hydroxypropyltriazolylmethyl) amine (THPTA)[17] were prepared and purified from previously reported protocols. Milli Q water was used for all experiments.

3.2.2 Synthesis

3.2.2.1 Synthesis of alkyne functionalized poly ethylene glycols (PEG-alkyne) and triethylene glycol (TEG-alkyne)

In a dry round bottom flask, 0.240 g (6 mmoles) of sodium hydride was taken under argon atmosphere. 50 mL of anhydrous tetrahydrofuran (THF) was added and the flask was cooled in ice bath. 0.873 mL of TEG or 10 g PEG ether (5 mmoles) was then added drop wise by syringe under inert atmosphere. The reaction mixture was stirred magnetically at 0 °C for 1 h. 0.67 mL (6 mmoles) of propargyl bromide was then added drop wise. The mixture was brought to ambient temperature and allowed to react for 7 h. finally the reaction was quenched by adding few drops of ethyl acetate.The solvent was removed under reduced pressure and residue was dissolved in 50 mL of anhydrous acetonitrile. The product was precipitated by adding 50 mL n-hexane and cooling at -18 °C overnight. The mixture was filtered through Whatmann paper no.1 and precipitate was collected and dried in vacuum to obtain pure products with practical yields of ~ 80%. The alkynylated products were referred as triethylene glycol-alkyne (TEG-alk) and polyethylene glycol-alkyne (PEG-alk) respectively.
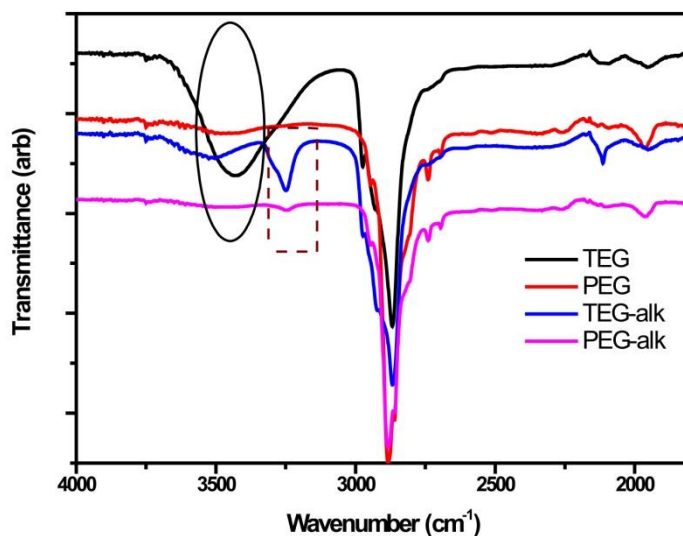
Figure 3.1 FT-IR spectra of TEG and PEG before and after functionalization with propargyl groups.

Monoether functionalized PEG and TEG were modified by propargyl group through well known chemical modification protocol. Here each chain contains one hydroxyl group which was then functionalizes with propargyl group using propargyl bromide reagent and sodium hydride as base. The FT-IR spectra of these different molecules shown in figure 3.1. A broad peak centered around 3450 and 3425 cm^{-1} is observed in IR spectra of TEG and PEG. This is attributed to the O-H stretching vibtration of terminal hydroxyl group of mono ether molecules. After the reaction with propargyl bromide a sharp peak is observed at 3250 cm^{-1} in both TEG-alk and PEG-alk samples which is characteristic frequency of acetylinic C-H stretching vibrations. Along with this a sharp C-C tripple bond stretching vibrational peak is also observed at 2110 cm^{-1} in TEG-alk sample. This clearly suggests the incorporation of propargyl functionality by reaction with terminal hydroxyl group.

The NMR analysis also confirms the same. The NMR signal for various samples are mentioned below-

PEG: CDCl$_3$ 3.62 ppm (s, 178 H) and 3.36 ppm (s, 3H); **PEG-alk**: CDCl$_3$ 4.2 ppm (d, 2H), 3.69 ppm (s, 179 H) and 3.38 ppm (s, 3H); **TEG**: CDCl$_3$ 3.67 ppm (m, 14H), 2.75 ppm (s broad, 1H) and 1.20 ppm (t, 3H); **TEG-alk**: CDCl$_3$ 4.15 ppm (d, 2H), 3.52 ppm (m, 14H), 3.34 ppm (s, 1H) and 1.11 ppm (t, 3H).

From ^{1}H NMR spectra it is clearly observed that there is an emergence of propargyl methylene peaks in the range of 4.1-4.2 ppm for both TEG-alk and PEG-alk samples. In TEG sample the signal for O-H proton vanishes and acetylene proton appears at 3.34 ppm. These results clearly indicate the alkynylation of TEG and PEG to yeild TEG-alk and PEG-alk respectively.
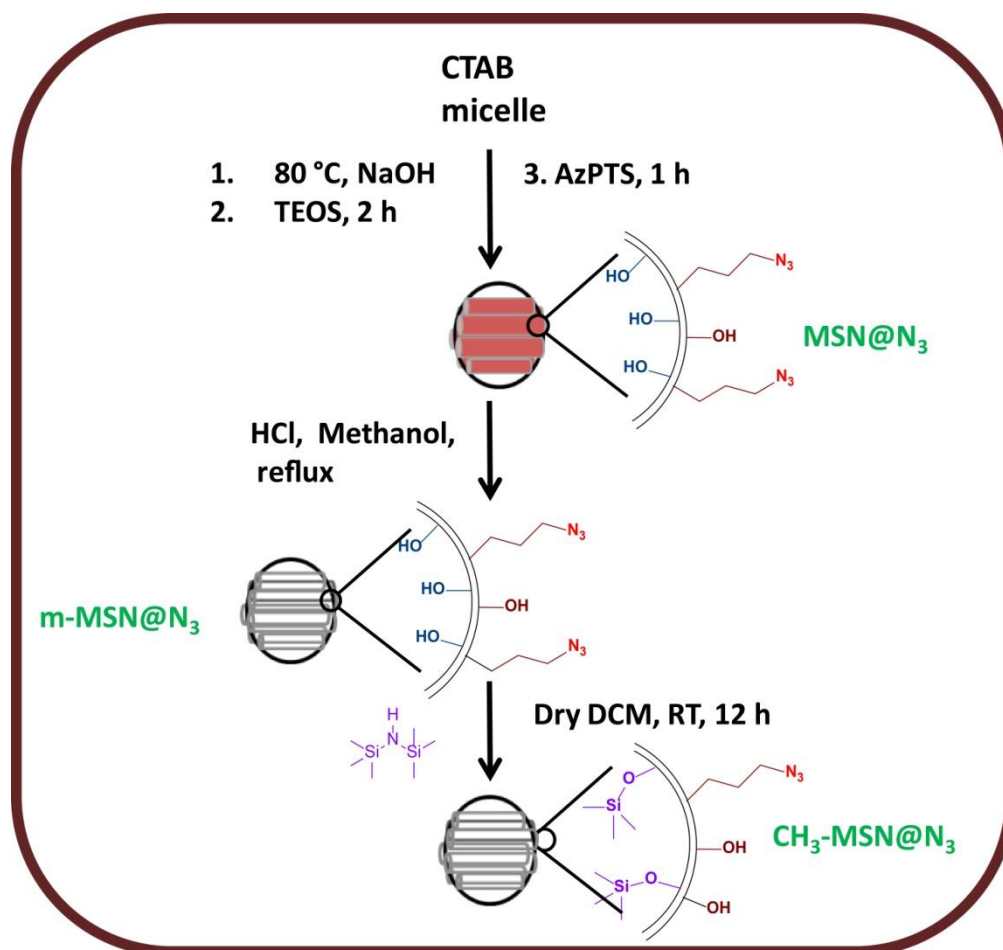
Scheme 3.2 Synthesis of amphi-functional MSN

3.2.2.2 Synthesis of selectively functionalized MSN

Scheme 3.2 briefly illustrates the methodology used for synthesis of selectively functionalized mesoporous silica nanoparticles. Here we modified the protocol reported in chapter II (section 2.3.2.1) where in the first two steps i.e. synthesis of MSN and grafting of AzPTS was condensed by using a co-condensation approach. 1.0 g of CTAB (0.0027 mol) was dissolved in 480 mL of water in a jacketed reaction flask and heated to 80 °C with

constant stirring using overhead stirrer for 30 minutes. 3.5 mL of 2 M NaOH was added into above mixture followed by drop wise addition of 5.0 mL of TEOS (22.3 mmol). The reaction was stirred for 2 hours at 80 °C after which 0.25 mL of AzPTS (1.0 mmoles) was added sequentially with an interval of 15 minutes (total of 0.75 mL; 3.0 mmoles). The reaction was allowed to proceed for another 1 h after last addition. It was immediately filtered through Whatman no. 1 filter paper and washed with copious amount of water to remove excess alkali (till filtrate became neutral to litmus). Finally the product was washed with 100 mL of ethanol and aged at 80 °C for 12 hours. This sample termed as MSN@N_3. Yield ~ 2.1 g.

This product was then dispersed in 100 mL methanol and acidified with 2 mL of concentrated HCl. Azide grafted particles were refluxed in methanol for 6 hours to remove CTAB after which it was centrifuged at 20000 rpm for 20 min and the supernatant containing acidic methanol was discarded. It was again dispersed in 100 mL fresh methanol and refluxed for another 24 hours. It was then subjected to centrifuge and purified by washing for three times as mentioned above. Finally the precipitate was dried in vacuum oven at 80 °C. Yield ~ 1.1 g. this sample was labelled as m-MSN@N_3.

For functionalization of mesoporous pores by hydrophobic functionality; 0.5 g of m-MSN@N_3 was dispersed in 50 mL of anhydrous dichloro methane under dry and inert atmosphere. 0.150 mL (1.2 mmol) of hexamethyl disilazane (HMDS) was injected while stirring at room temperature. After 24 hours of reaction, the product was isolated by centrifugation at 20000 rpm for 20 minutes and washed with ethanol three times similar to previous experiment. Finally the precipitate was dried in a vacuum oven for 12 hrs @ 80 °C. The material was labelled as CH_3-MSN@N_3, yield ~ 0.430 g.

3.2.2.3 Synthesis of functionalized SBA and KCC materials

SBA-15 and KCC-1 silica materials were supplied by Prof. Vivek Polshettiwar's (TIFR, Mumbai) group. These were synthesized using previously reported protocols[18-19].

For surface grafting azide groups; 1.5 g of SBA-15 or KCC-1 dispersed in 100 mL dry toluene under nitrogen atmosphere. The reaction flasks were heated to attain 80 °C followed by slow addition of 0.75 mL (3.0 mmol) of AzPTS. The mixture was allowed to react at 80 °C under nitrogen atmosphere for 12 hours and then cooled to ambient temperature. The product was separated by centrifuge at 20000 rpm for 20 minutes. The separated products were washed with ethanol three times. All the supernatants after centrifuge were discarded. At this stage products were labelled as SBA@N_3 and KCC@N_3 respectively.

For removal of CTAB from pores and grafting trimethylsilyl functional groups by treatment with HMDS; protocols described in above section 3.2.2.2 were followed. Final products were labelled as CH_3-SBA@N_3 and CH_3-KCC@N_3.
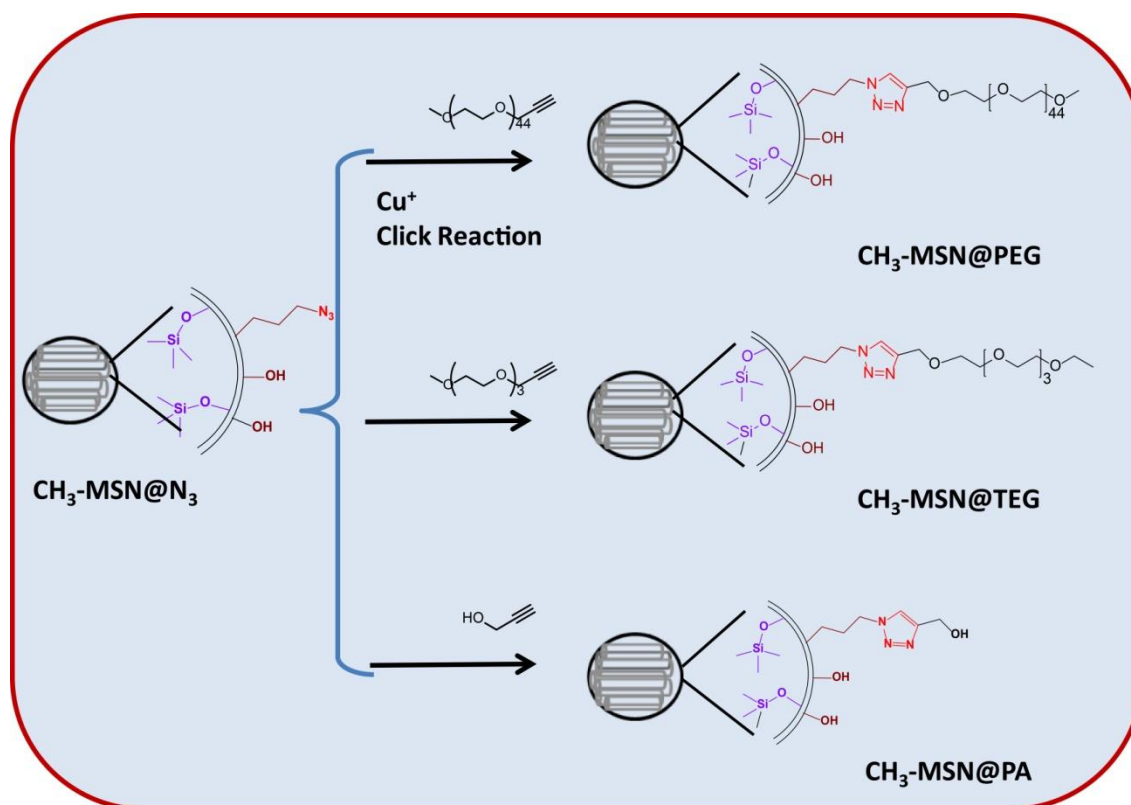
Scheme 3.3 Surface modification of amphi-functional MSN by click reactions with various alkynes

3.2.2.4 Synthesis of various functionalized silica with click chemistry

The reactions are schematically shown in scheme 3.3. In a typical reaction 0.2 g (0.194 mmol of azide) of amphi-functional silica material CH_3-MSN@N_3, CH_3-SBA@N_3 and CH_3-KCC@N_3 were taken in a separate two neck round bottom flasks to which 0.77 g of sodium ascorbate (3.88 mmol) and 0.253 g(0.582 mmol) of THPTA were added. For different functionalization of CH_3-MSN-N_3 different alkyne moieties were added such as, 0.033 mL (0.582 mmol) of propargyl alcohol (PA), 0.126 mL (0.582 mmol) of triethylene glycol-alkyne (TEG-alk) and 1.18 g (0.582 mmol) of polyethylene glycol-alkyne (PEG-alk) in separate flasks. For CH_3-SBA@N_3 and CH_3-KCC@N_3 materials only PEG-alk was used. 10 mL of milli Q water was added to each flask followed by sonication for about 15 minutes to

homogenize the reaction mixture. The flasks were then flushed with nitrogen and kept under nitrogen atmosphere. 1.0 mL (16 mg; 0.097 mmol) of aqueous cupric chloride solution (16 mg/mL) was injected into each of the reaction mixture through rubber septum. The reaction mixtures were stirred at room temperature under nitrogen for 48 hours.

After reaction the products were separated by centrifuge @ 20000 rpm for 20 minutes. The products were thoroughly washed with 10 mL of water (3 times), 5 mL of 0.1M aqueous EDTA solution, 10 mL of water (2 times) and finally with 10 mL of acetone. The washed products were dried in vacuum oven at 80 °C for 12 hours.

3.2.2.5 Preparation of proflavine free base from proflavine hydrochloride

The commercially availabe proflavine is in the form of mono hydrochloride salt. As we are using a hydrophobic vehicle, we envisioned that loading free base form of proflavine which willbe more hydrophobic than its salt form; can result in enhanced loading. The neutralization was performed in the following way (Scheme 3.4). 1.0 g (4.07 mmol) of proflavine hydrochloride was taken in a round bottom flask and was dissolved in 100 mL methanol and cooled to 0 °C in an ice bath. 0.854 g (10.0 mmol) of solid sodium bicarbonate was added slowly. The reaction mixture was brought to ambient temperature and stirred for 1 hour. The mixture was then filtered through Whatmann no.1 to remove unreacted bicarbonate and the filtrate was evaporated to dryness. The solid product was further purified by re-crystallization from methanol and dried under vacuum oven to remove traces of methanol. Practical yield obtained was 90%.
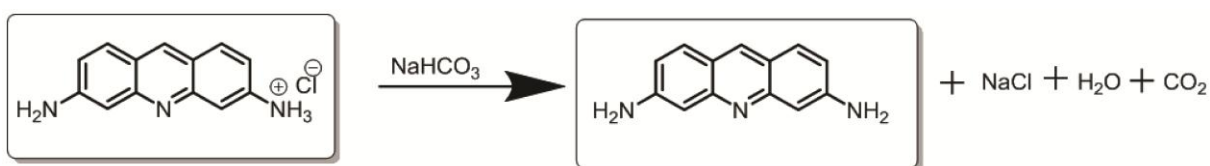
Scheme 3.4 Neutralization of proflavine hydrochloride to free base

The sucess of neutralization was confirmed from proton NMR of salt and product.

[1]H of Proflavine hydrochloride

DMSO: 8.71ppm (s, 1H), 7.79 ppm (d, 2H), 7.27 ppm (s, 5H), 6.95 ppm (dd, 2H) and 6.75 ppm (s, 2H)

^{1}H of Proflavine hydrochloride

DMSO: 8.60 ppm (s, 1H), 7.74 ppm (d, 2H), 6.90 ppm (m, 6H) and 6.78 ppm(s, 2H)

Mass spectrometry (LCMS) m/z : 210

The hydrochloride salt shows total of 12 protons while neutralized base shows signal for 11 protons. The 5 protons for protonated and free amine group appear at 7.79 ppm in salt. After removal of acidic proton the 4 amine proton apear at much sheilded region and overlap with a signal from acridine ring protons showing a multiplet at 6.90 ppm. The effect of availability of both lone pairs from amine nitrogen are evident in almost every signal of free base causing upfield shifts.

3.2.2.6 Comparative study of loading efficiency of proflavine hydrochloride and proflavine free base

The loading capacity of proflavine hydrochloride or proflavine free base was calculated by mixing their solutions with aqueous dispersion of CH$_3$-MSN@N$_3$ independently. The final concentration of particles and drugs were 10 mg/mL and 0.9 mM respectively in a volume of 0.5 mL. The mixture in eppendorf tubes were then mixed thoroughly by rotating for 12 hours at 30 RPM on a tarson rotospin. The tubes were then subjected to centrifuge to isolate the silica particles and the supernatants were then analyzed by UV-Vis spectroscopy. The amount of adsorbed drug was calculated by using following formula.

$$q_t = \frac{(C_0 - C_e)V}{W}$$ 3.1

Where, q_t is adsorption capacity (mmol.g^{-1}), C_0 & C_e are initial and equilibrium concentration (mmol.dm^{-3}) of dyes after sorption respectively, V is volume of solution (dm^3) and W is mass of sorbent (g).

3.2.2.7 Loading of proflavine free base in the various functionalized MSN

0.5 g of CH$_3$-MSN@N$_3$ sample was dispersed in 1.0 mM solution of proflavine free base. The dispersion was subjected to sonication for 30 minutes and mixed on a tarson rotospin for 12 hours. The supernatant was removed by decantation and precipitate was gently washed with 10 mL of water 3 times to remove non adsorbed drug.

In case of various functionalized silica materials such as CH$_3$-MSN@PA, CH$_3$-MSN@TEG and CH$_3$-MSN@PEG; 0.05 g of materials were dispersed in 1.5 mL of 1.0 mM proflavine. The incubation and washings were performed similarly as above. The amount of proflavine

remaining in supernatant and the washings was measured by UV-Vis spectroscopy. The loading capacities were determined by using equation 3.1 mentioned above in 3.2.2.6.

3.2.2.8 One pot loading of proflavine free base and subsequent modification of surface by click chemistry

0.5 g of CH_3-MSN@N_3 was dispersed in 15 mL of 1.0 mM proflavine free base solution in water. The dispersion was made homogenous by sonication for 30 minutes. The mixture was stirred magnetically for 12 hours at ambient conditions. The click reagents were added to functionalize the outer surface of MSN after loading drug was carried out in similar way as followed above in 3.2.2.3. After the reaction was over the product was separated by centrifuge and washed with 15 mL of water thrice. Finally it was dried under vacuum at 60 °C for 12 hours to obtain the final product. The loading of drug was determined by TGA analysis of dried samples by using following equation.

$$q_t = (W_b - W_a - W_c) * \frac{1000}{100*M_w}$$

3.2

Where, q_t is adsorption capacity (mmol.g^{-1}), W_a and W_b are the weight loses of CH_3-MSN@N_3 and proflavine loaded surface functionalized sample respectively. Wc is the weight loss corresponding to the presence of different surface functionality viz. PA, TEG or PEG calculated by grafting their alkyne counterparts in similar reaction conditions. M_w is the molecular weight of proflavine.

$$W_C = W_d - W_a$$

3.3

Here, W_d is the weight loss by alkyne modified samples without any drug.

3.2.2.9 Uptake of Nile Red in functionalized MSN, SBA and KCC to study molecular gating effect

To 0.5 mL of particle dispersions (2.0 mg/mL) of CH_3-MSN@N_3, CH_3-MSN@PEG, CH_3-SBA@N_3, CH_3-SBA@PEG, CH_3-KCC@N_3 and CH_3-KCC@PEG silica particles in millipore water; 10 µl Nile Red solutions (2.3 mg/mL) in ethanol were added. The mixtures were then incubated on a rotospin spinning at 25 rpm at room temperature for 3 hours. 0.1 mL of aliquot was diluted to 1.0 mL with water and used to measure photoluminescence by exciting at 530 nm using 5nm slit widths for both excitation and emission. The intensity at 645 nm was used to compare quantitative uptake of dye in particles. The digital photographs of dispersions were captured for visualization.

3.2.2.10 Release study of proflavine drug from various surface functionalized MSN particles

Firstly we attempted to determine the maximum amount of drug that can be extracted from each particle in a good solvent like DMSO. 20 mg of each silica sample loaded with proflavine and then clicked *in situ* viz. CH$_3$-MSN@N$_3$, CH$_3$-MSN@PEG, CH$_3$-SBA@N$_3$ and CH$_3$-SBA@PEG were taken in separate eppendorf tubes. 1.0 mL of DMSO solvent was added to each of them and the mixture was subjected to sonication for 15 minutes. The tubes were then taken to centrifuge to separate silica and the supernatants were separated with a micropipette. The residues were washed four more times in similar fashion and all washings were collected together for each sample. The amount of drug was measured by UV-Vis spectroscopy using molar absorption coefficient of 34,600 M^{-1}.cm^{-1}.

To find out release behaviour in physiological conditions we used phosphate buffer saline (PBS) solution of pH= 5.5. 50 mg of each sample was dispersed in 50 mL of PBS solution in a conical flask. The flasks were shaken on a rotary shaker maintained at 37 ºC and shaken at 200 rpm in bidirectional mode. The 1.0 mL aliquots were taken for specified time intervals and immediately subjected to centrifuge. The supernatants were then analyzed by UV-Vis spectroscopy to determine the amount of drug released. The stock was topped up by 1.0 mL PBS each time to counter the volume change.

3.3 Physicochemical Characterizations

FTIR spectra were obtained on Perkin Elmer Spectrum Two spectrophotometer in 4000-400 cm^{-1} range with a resolution of 4 cm^{-1}. The samples were thoroughly mixed with dried KBr (0.5 % wt/wt) and pressed into 13 mm diameter pellets at a pressure of 8 ton.cm^{-2}. UV-Visible spectra were recorded on a Carry 300 Conc UV-Visible spectrophotometer in quartz cuvette having path length of 10 mm. Photoluminescence was measured on a Carry eclipse fluorescence spectrophotometer with excitation and emission slit widths of 5 nm. Photoluminescence was measured in a quartz cuvette with path length of 10 nm at a resolution of 1 nm. TEM images were taken on a FEI Technai T20 operating at a voltage of 200 kV. The samples were prepared by dispersing a 0.1 mg.mL^{-1} of nanoparticles in ethanol by sonication. The dispersion was drop casted on a carbon coated copper grid of 400 mesh and allowed to dry in air. Thermo gravimetric analysis (TGA) of the silica nanoparticles was carried out using a TA Instrument SDT Q600 analyzer between ambient and 800 °C in nitrogen atmosphere (flow 100 mL.min^{-1}) at a heating rate of 10 °C.min^{-1}. All samples were dried under vacuum at 60 °C overnight prior to the analysis. NMR experiments were carried

out on a Bruker AVANCE AV 200 spectrometer equipped with a superconducting magnet with a field of 4.7 Tesla. All the chemical shifts were referenced to TMS.

3.4 Results and Discussion

3.4.1 Surface modification of various amphifucntional silica with click chemistry
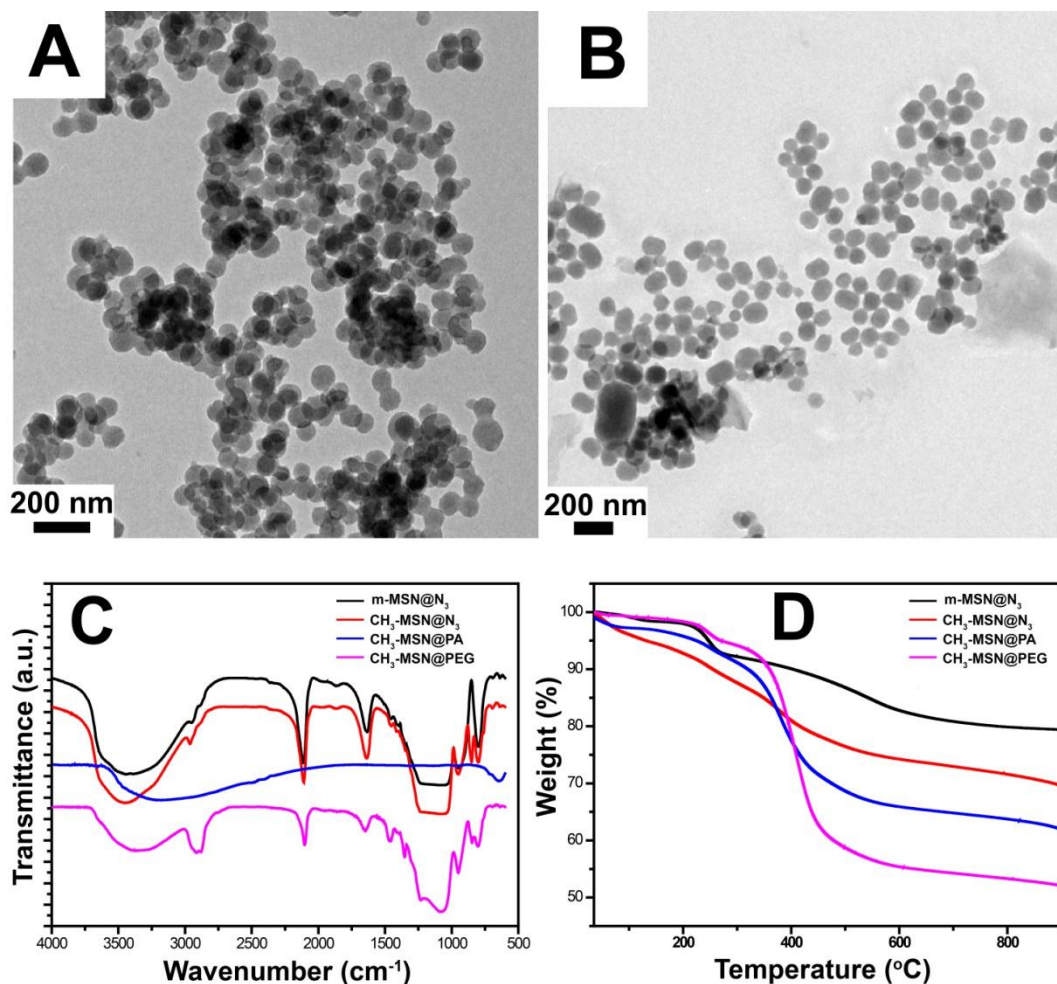
Figure 3.2 Characterization functionalized MSN. TEM micrographs of A) m-MSN@N₃ B)CH₃-MSN@PEG C) FT-IR spectra and D) TGA thermograms.

Here, we have performed synthesis of amphifunctional MSN as per scheme 3.2. The synthesis is very similar to that described in chapter II except for a small modification in the first two steps where azide groups have been grafted in a co-condensation approach. By using

this co-condensation apporach we have eliminated one step from the stepwise modification protocol. By this approach the grafting density(as calculated from TGA analysis) of azide group gets increased by 3.5 times (from 0.27mmol/g in the post synthesis grafting to 0.97 mmol/g). Similarly, SBA-15 and KCC were also subjected to further modifications as descibed in chapter II to imaprt amphi-functionlaity to them. The final samples of amphi-functional SBA and KCC were labelled as CH_3-SBA@N_3 and CH_3-KCC@N_3 respectively. Subsequently, various silica samples such as CH_3-MSN@N_3, CH_3-SBA@N_3, and CH_3-KCC@N_3 were functionlaized with propargyl alcohol and alkynyl functionalized TEG-alk and PEG-alk by azide-alkyne click chemistry. The click was catalysed by Cu(I) ions and THPTA was used as ligand for facilitating the click. The clicked samples were denoted by names such as CH_3-MSN@PA, CH_3-MSN@TEG and CH_3-MSN@PEG for products of CH_3-MSN@N_3 clicked with PA, TEG-alk and PEG-alk respectively. The clicked sample of SBA and KCC were also lablled in similar fashion viz. CH_3-SBA@PEG and CH_3-KCC@PEG, respectively.

Figure 3.2 A and B show TEM micrographs of CH_3-MSN@N_3 before and after final click reactions with PEG respectively. The TEM images show no significant change in size distribution as well as morphology of the materials. The mean size of particles is 80 nm. The evidence of functionalization can be derived from FT-IR analysis of the samples. As shown in figure 3.2 C, in the FT-IR spectra of m-MSN@N_3 and CH_3-MSN@N_3 all characteristic features as mentioned before in chapter II (please see section 2.5 and Figure 2.3 B) could be clearly seen. The azide peak at 2100 cm^{-1} can be followed to check click reactions with various groups[20]. The peak completely disappeared for CH_3-MSN@PA sample while reduced significantly in intensity for CH_3-MSN@PEG sample. This indicates the progerss of click reaction. In case of CH_3-MSN@PEG sample, the strong absorption at 2913 cm^{-1} and 2890 cm^{-1} due to asymmetric and symmetric -CH_2 stretch respectively is very much evident. These signals can be attributed to the ethylene groups in poly ethylene glycol backbone. Surface functionalization by click can also be evidenced by TGA analysis of MSN samples at various stages[21]. We have already discussed the grafting of azide and trimethyl groups and their characteristic thermogravimentric behaviour in previous chapter (figure 2.4 and section 2.5). Here we will discuss only further functionlizations. As it can be scene by figure 3.2 D the thermograms of various functional groups show varying degree of weight loses.

Table 3.1 Analysis of TGA data for various MSN samples

Sample	Total wt. Loss from 130-800 ºC (%)	Wt. of clicked alkyne (%)	Mol. wt. of alkyne (g/mol)	Amount of alkyne functional groups (mmol/g)	Efficiency of click w.r.t. azide groups (%)
CH$_3$-MSN@N$_3$	18.67	-	-	-	-
CH$_3$-MSN@PA	23.46	4.79	56.10	0.85	87.63
CH$_3$-MSN@TEG	33.31	14.64	216.28	0.68	70.10
CH$_3$-MSN@PEG	45.72	27.05	2038.0	0.13	13.40

Table 3.1 sumarises the TGA results of MSN samples clicked with various alkynes. The weight loss below 130 ºC corresponds to adsorbed moisture hence neglected. Therefore, we have calculated weight loss of all samples from 130 ºC- 800 ºC. The weight loss in this region includes loss of surface functionlaized groups as well as loss due to surface silanol condensation. We subtracted weight loss of CH$_3$-MSN@N$_3$ in this region from all other samples to obtain the weight loss corresponding only to alkyne groups attached due to click reaction. The amounts of various alkyne groups in PA, TEG-alk and PEG-alk modified samples are 0.85, 0.68 and 0.13 mmol/g respectively. The azide density in CH$_3$-MSN@N$_3$ was 0.97 mmol/g which was used as starting material in all material synthesis mentioned above. So the efficiency of click reaction w.r.t. azide groups performed under exactly similar conditions are 87.63, 70.10 and 13.40% for PA, TEG-alk and PEG-alk respectively. We attribute the decrease in efficiencey with increasing chain length to steric crowding.

3.4.2 Comparative study of loading efficiency of proflavine hydrochloride and proflavine free base

The spectral characteristics of both proflavine hydrochloride salt and free base are very similar as observed in UV-Vis spectra of their aqueous solutions (figure 3.3 A). Both show a strong absorption peak at 445 nm which has been used for quantification thoughout this work. The molar absorption coefficient in aqueous solution was found to be 28100 $M^{-1}.cm^{-1}$ which is not much succeptible to change in pH.

As mentioned earlier the free base is expected to have more hydrophobic character than the salt. So it is possible that the base might show enhancement in the loading capacity compared to salt. So we tested the loading of both salt and base on to CH_3-MSN@N_3. The loading capacity at 0.9 mM concentartion was taken for comparison. Figure 3.3 B shows the normalized relative adsorption capacity of free base and salt on to same material. It is clearly evident that the base has more than two fold upatake than the salt. So we decided to load free base as drug in further experiments. This also might be useful during release process. We speculate that the drug release might be facilitated in slightly acidic environments such as lysosomal compartments due to salt formation.
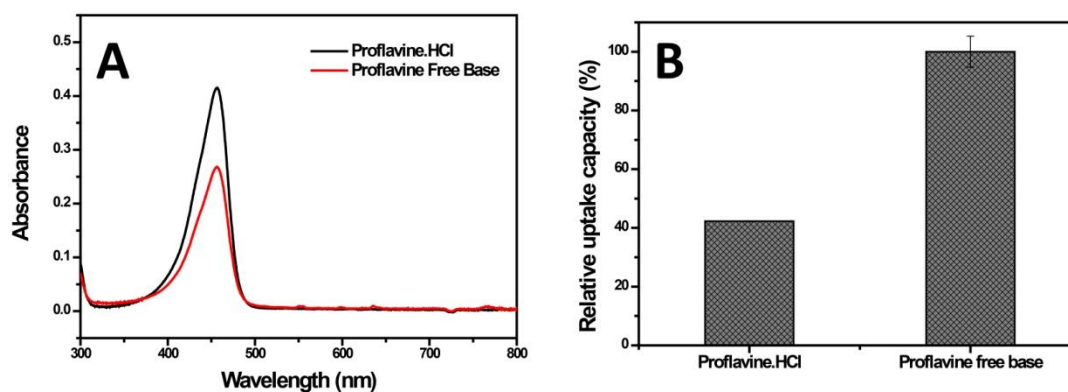
Figure 3.3 Evaluation of proflavine hydrochloride salt and free base A) UV-Vis Spectra B) relative uptake by CH_3-MSN@N_3 particles

3.4.3 Comparison between two methods of loading

As we have discussed in the begining of this chapter, the methods of loading of drug can greatly affect its loading capacity. To investigate this we have performed the loading of

proflavine on in the pores of functionalized MSN by two methods viz. 1) first modifying outer surfaces with click chemistry and then loading the drug (Path A Scheme 3.1) and 2) loading the drug in CH_3-MSN@N_3 sample and then surface functionalizing the material with various alkynes using the click chemistry (Path B Scheme 3.1). In first experiment various samples such as CH_3-MSN@N_3, CH_3-MSN@PA, CH_3-MSN@TEG and CH_3-MSN@PEG were incubated with proflavine solution in water. After 12 hours all materials were separated by centrifuge and the supernatents were analyzed by UV-Vis spectroscopy. Figure 3.4 A shows the spectra of all supernatent as well as proflavine blank. Here, note that the blank represented the amount of proflavine available for uptake before addition of silica particles.The loading was calculated by subtracting the amount present in supernatant from the initial amount present in blank sample for all adsorbent materials. The amount adsorbed by each material is presented as relative adsorption capacity calculated by using equation 3.1(figure 3.4 B). The uptake by CH_3-MSN@N_3 was found to be 0.0076 mmol/g. The sample CH_3-MSN@PA has shown dramatically increase in upatke to about double of azide sample to 0.0158 mmol/g. The CH_3-MSN@TEG asnd CH_3-MSN@PEG samples show 0.0131 and 0.0025 mmol/g of uptake respectively. The most notable result here is the higher uptake of drug into CH_3-MSN@PA and CH_3-MSN@TEG when compared to CH_3-MSN@N_3. The CH_3-MSN@N_3 samples are difficult to disperse easily in aqueous solutions. This may be due to presence of some trimethyl silyl functionality on the surface during HMDS treatment. But after click we observed that the dispersions with PA, TEG and PEG modified samples are way more easy to prepare as well as stable. So better dispersed materials such as CH_3-MSN@PA and CH_3-MSN@PA show higher uptake even compared to CH_3-MSN@N_3. We ascribe the higher uptake of proflavin into CH_3-MSN@PA and CH_3-MSN@TEG as compared to CH_3-MSN@PEG to the lower interfernce towards the transport of drug molecule inside pores due to the smaller chain length of PA or TEG. Similar trends were also observed when we repeated the uptake experiments with R6G (figure 3.4 D). The uptake capacities of the different MSN sampels with both proflavine and R6G have also been summarized in table 3.2.
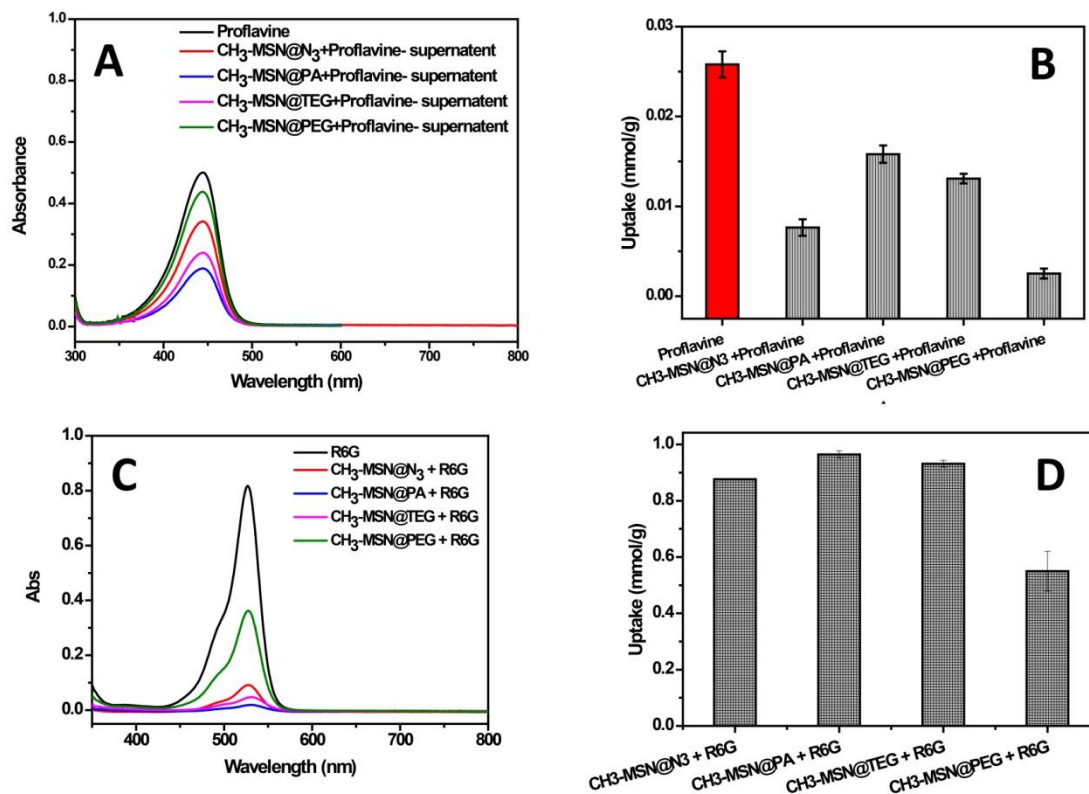
Figure 3.4 Loading of proflavine A and B and R6G C and D after outer surface modification of MSN A) UV-Vis spectra of different supernatants after separation B) relative comparison of uptake among various surface functionalized MSN

Table 3.2 Uptake capacities of silica samples for proflavine and R6G after click reactions with various alkynes

Sr.no.	Sample	Drug uptake capacity (mmol/g)	
		Proflavine	**R6G**
1	CH$_3$-MSN@N$_3$	0.0076	0.8765
2	CH$_3$-MSN@PA	0.0158	0.9647
3	CH$_3$-MSN@TEG	0.0131	0.9315
4	CH$_3$-MSN@PEG	0.0025	0.5498

In other experiment we loaded the drug in CH$_3$-MSN@N$_3$ material and then performed click reactions on them using diffrent alkynes (Scheme 3.1 Path B). In this case we could not measure the amount of drug remaining in the supernatent after separation of materials by UV-Vis spectroscopy due to intereference of various reagents used for click reaction. So we decided to determine the loaded drug by TGA analysis. All samples were analyzed by TGA. Figure 3.5 A shows the thermograms of various samples. The weight loss between 130 to 800 ℃ contributes for loss of surface functionalities, silanol condensationas well as physisorbed drug present. Thus we could determine the weight corresponding to alkyne group and proflavine only after subtracting the weight loss of CH$_3$-MSN@N$_3$ from all samples. . As mentioned in table 3.1 amounts of various alkyne groups were then subtracted from that to obatin the amount of proflavine loaded. The loading capacity values obtained from samples CH$_3$-MSN@N$_3$, CH$_3$-MSN@PA, CH$_3$-MSN@TEG and CH$_3$-MSN@PEG were 0.0560, 0.1936, 0.0649and 0.1836 mmol/g respectively (figure 3.5 B). Here we do not see any particular pattern and the loading in all samples is in the range of ~ 0.06-0.2 wt. %. But most notably, if we compare individual sample data by two methods; we find that the uptake is always higher in second method (Path B Scheme 3.1).

From the above observations it can be conlcuded that the loading before outer surface modification do not affect on loading capacity. However, the outer surface functional group does alter the uptake process if the material was functionalized first and then the drug was loaded. Among the surface modified samples the bulkier group tend to hinder the uptake more.
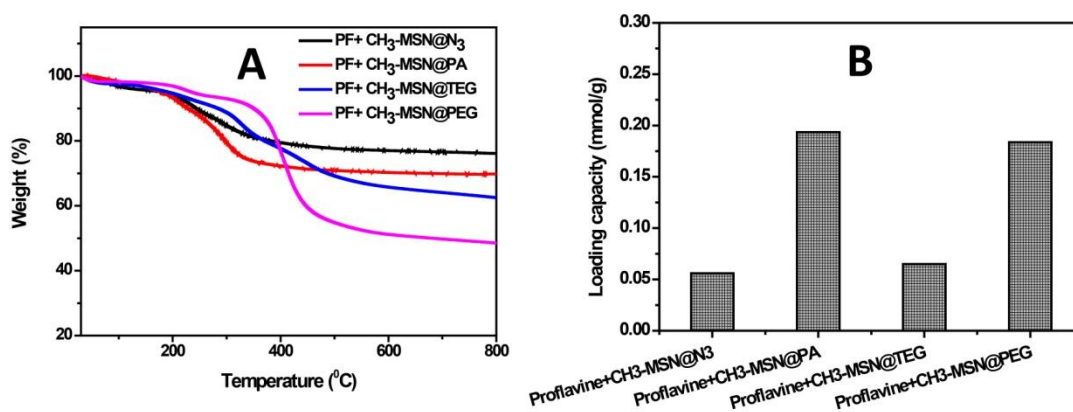
Figure 3.5 Loading of proflavine followed by one pot surface modification via click chemistry. Comparative study of loading of proflavine into various MSN post

functionalized after loading A) TGA thermograms of all samples B) quantitative loading in different samples.

3.4.4 Effect of surface functional groups on loading

As we have done few experiments with Nile red (NR) earlier in chapter II (section 2.5 figure 2.6 II); we thought it is worth to extend those experiments with alkyne modified samples. So, we performed the uptake of NR into the various functionalized MSN materials via Path A Scheme 3.1 and the results are shown in figure 3.6 A. Here we observations are consistant with earlier experiment where the photoluminescence intensity of NR form aqueous dispersion was suddenly increased by the addition of CH_3-MSN@N_3 particles. This of course due to the sequestration of NR from aggregated state into the hydrophobic pockets of amphi-functional material. But, with CH_3-MSN@PA particles the dye shown significantly decreased PL intensity in the aqueous medium. This trend of decrease in PL signal intensity continued for CH_3-MSN@TEG and CH_3-MSN@PEG as well. In fact, CH_3-MSN@PEG sample shown almost similar signal intensity as that of non functionalized m-MSN sample. The intensities of PL emmisions were normalized with respect to CH_3-MSN@N_3 and shown in figure 3.6 B. The corresponding digital images can also be seen alongside. This clearly demonstrates the phenomenon that the presence of bulkier surface groups do hinder the acces of dye to hydrophobic pockets of particles.
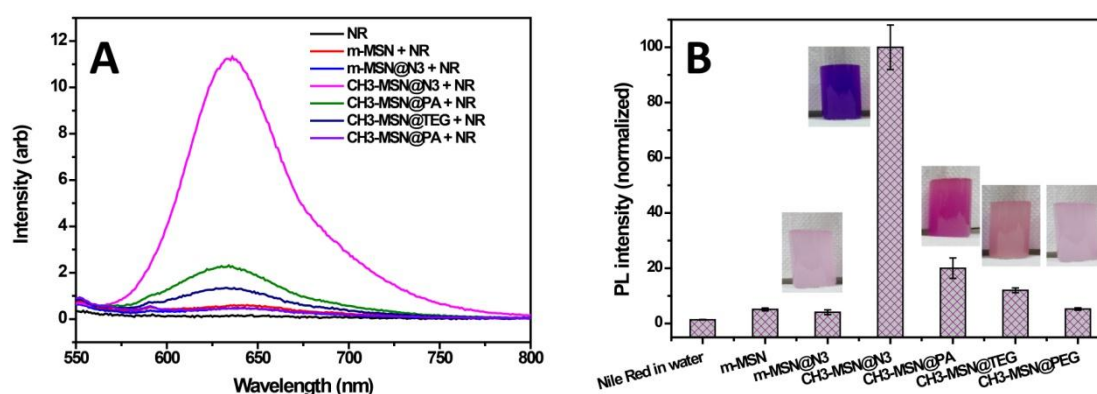
Figure 3.6 PL measurements of NR encapsulation by functionalized silica particles in water A) PL spectra B) quantitative comparison of various materials.

We wish to highlight here that while we have obeserved clear trend of decreasing loading capacity with increase in chain length of outer surface functionality in case of NR, there was

a little deviation from the trend when we loaded the real drug proflavin. This can be visualized by obesrving figure 3.4 B and table 3.2. In case of proflavin, the uptake capacities for CH_3-MSN@PA and CH_3-MSN@TEG samples were slightly higher than CH_3-MSN@N_3 sample. We ascribe this to the dispersiblity factor as mentioned earlier. As opposed to NR which was totally insoluble in water; proflavine is water soluble. So in this case the drug is in continuous phase. It is therefore not very surprising that the uptake capcities of MSN functionlaized with different functionalities (figure 3.4 D and table 3.2) with another water soluble dye R6G were similar to that observed with proflavin. From these obervations we postulate that the uptake of drug/dye depends on following factors- 1) the outer surface functionality of MSN 2) solubility of dye/drug in the given solvent. Bulkier surface functionalities try to hinder the passage of cargo molecules towards the pores. The surface functionality also determines the dispresion stability of MSN. The solubility of dye/drug determines the extent of its partition between solution and adsorbent. So, by taking all these factors in to account the observed behaviours can be explained as follows. For NR as it is in aggregated form, the partition from water to CH_3-MSN@N_3 sample is very high. For other samples viz. CH_3-MSN@PA, CH_3-MSN@TEG and CH_3-MSN@PEG; the chain length of outer surafce groups plays the most crucial role. The hindernace to NR for passage into pores is directly related to its uptake by respective material. In case of proflavine and R6G, both of them are soluble in water. So there is an equilibrium established for partition between MSN and water. In case of CH_3-MSN@PA and CH_3-MSN@TEG; the outer surface functionality is smaller but effectively imparts more hydrophillicity to MSN compared to CH_3-MSN@N_3 sample. So we see more uptake in these to samples. While in case of CH_3-MSN@PEG the blocking by PEG dominates that effect. The effect of blocking the passage by PA, TEG and PEG is consistent in case of both proflavine as well as R6G uptake(figure 3.4 B & D).

This phenomenon of blocking by surface groups is analogous to the frame and gate mechanism. The pore walls with azide groups constitute the frame while the surface groups attached by click chemistry serves as gate. The room or pore is hydrophobic. The length of attached group is analogous to the length of the gate. So we have three diffrent sized gates such as CH_3-MSN@PA, CH_3-MSN@TEG and CH_3-MSN@PEG. As we have seen in the above experiments as the size of gate increases it closes the frame to greater extent and in case of PEG-alk it blocks it completely. This we believe has great ramifications for the design of future drug delivery vehicles based on porous materials.
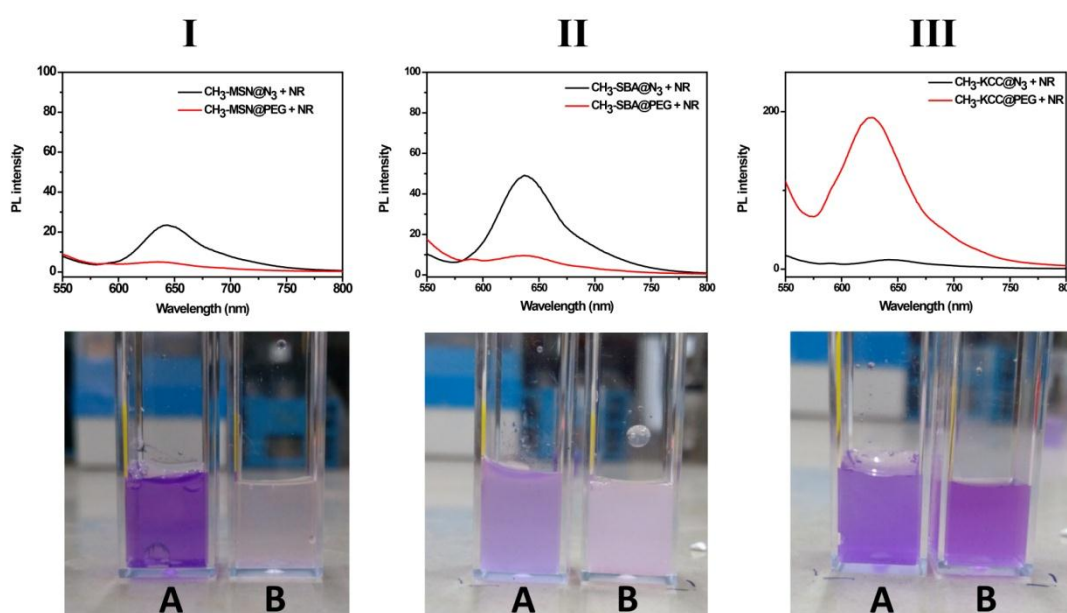
Figure 3.7 Effect of pore diameter on uptake of NR by particles with only azide and those with PEG modified surface. The PL spectra for I) MSN II) SBA and III) KCC materials with azide and PEG modified surfaces the corresponding images of dispersions shown below for each set as A and B respectively.

To prove this "molecular gating" effect in another way we decided to vary the frame size i.e. pore size while keeping the gate size i.e. chain length of surface group constant. At certain fixed gate size, when the frame size is larger than what gate could cover, we should be able to see the passage of cargo. For this, we selected three diffrent pore size material viz. MSN, SBA and KCC with 2 nm, 4 nm and open pore structure respectively. All of these materials were synthesized by sol-gel method by soft templating of surfactants; hence our stepwise functionalization strategies can be applied without any problem. For each material two diffrent samples were prepared, 1) with azide groups only and 2) PEG-alk functionalized viz. CH_3-MSN@N_3 and CH_3-MSN@PEG in case of MSN respectively. These samples were then subjected to adsorb NR from aqueous dispersions. Figure 3.7 I-III shows the PL spectra for functionalized MSN, SBA and KCC materials. In MSN and SBA case the azide sample shows uptake of NR while the PEG modified sample shows reduced uptake. This indicates that after click the pore openings of MSN as well as SBA materials gets blocked and NR can not access it. In case of KCC which has a open pore fibrous structure; the azide groups are expected to be grafted on the fiber tips. After click our PEG is also gets attached to it covalently by formation of triazole ring. Such a surface modification still leaves wide gap

between the two fibers eventhough a large molecule like PEG was used. Figure 3.7 III shows that the PL emmision after surface modification in KCC does not decrease as observed in case of MSN and SBA. That means PEG is not able to block the frame in this case. These experiments conclusively proves our hypothesis of "molecular gating" by ligands on outer surface. This can also be visualized by naked eye (see digital images in figure 3.7).

3.4.5 Effect of various surface functional groups on release of loaded drug

While the above observations clearly demonstrate the role of outer surface groups, it also poses an important question - how do the different molecules used for outer surface functoionalization effect the realease of loaded dye/drugs? This will have many consequences in drug delivery applications. Many drug delivery vehicles use targeting ligands which are macromolecules such as peptides, antibodies etc. To understand this we used path B approach in drug loading i.e. first loading drug in CH_3-MSN@N_3 and then surface modification by click. In this way we have maximum and almost equivalent loading in all samples. Proflavine was used as drug in this case. Firstly we wanted to determine how much drug can be extracted from each of these samples at maximum. To do that we decided to extract it with DMSO as solvent. The drug was extracted in several cycles and all of the extract was collected to measure the amount of drug. The amounts of proflavine extracted from various samples is shown in figure 3.8 A. Here we observed that CH_3-MSN@N_3 sample which is devoid of any additional functional group shows highest release of 0.227 mol/g. The samples modified with click CH_3-MSN@PA, CH_3-MSN@TEG and CH_3-MSN@PEG show decreasing amounts of released proflavine as 0.023, 0.015 and 0.003 mmol/g respectively. The loading capacities obatined by path B were 0.056, 0.196, 0.065 and 0.184 mmol/g for CH_3-MSN@N_3, CH_3-MSN@PA, CH_3-MSN@TEG and CH_3-MSN@PEG respectively. So here it can be deduced that the presence of bulkeir surface group can hinder the diffusion of drug molecule outside the particles even in a good solvent. This also corroborates with earlier observation of uptake via path A where we observed that the uptake decreased gradually in CH_3-MSN@PA , CH_3-MSN@TEG and CH_3-MSN@PEG samples.

We then studied the release of proflavine in PBS solution (pH= 5.5) which is comparable atmopshere to lysosomal conditions. The release profiles have shown in figure 3.8 B. Here we observed that the total released amount show similar trend i.e. CH_3-MSN@N_3 (0.0186 mmol/g) > CH_3-MSN@PA (0.0020 mmol/g) > CH_3-MSN@TEG (0.0019mmol/g) > CH_3-

MSN@PEG (0.0015 mmol/g). The saturation is attained for all samples within 1day though the amount released was far less to that which could be extracted in DMSO.
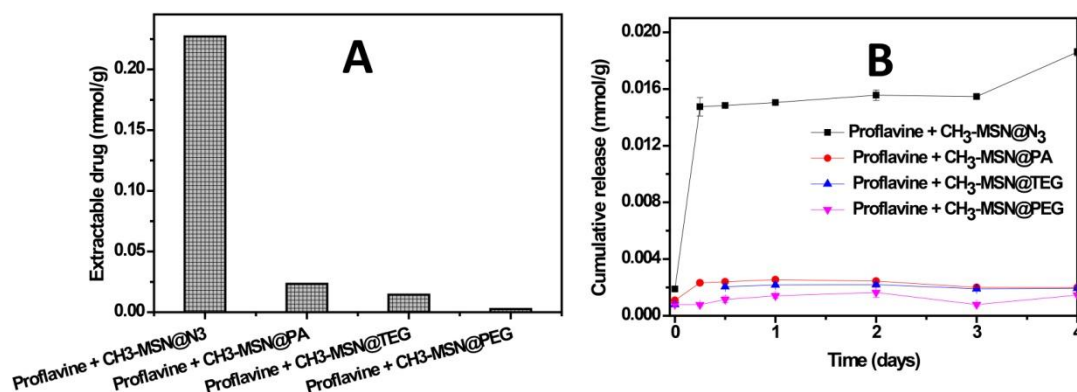
Figure 3.8 Release behaviour of proflavine loaded MSN with different outer surface groups attached after loading. A) Extraction by DMSO to determine maximum amount that can be extracted B) actual cumulative release in PBS buffer pH = 5.5.

3.5 Summary and Conclusions

In this chapter we have optimized the stepwise functionalized approach to minimize a step of grafting of azide group of silica. The new co-condensation apporach can functionalize silica more efficiently than previous method. The outer surface of the silica is then modified with diffent functional groups such as PA, TEG and PEG with varying chain length of ethylene oxide moeities. The major speculation about method of loading of cargo is evaluated. As we proposed in the begining of the chapter, two diffrent methods were tested. path A where the cargo is loaded after all fucntionalizations has resulted in far less loading (almost by 10 times in all samples). The other apporach (path B) where the cargo is loaded first followed by outer surface functionalizations resulted in better loading in all samples. The role of outer surface groups in the process of uptake has also been evaluated. Its is quite clear from trends that the bulkiness of outer surafce functional do affect the uptake process. The observation of this kind has been noted in pristine MSN. In a particular example, Wang et al. reported that surface modification prior to functionalization results in lower encapsulation efficiency of doxorubicin drug[22]. However, this phenomenon has not been demonstrated experimetally in materials where the pores are modified for enhanced uptake. With NR uptake experiments with different surface functionality we have clearly demonstrated this. The effect was

certainly arise due to "molecular gating" effect of bulky groups present on the surface. By varying the pore size of materials, this effect has also been demonstrated. The trade off between dispersibilty of MSN and blocking of access to the pores is critical for choice of apporpiriate surface functional group. Further we also found that the partition of a particular cargo molecule is also a driving factor. We believe that these findings will set platform for designing porous material based drug delivery systems in future.

3.6 References

(1)   Biju, V. *Chem. Soc. Rev.* **2014**, *43*, 744.

(2)   Bharti, C.; Nagaich, U.; Pal, A. K.; Gulati, N. *Int. J. Pharma. Investig.* **2015**, *5*, 124.

(3)   Pan, L.; Liu, J.; He, Q.; Wang, L.; Shi, J. *Biomaterials* **2013**, *34*, 2719.

(4)   Zhao, J.; Liu, Y.; Park, H.-J.; Boggs, J. M.; Basu, A. *Bioconjugate Chem.* **2012**, *23*, 1166.

(5)   Popat, A.; Hartono, S. B.; Stahr, F.; Liu, J.; Qiao, S. Z.; Qing Lu, G. *Nanoscale* **2011**, *3*, 2801.

(6)   Lihua, L.; Yao, L.; Chunyan, J.; Ye, Z.; Xianfeng, Y.; Xiaoming, H.; Zefeng, L.; Yu, Z.; Mingying, P.; Hong, X.; Chuanbin, M. *Adv. Funct. Mater.* **2018**, *28*, 1704623.

(7)   Badruddoza, A. Z. M.; Rahman, M. T.; Ghosh, S.; Hossain, M. Z.; Shi, J.; Hidajat, K.; Uddin, M. S. *Carbohydr. Polym.* **2013**, *95*, 449.

(8)   Monaco, I.; Arena, F.; Biffi, S.; Locatelli, E.; Bortot, B.; La Cava, F.; Marini, G. M.; Severini, G. M.; Terreno, E.; Comes Franchini, M. *Bioconjugate Chem.* **2017**, *28*, 1382.

(9)   Saint-Cricq, P.; Deshayes, S.; Zink, J.; Kasko, A. *Nanoscale* **2015**, *7*, 13168.

(10)   Chen, F.-H.; Zhang, L.-M.; Chen, Q.-T.; Zhang, Y.; Zhang, Z.-J. *Chem. Commun.* **2010**, *46*, 8633.

(11)   Zalipsky, S. *Adv. Drug Deliv. Rev* **1995**, *16*, 157.

(12)   Kingshott, P.; Wei, J.; Bagge-Ravn, D.; Gadegaard, N.; Gram, L. *Langmuir* **2003**, *19*, 6912.

(13)   Sano, K.; Nakajima, T.; Miyazaki, K.; Ohuchi, Y.; Ikegami, T.; Choyke, P. L.; Kobayashi, H. *Bioconjugate Chem.* **2013**, *24*, 811.

(14)   Yang, P.; Gai, S.; Lin, J. *Chem. Soc. Rev.* **2012**, *41*, 3679.

(15)   Vallet-Regí, M.; Balas, F.; Arcos, D. *Angew. Chem. Int. Ed.* **2007**, *46*, 7548.

(16)   Malvi, B.; Sarkar, B. R.; Pati, D.; Mathew, R.; Ajithkumar, T.; Gupta, S. S. *J. Mater. Chem.* **2009**, *19*, 1409.

(17)   Hong, V.; Presolski, S. I.; Ma, C.; Finn, M. *Angew. Chem. Int. Ed.* **2009**, *48*, 9879.

(18)   Singh, B.; Mote, K. R.; Gopinath, C.; Madhu, P.; Polshettiwar, V. *Angew. Chem. Int. Ed.* **2015**, *127*, 6083.

(19)   Polshettiwar, V.; Cha, D.; Zhang, X.; Basset, J. M. *Angew. Chem. Int. Ed.* **2010**, *122*, 9846.

(20)   Kumari, S.; Dhar, B. B.; Panda, C.; Meena, A.; Sen Gupta, S. *ACS Appl. Mater. Interfaces* **2014**, *6*, 13866.

(21)   Shinde, P.; Gupta, S. S.; Singh, B.; Polshettiwar, V.; Prasad, B. L. *J. Mater. Chem. A* **2017**, *5*, 14914.

(22)   Wang, Y.; Sun, Y.; Wang, J.; Yang, Y.; Li, Y.; Yuan, Y.; Liu, C. *ACS Appl. Mater. Interfaces* **2016**, *8*, 17166.

Chapter IV

Design and Synthesis of MRI Responsive Theranostic Core-shell System

4.1 Introduction

As we have mentioned in the introduction chapter our ultimate aim is to design and synthesize a theranostic nano carrier based on mesoporous silica nanoparticles (MSN). Towards this goal in the earlier chapters of this thesis we have made an attempt to create a methodology for differential pore and surface functionalization of MSN particles so that they could become effective carriers for hydrophobic drug molecules. During these experiments we have also delineated few basic principles that underlay the phenomenon of drug adsorption into cargo and its diffusion. With this knowledge we believe that the design of drug delivery vehicles to be practically more efficient. The next step was to incorporate a diagnostic entity so that the design of the theranostic system is complete. Among the different diagnostic tools available, imaging is the most versatile as it can give both biological and functional information about tissues and organ system that is helpful in both basic biology [1] as well as medicine[2]. There are several imaging tools that have been used in literature to design theranostic systems such as luminescent materials[3], radio nuclides[4], ultrasound[5] and magnetic resonance imaging (MRI)[6]. Among these MRI is very promising tool because of its use in routine diagnosis for many disease conditions, established network of facilities through hospitals and most importantly due to its non invasive nature. The technique was developed in 70's by Peter Mansfeild and Paul Lauterbur who were awarded 2003 Nobel Prize in physiology and medicine. As opposed to CT and PET scanners, MRI is considered much safer as it does not expose patients to high energy radiations. Apart from its growing applications in cancer diagnosis it has been routinely used for neuroimaging[7], angiography[8] as well as cardio vascular imaging, organ[9] and gastrointestinal[10] and musculoskeletal imaging[11].

In MRI the contrast is based on density of protons in given space as well as relaxation of those protons in an applied magnetic field. The basic principle is proton nuclear magnetic resonance (NMR). When a magnetic field is applied the nuclear states of protons undergo degeneration and precess at Larmor frequency. So when a pulse of radiofrequency which is identical to this precession frequency of protons is applied they absorb this energy and undergo excitation. This process is called resonance. Then the excited energy is released the nuclei comes back to its ground state and becomes ready to absorb radio energy from next pulse. The time taken to undergo relaxation is known as relaxation time. The relaxation can happen mainly through two different mechanisms. It can happen through spin-lattice (longitudinal) mechanism known as T1 or by spin-spin mechanism (transverse) known as T2.

The image weighting based on T1 or T2 can show different contrasts for different tissues. The proton in different tissues has different relaxation times depending upon amount of water present there. This is primary source of contrast in MRI. The contrast in an image can also be generated by using a specified pulse sequence and weighting on either T1 or T2 relaxation. This flexibility gives MRI an edge over other *in vivo* imaging techniques. However, this contrast many times is not sufficient and hence practically it becomes difficult to detect a disease condition. Fortunately, this can further be enhanced by injecting contrast agents.

Presently Gd^{+3} ion based chelates have been primarily used as T1 contrast agents[12] (e.g. Magnevist® and Gadovist®) especially for studying the breakage of blood brain barrier (BBB). In presence of these contrast agents the relaxation time is shortened by the interaction of protons with the electron density of Gd^{+3} ions and therefore the protons usually appear brighter. Gd (III) complexes however suffer from some serious clinical disadvantages such as rapid excretion from urine and hence short circulation time. The functionalization of these complexes is rather difficult and leaching of Gd^{+3} ions can cause toxic effects e.g. nephrogenic system fibrosis (NSF)[13], etc. On the other hand T2 contrast agent create microscopic field in homogeneity in applied magnetic field and activate dephasing of protons leading to shortening of T2 relaxation. Super paramagnetic iron oxide nanoparticles (SPION) are first clinically approved NP based contrast agents[14] (e.g. dextran coated magnetite Ferridex®) which generate T2 contrast for liver. Iron oxide is more biocompatible than heavy metal like Gd or Mn. Human body can store iron in ferritin. So making MRI contrast agents based on iron oxide nanoparticles is quite logical and looks a very attractive alternative to T1 contrasting agents based on Gd^{+3} ions.

Iron oxide can be synthesized very easily in size and shape controlled manner[15]. The critical size for iron oxide (magnetite/maghemite) to become super paramagnetic is ~ 16 nm. Above the critical size the material becomes ferromagnetic. It is well documented that SPION can be easily coated by silica shell that imparts several advantages to them such as preventing their aggregation yet retaining their magnetic properties. Since silica is amorphous it can easily coat the SPION surface and the combination i.e. iron oxide core-silica shell is a convenient design from synthesis point of view[16]. Indeed, there have been several attempts to make such systems[17]. Unfortunately, in most of the reported literature a solid silica shell has been used to coat the SPIONS[18]. Though a thick shell allows the separation of magnetic cores and prevents their aggregation, practically this is not much useful for drug loading purposes and hence this design cannot be a good theranostic system. Here, keeping in mind the goal of

theranostic system it is very important to have a porous shell. In this regard, Hyeon and co-workers[19] as well as Xia and co-workers[20] have attempted to make such systems. Although they have created SPION core-porous silica shell architectures, the appropriate functionalization of silica in general and pores in particular is still missing even in their design. Therefore, we intended to use our amphi-functional silica particle preparation strategy and create a iron oxide core amphi-functional porous silica shell system by combining our silica functionalization approach combining with incorporation of SPION core to complete this piece of the puzzle in the theranostic system design.

4.2 Materials and Methods

4.2.1 Materials

$FeCl_3.6H_2O$ (99%) and sodium sulphate anhydrous were procured from s.d. fine chemicals India Ltd. Sodium oleate (AR grade) was purchased from Fluka India. Ethanol and n-hexane were purchased from Merck India. 1-octadecene (95%, technical grade) was purchased from Alfa Aesar. D_2O, Oleic acid (90%, technical grade) paraformaldehyde, glutaraldehyde, osmium tetra oxide, uranyl acetate, epoxy resin and TEOS was bought from Sigma-aldrich Inc. HeLa cell lines were purchased from ATCC. DMEM, FBS, PBS were purchased from HiMedia. Milli Q water was used throughout all synthesis.

4.2.2 Experimental

4.2.2.1 Synthesis of super paramagnetic iron oxide nanoparticles (SPION)

As shown in Scheme 4.1 the SPION were prepared by thermal decomposition of iron-oleate complex in a high boiling solvent as reported previously by Hyeon and co-workers[21] with slight modifications. For this, an iron-oleate complex was first prepared by reacting 40 mmol of $FeCl_3.6H_2O$ with 120 mmol of sodium oleate in mixture solvent (80ml ethanol + 60ml water + 140ml n-hexane) at 70° C for 4 hours. After the reaction was over the upper hexane layer containing iron-oleate complex was washed with water excessively to remove unreacted salt. Anhydrous sodium sulphate was added to this to remove moisture and dried under reduced pressure to yield waxy solid iron-oleate.

To synthesize SPION 2.75 mmol of iron-oleate complex was dissolved in 35 mL of 1-octadecene and 0.21 mmol of oleic acid. The reaction mixture was then heated to 320 °C under inert atmosphere of Argon while stirring and kept at that temperature for 1 hour. The

initial dark brown solution turns totally black after the reaction indicating the formation of SPIONS as a suspension. The SPION were then recovered by centrifugation and washed several times with ethanol. Finally these were dispersed in chloroform and stored for further use. This sample will be referred to as SPION further in the chapter.

$$FeCl_3 + 3\ Na\text{-}Oleate \xrightarrow[70\,°C,\ 4\ h]{Ethanol:\ water:\ hexane} Fe\,(Oleate)_3 + 3\ NaCl$$

$$Fe(Oleate)_3 \xrightarrow[320\,°C,\ 1\ h]{1\text{-}octadecene} Iron\ Oxide\ NP$$
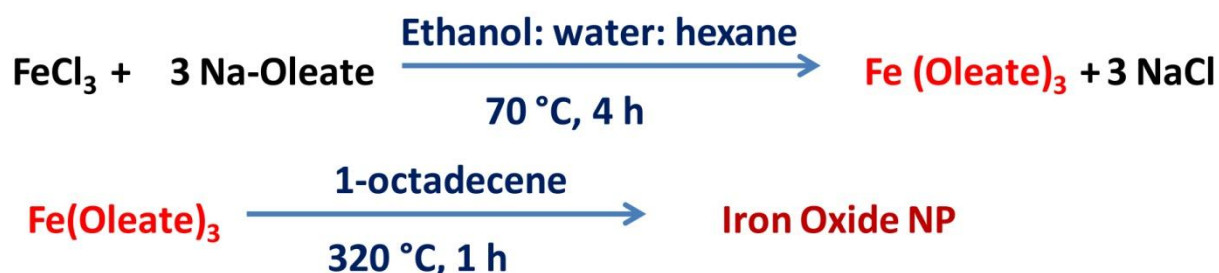
Scheme 4.1 Synthesis of iron oxide NP by thermal decomposition method

4.2.2.2 Synthesis of SPION-silica core-shell nanoparticles grafted with azide groups (SPION@SiO₂@N₃)

The synthesis protocol as demonstrated by Kim et.al. shown in Scheme 4.2 was used for this purpose[19]. 0.78 mL of stock solution of SPION in chloroform (0.110 g of SPION) was added to 5 mL of 0.55 M of CTAB solution. The solution was stirred for 1 hour to form an emulsion. This was then heated up to 70 °C for 30 minutes to remove chloroform. The solution appears dark brown in colour. 45 mL of Milli Q water was added followed by 0.3 mL of 2 M NaOH solution. The solution was stirred for 10 minutes and 0.5 mL of TEOS (2.23 mmol) was added to it. The reaction was allowed to continue for 3 hours. After 3 h, 0.075 mL of AzPTS (0.3 mmol) was added into the reaction and the reaction was continued for 1 hour before it was stopped.

The reaction mixture was centrifuged at 10000 rpm for 10 minutes to separate particles. The product was washed with ethanol (50 mL) for three times and separated by centrifugation. Finally they were dispersed in 50 mL ethanol. This sample was labelled as SPION@SiO₂@N₃.

4.2.2.3 Removal of surfactant from SPION@SiO₂@N₃

To the above synthesized dispersion of SPION@SiO$_2$@N$_3$ 0.040 mL of concentrated HCl was added. The mixture was then heated at 60 °C with stirring for 3 hours. The reaction mixture was then cooled to room temperature and product was separated by centrifuge at 15000 rpm for 15 minutes. The supernatant was discarded and residue was re-dispersed again in 15 mL of ethanol. The washing was repeated for three times with 15 mL of ethanol and finally dispersed in 15 mL ethanol. The sample was labelled as SPION@m-SiO$_2$@N$_3$.
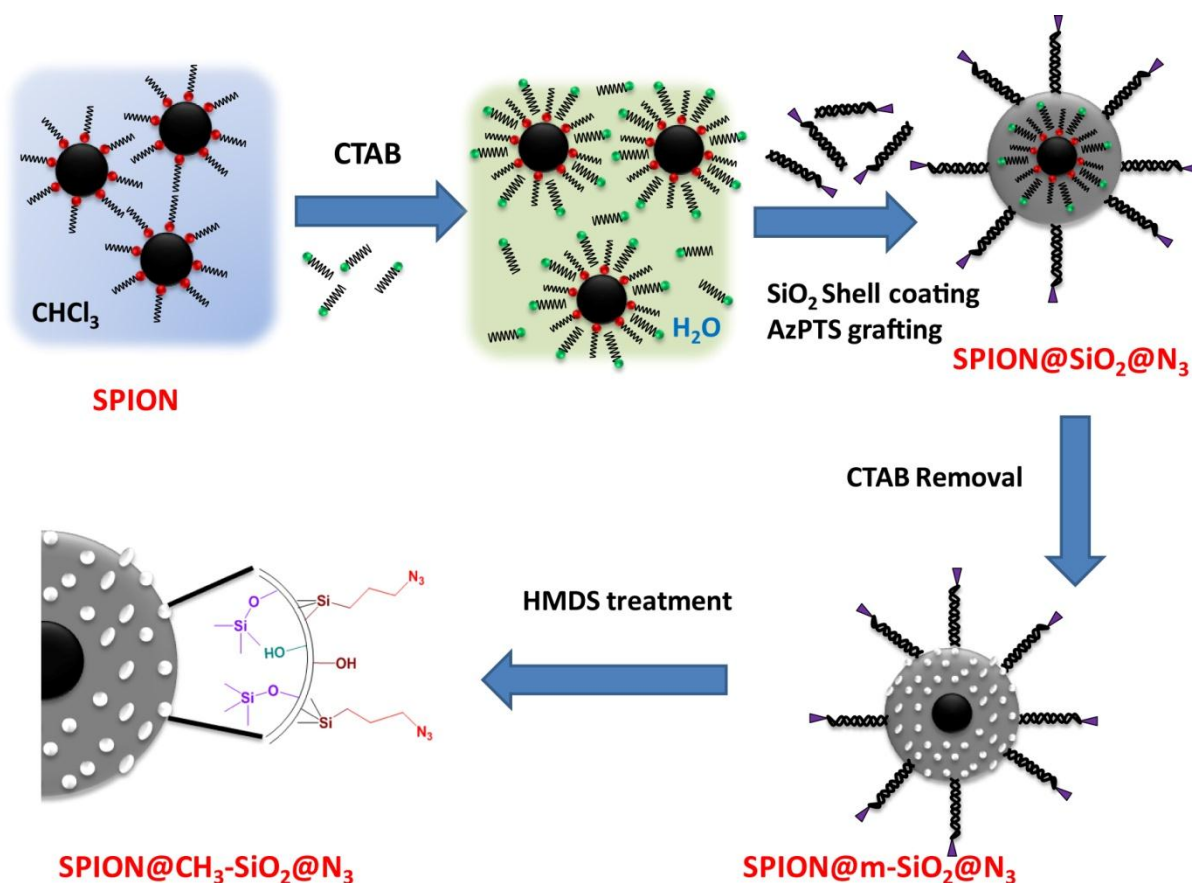
Scheme 4.2 Coating of SPION by silica and functionalization

4.2.2.4 Measurement of saturation magnetization and blocking temperatures

For measurement of saturation magnetization as well as blocking temperatures the samples were dried in vacuum oven at 70 °C overnight. The samples were then loaded (2-5 mg) in a cleaned VSM sample holder and sealed with Teflon tape.

4.2.2.5 Measurement of T1/T2 relaxivities of SPION@m-SiO$_2$@N$_3$ of core shell nanoparticles

For measurement of T1/T2 values the dispersion in ethanol was subjected to centrifuge at 15000 rpm for 15 minutes. The supernatant was discarded and precipitate was dispersed in D$_2$O. A stock solution of 0.8 mM (Fe concentration determined by AAS) was prepared. The dilutions of 0.4, 0.2, 0.1 and 0.05 mM were prepared serially from this stock. T1/T2 values were measured for these samples for proton signal of residual water.

4.2.2.6 Cellular uptake of SPION@m-SiO$_2$@N$_3$ NP

HeLa cells were cultured in Dulbecco's modified Eagle medium containing 10% fetal bovine serum (FBS) and 1% each of non-essential amino acid solution and penicillin-streptomycin in 3 cm culture dishes at 37 °C in a humidified atmosphere containing 95% air and 5% CO$_2$ (v/v). Before incubation with SPION@m-SiO$_2$@N$_3$ NP this medium was removed by aspiration, and the cells were washed twice with PBS (1× DPBS). Then, 2 mL suspension of nanoparticles in fresh medium of the same formulation was added, and the cells were incubated for the 2 hours under the above conditions. Cells were 80% confluent at the time of processing for TEM.

4.2.2.7 Fixing of cells in epoxy resin and TEM of SPION@m-SiO$_2$@N$_3$ in HeLa

The fixing in epoxy followed by imaging was performed by following a previously reported protocol[22]. After incubation of the cells, the medium containing the excess SPION@m-SiO$_2$@N$_3$ NP was removed and the cells were washed three times with PBS. Primary fixation of the cells was carried out with a 0.1 M PBS solution of 0.5% paraformaldehyde and 3% glutaraldehyde for 1 h. The cells were then washed with PBS and post fixed using a 1% aqueous solution of OsO$_4$ for 1 h followed by successive washings with PBS, water, and 30% ethanol. Staining with 0.5% uranyl acetate in ethanol was carried out for 1 h. Cells were then dehydrated using increasing concentrations of ethanol (30%, 60%, 70%, 80%, and 100%). Finally the cell pellets were infiltrated first with a mixture of 1:1 epoxy resin in 100% ethanol and then with the resin only and were left to polymerize at 60°C for 48 h. Ultrathin sections (∼70-100 nm) were cut using a Leica Ultramicrotome using a diamond knife. The sections were then mounted on Formvar coated copper grids and then stained with 5% uranyl acetate in 50% ethanol and 2% aqueous lead citrate solution. Finally, TEM imaging of the sample was done at lower voltage of 100 kV.

4.3 Physico-chemical Characterizations

FTIR spectra were obtained on Perkin Elmer Spectrum Two spectrophotometer in 4000-400 cm^{-1} range with a resolution of 4 cm^{-1}. The sample were thoroughly mixed with dried KBr (0.5 % wt/wt) and pressed into 13 mm diameter pellets at a pressure of 8 $ton.cm^{-2}$. Powder X-ray diffraction of all the mesoporous samples was carried out in a PANalytical X"pert Pro diffractometer with a proportional counter detector. The radiation source was Cu Kα (1.5418 Å) with a Ni filter and the data collection was carried out with a flat holder in Bragg–Brentano geometry (0.5 to 10°; 0.2° min^{-1}). Ultrathin sections (70–100 nm) were cut using a diamond knife on a Leica Ultramicrotome. The biological samples were analyzed using FEI Tecnai Spirit TEM at 100 kV. Inorganic materials were imaged on TEM images were taken on a FEI Technai T20 operating at a voltage of 200 kV. The samples were prepared by dispersing nanoparticles in ethanol by sonication. The dispersion (6-10 μL) was drop casted on a carbon coated copper grid of 400 mesh and allowed to dry in air. Magnetic properties were measured on a Quanta design SQUID-VSM magnetometer. For ZFC measurements a static field of 100 Oe was applied. For field cooled sample (FC), the samples were cooled under static field of 100 Oe and measurement of magnetic moments under a field of 100 Oe was carried out in temperature range of 5-300 K. Magnetization vs. field measurements were measured in a field of − 6 to +6 T (60000 Oe). The T1 and T2 relaxation time were measured in D_2O on a Bruker Avance AV 500 NMR spectrometer operating at 11.7 T and 500 MHz with an acquisition time of 1.31 s.

4.4 Results and Discussion

4.4.1 Synthesis of iron oxide nanoparticles

The FTIR spectrum in figure 4.1 A shows absorption at 1716 cm^{-1}, which is characteristic signal for metal–oleate complexes. The peaks at 2927 cm^{-1} and 2851 cm^{-1} are due to $-CH_2$ stretching vibrations of oleate ligand. The $-CH_3$ bending vibrations are observed at 1534 cm^{-1} and 1446 cm^{-1} respectively. Fe-O stretching vibration is detected at 605 cm^{-1}. The broad absorption around 3305 cm^{-1} is observed which can be attributed to –OH stretching vibrations. PXRD pattern of as synthesized iron oxide nanoparticles are shown in figure 4.1 B. The peaks at 2 theta values 18.17, 30.28, 35.65, 43.33, 53.67, 57.17, 62.85, 74.53 are identified for 111, 220, 311, 400, 422, 511, 440, 533 planes of magnetite Fe_3O_4 phase (PDF card no 85-1436) respectively. The broadening of the peaks suggests formation of nanosized crystals. The average crystallite size determined by using Scherrer equation turns out to be 11

nm. The transmission electron microscope images of SPION are shown in figure 4.1 C. The particles were drop casted from their dispersion in n-hexane upon carbon coated copper grid. The image shows discrete particles of average size 13.6 nm. The morphology of the particles was spherical. This corroborates with crystallite size obtained by Scherrer equation. This also suggests that each particle is crystalline in nature. From the M vs H magnetization plot it can be concluded that these SPIONs show super paramagnetic behaviour (figure 4.1 D). They show a coercivity of 260 Oe at 5K and only 15 Oe at 300K. Figure 4.1 D inset shows the magnified region around zero applied fields. The saturation magnetization values are determined to be 20 emu/gm and 25 emu/gm at 300K and 5K temperatures respectively. The low saturation magnetization values compared to the bulk value of magnetite (90 emu/gm) can be attributed to surface canting of spins as well as the weight of capping agent oleic acid. From the field cooled (FC) and Zero field cooled (ZFC) data plot for Fe_3O_4 NPs; blocking temperature (T_B) was determined to be ~78 K. This suggests that above this temperature the particles exhibit superparamagnetism.
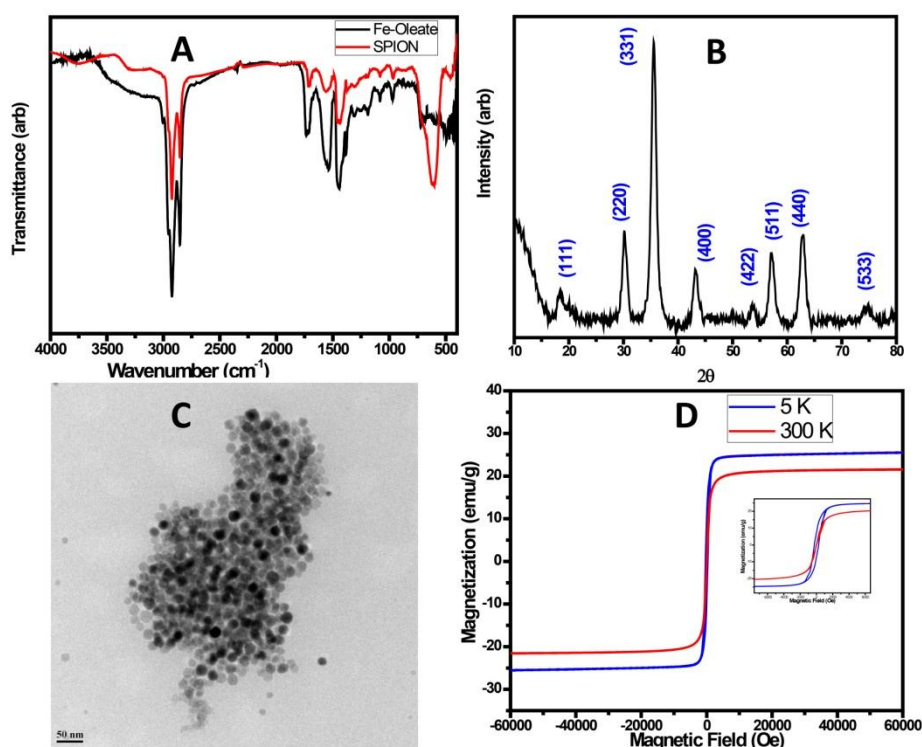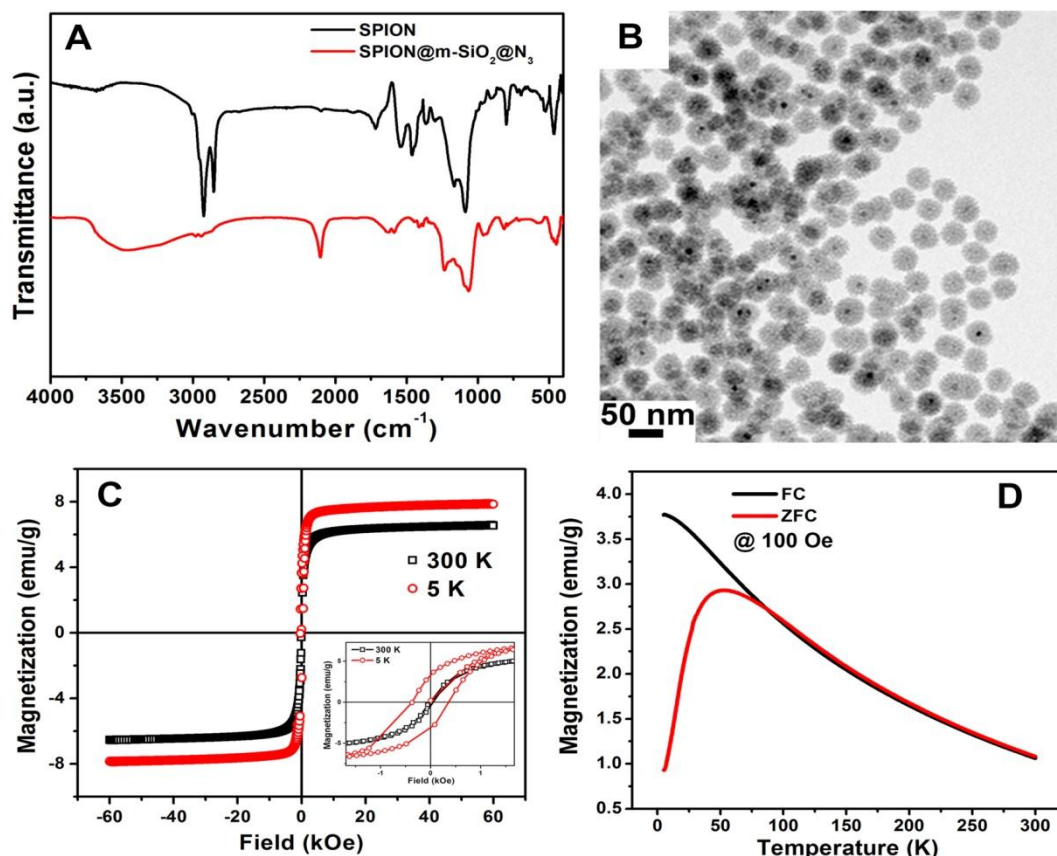

Figure 4.1 Characterization of SPION A) FT-IR spectra of iron-oleate and oleate capped SPION B) wide angle PXRD pattern of SPION C) TEM micrograph of SPION and D) M-H curve of SPION.

4.4.2 Synthesis of iron-oxide silica core-shell nanoparticles

As seen from the FTIR spectra of SPION@SiO$_2$@N$_3$ shown in figure 4.2, the broad peak at 1100 cm^{-1} is characteristic signature of Si-O-Si stretching vibrations which also overlaps with Fe-O-Fe stretch. Another broad peak which appears ~ 3400 cm^{-1} can be attributed to O-H stretching vibrations of silanol Si–OH groups. The characteristic signal for azide stretching vibration appears at 2100 cm^{-1} SPION@SiO$_2$@N$_3$. This clearly indicates grafting of azide groups onto the silica coated sample. The aliphatic stretching vibrations 2930 and 2850 cm^{-1} are characterized with decreased intensity due to relative decrease of oleic acid in final composition as well as removal of CTAB surfactant. The data can also be corroborated with our previous observations in case of silica (section 2.5 and figure 2.3 B FT-IR). All other peaks are common to both SPION and SPION@SiO$_2$@N$_3$ nanoparticles.

The transmission electron microscopy (figure 4.2 B) clearly reveals the formation of core-shell structure of SPION@SiO$_2$@N$_3$. The morphology of the core-shell structure is spherical. The porous nature of the silica shell can be observed in the TEM micrograph. The iron-oxide core appears dark in contrast while silica shows lighter contrast due to lower atomic number. From TEM the average size of core-shell particles is found out to be 39 nm. From field cooled (FC) and zero field (ZFC) cooled magnetization measurements in a field of 100 Oe (figure 4.2 C) it can be seen that the blocking temperature (T$_B$) is marginally decreased from 78 K to 55 K after surface coating with silica. This again is indicative of coating since decrease in T$_B$ here can be correlated to the decrease in inter-particle interaction due to coating[23]. The saturation magnetization is decreased dramatically to 7.5 and 6.4 emu/gm at 5 K and 300 K respectively (Figure 4.2 D). This is known to be a direct consequence of non magnetic silica coating. The coercivity (H$_C$) values are 30 Oe and 365 Oe at 300K and 5 K respectively indicating the particles are still super paramagnetic at room temperature. The above observations clearly prove that the SPION are coated with silica forming core-shell morphology with discrete particles and porous shell. The presence of azide functionality which has been incorporated on the SPION@SiO$_2$@N$_3$ by the co-condensation approach is concluded from the FTIR data. It is also clear that the particles retain their super paramagnetic nature after functionalization. This property can be an added advantage when the system is used to diagnose malignant tumour. After diagnosis, the super paramagnetic systems can be used to heat up the tumour environment by using an alternating magnetic field. This phenomenon is known as magnetic fluid hyperthermia. Combined with an anti cancer drug the effect can magnificently enhance the therapeutic effect.

Figure 4.2 Characterizations of SPION@SiO₂@N₃ A) FT-IR spectra of SPION and SPION@SiO₂@N₃ B) TEM image C) FC and ZFC curves and D) Magnetization vs. field curve

4.4.3 Measurement of relaxivities of SPION@m-SiO₂@N₃ particles for MRI contrast applications

The application of this functionalized SPION@m-SiO₂@N₃ for MRI applications depends on their ability to shorten the relaxation time of protons in their surroundings. To test that we dispersed these particles in D_2O solvent and measured the relaxation times for both T1 and T2. For T2 spin-spin relaxation Carr-Purcell-Meiboom-Gill (CPMG) sequence was used. The water signal at 4.71 ppm of residual water was considered for these measurements. As seen from the figure 4.3 A the r_2 value which is inverse of T2 obtained was 0.38 mM^{-1} s^{-1}. This very low relaxivity value can be correlated to high magnetic field (11.7 T) used for measurements of relaxivity. The relaxivity values are known to be greatly dependent on magnetic field (B) used. A reported value for magnetite with a particles size of ~12 nm[24] was found to be ~ 200 mM^{-1} s^{-1} which was measured at a field of 1.5 T. In an another closer example where higher magnetic field (3.0 T) was used for measurement where 22 nm sized

iron oxide nano cubes coated with PEG-phospolipids[25] show r_2 relaxivity of 761 mM^{-1} s^{-1}. It is also reported in the literature[23] that for sizes around 5 nm of iron oxide (magnetite) the relaxivity varies between 60-180 mM^{-1} s^{-1} when measured at a field of 1.5 T. The r_2 values depend upon the size of magnetic core, magnetization values and also the surface coating of material. In case of T1 relaxation (longitudinal or spin lattice), we found that the relaxation time data for T1 obtained is very much constant over the measured range of concentrations. This data cannot be fitted in with an intercept in origin. From the above observations it is clear that the synthesized material SPION@m-SiO$_2$@N$_3$ can generate contrast by T2 relaxation mechanism. It is possible that because of larger size of the magnetic core the effective magnetic moment is high showing predominantly T2 relaxation. It has been shown that if we reduce the size of the NP the surface canting of spins leads to reduction in magnetization of the particle. In such cases T1 relaxation gets improved[26]. Thus the above measurements clearly establish the effectiveness of SPION@m-SiO$_2$@N$_3$ NP as MRI contrast enhancing agents via T2 relaxation mechanism.
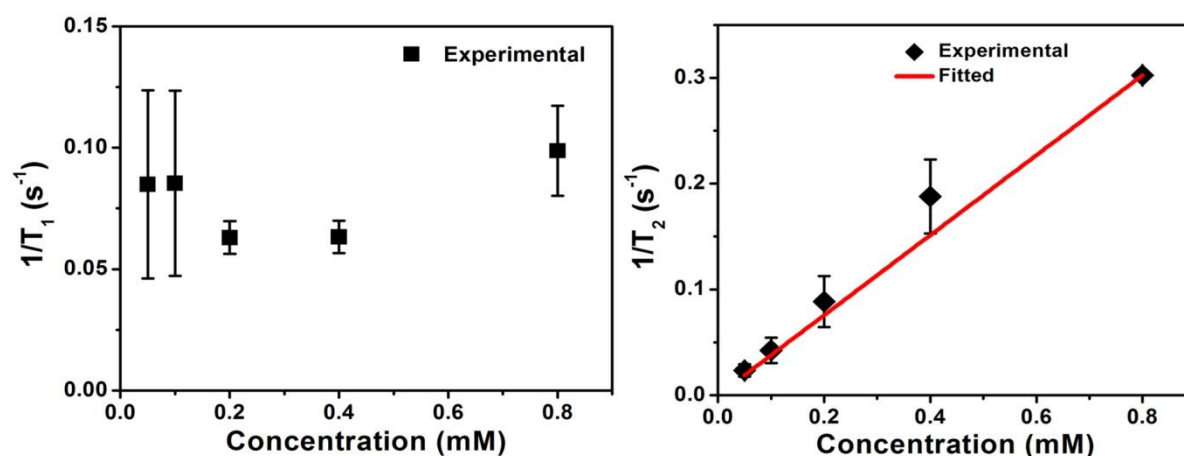
Figure 4.3 A) T1 and B) T2 relaxivity of SPION@m-SiO$_2$@N$_3$

4.4.4 Cellular uptake of SPION@m-SiO$_2$@N$_3$

While the NMR experiments show the effectiveness of SPION@m-SiO$_2$@N$_3$ NPs as contrast agents, in the real situation it is important that these NPs once injected into a patient body get internalized by the cells/tissue. To get some insight into this aspect we wanted to check the ability of cells to internalize these NPs. The internalization of SPION@m-SiO$_2$@N$_3$ can be conclusively evidenced by electron microscopy. The cells after incubation with SPION@m-SiO$_2$@N$_3$ particles were washed to remove excess particles. They were then fixed in epoxy

resin by using routinely used protocol of slow and gradual dehydration while preserving the morphology and structure of the cell. The epoxy resin was then polymerized to form solid matrix. This enables to make thin sections by a microtome. These sections were then analyzed by TEM after negative staining with uranyl acetate. From the TEM images of HeLa cells (figure 4.4) incubated with SPION@m-SiO$_2$@N$_3$ NP, it can be visualized the cells were healthy at the time of fixing with distinct nuclei. The TEM images also conclusively show that the particles are indeed internalized. Almost in all cases they are confined in endosomic vesicles. They were mostly found in the cytoplasm and none were observed in nucleus or any other cell organelle. While this is not entirely desirable, the presence of SPION in the core provides a tool for destroying these cells by magnetic hyperthermia. The duration of stay of NP inside these vesicles is limited. Interestingly in recent reports from Brust and co-workers have shown that it is possible to break these endosomes by moderate phototherapy releasing NP into the cytosol[27]. This can allow the drug loaded NP to be available for participating in their intended action.
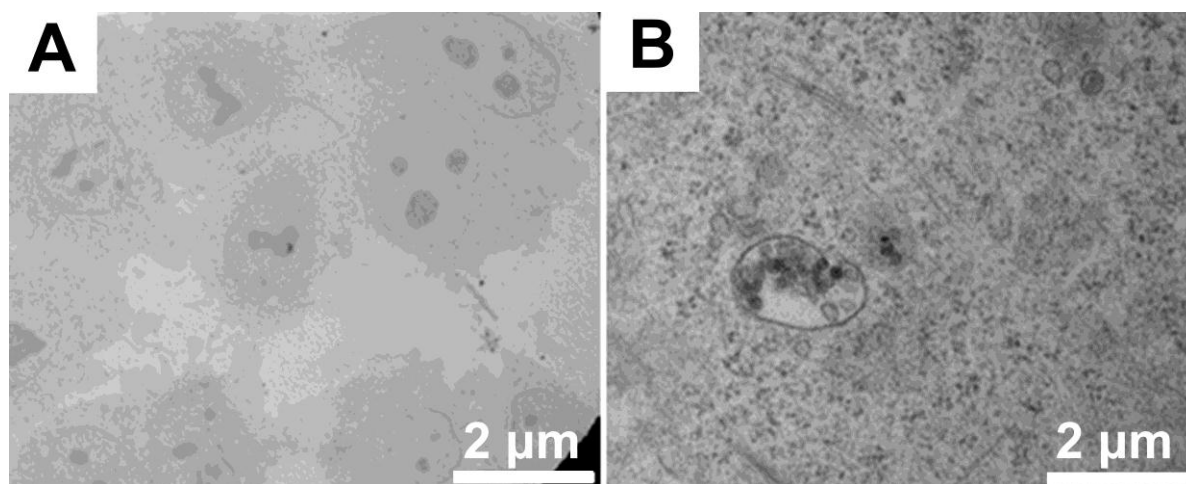
Figure 4.4 TEM images of HeLa cells after incubation with SPION@SiO$_2$@N$_3$

4.5 Summary and Conclusions

In this chapter we have successfully demonstrated the incorporation of magnetically active iron oxide (magnetite) core in silica shell. The silica shell is designed to be porous and has surface functionality for use as cargo carrier. The SPION@m-SiO$_2$@N$_3$ can be easily functionalized with HMDS as we have proposed in the scheme 4.2 and done in previous chapters. The synthesized material has core-shell morphology with porous shell. The material

has been thoroughly characterized by FT-IR, TEM, SQUID-VSM and PXRD techniques. The material has been tested for its ability for applications as MRI contrast agent. SPION@SiO$_2$@N$_3$ shows MRI contrasting ability by T2 or spin-spin relaxation mechanism. The r$_2$ relaxivity of 0.38 mM^{-1} s^{-1} was obtained for static applied magnetic field of 11.7 T. Recent report shows that SPION can also be developed as T1contrast agents by reducing their particles size below 5 nm. The particles have also been tested for their uptake into HeLa cell line. The uptake has been visualized by TEM imaging. The material can be readily subjected to further functionalization as per strategies developed in earlier chapters. Combining the ability of click chemistry to functionalize surface with variety of targeting ligands, this system can be used as a platform for multifunctional theranostics. The presence of super paramagnetic core in the theranostic NP also offer possibility of magnetic hyperthermia in combination with drugs[28].

4.6 References

(1)   Schoder, H.; Erdi, Y. E.; Larson, S. M.; Yeung, H. W. *Eur. J. Nucl. Med. Mol. Imaging* **2003**, *30*, 1419.

(2)   Sujlana, P.; Skrok, J.; Fayad, L. M. *J. Magn. Reson. Imaging* **2018**, *47*, 875.

(3)   Wu, X.; Sun, X.; Guo, Z.; Tang, J.; Shen, Y.; James, T. D.; Tian, H.; Zhu, W. *J. Am. Chem. Soc.* **2014**, *136*, 3579.

(4)   Baum, R. P.; Kulkarni, H. R.; Schuchardt, C.; Singh, A.; Wirtz, M.; Wiessalla, S.; Schottelius, M.; Mueller, D.; Klette, I.; Wester, H.-J. *J. Nucl. Med.* **2016**, *57*, 1006.

(5)   Fenster, A.; Downey, D. B. *EEE Eng. Med. Biol. Mag.* **1996**, *15*, 41.

(6)   Na, H. B.; Song, I. C.; Hyeon, T. *Adv. Mater.* **2009**, *21*, 2133.

(7)   Jack, C. R.; Bernstein, M. A.; Fox, N. C.; Thompson, P.; Alexander, G.; Harvey, D.; Borowski, B.; Britson, P. J.; L Whitwell, J.; Ward, C. *J. Magn. Reson. Imaging* **2008**, *27*, 685.

(8)   Wintermark, M.; Meuli, R.; Browaeys, P.; Reichhart, M.; Bogousslavsky, J.; Schnyder, P.; Michel, P. *Neurology* **2007**, *68*, 694.

(9)   Basaran, C.; Karcaaltincaba, M.; Akata, D.; Karabulut, N.; Akinci, D.; Ozmen, M.; Akhan, O. *Am. J. Roentgenol.* **2005**, *184*, 1103.

(10)   Marciani, L. *Neurogastroenterol. Motil.* **2011**, *23*, 399.

(11)   Gold, G. E.; Han, E.; Stainsby, J.; Wright, G.; Brittain, J.; Beaulieu, C. *Am. J. Roentgenol.* **2004**, *183*, 343.

(12)   Raymond, K. N.; Pierre, V. C. *Bioconjugate Chem.* **2005**, *16*, 3.

(13)   Marckmann, P.; Skov, L.; Rossen, K.; Dupont, A.; Damholt, M. B.; Heaf, J. G.; Thomsen, H. S. *J. Am. Soc. Nephrol.* **2006**, *17*, 2359.

(14)   Shen, Z.; Wu, A.; Chen, X. *Mol. Pharm.* **2016**, *14*, 1352.

(15)   Gupta, A. K.; Gupta, M. *Biomaterials* **2005**, *26*, 3995.

(16)   Ding, H.; Zhang, Y.; Wang, S.; Xu, J.; Xu, S.; Li, G. *Chem. Mater.* **2012**, *24*, 4572.

(17)   Hui, C.; Shen, C.; Tian, J.; Bao, L.; Ding, H.; Li, C.; Tian, Y.; Shi, X.; Gao, H.-J. *Nanoscale* **2011**, *3*, 701.

(18)   Choi, J.; Kim, J. C.; Lee, Y. B.; Kim, I. S.; Park, Y. K.; Hur, N. H. *Chem. Commun.* **2007**, 1644.

(19)   Kim, J.; Kim, H. S.; Lee, N.; Kim, T.; Kim, H.; Yu, T.; Song, I. C.; Moon, W. K.; Hyeon, T. *Angew. Chem. Int. Ed.* **2008**, *47*, 8438.

(20)   Lu, Y.; Yin, Y.; Mayers, B. T.; Xia, Y. *Nano Lett.* **2002**, *2*, 183.

(21)   Park, J.; An, K.; Hwang, Y.; Park, J.-G.; Noh, H.-J.; Kim, J.-Y.; Park, J.-H.; Hwang, N.-M.; Hyeon, T. *Nat. Mater.* **2004**, *3*, 891.

(22)   Krpetić, Ž.; Nativo, P.; Prior, I. A.; Brust, M. *Small* **2011**, *7*, 1982.

(23)   Sreeja, V.; Jayaprabha, K.; Joy, P. *Appl. Nanosci.* **2015**, *5*, 435.

(24)   Jun, Y.-w.; Seo, J.-w.; Cheon, J. *Acc. Chem. Res.* **2008**, *41*, 179.

(25)   Lee, N.; Choi, Y.; Lee, Y.; Park, M.; Moon, W. K.; Choi, S. H.; Hyeon, T. *Nano Lett.* **2012**, *12*, 3127.

(26)   Kim, B. H.; Lee, N.; Kim, H.; An, K.; Park, Y. I.; Choi, Y.; Shin, K.; Lee, Y.; Kwon, S. G.; Na, H. B. *J. Am. Chem. Soc.* **2011**, *133*, 12624.

(27)   Krpetic, Z.; Nativo, P.; Sée, V.; Prior, I. A.; Brust, M.; Volk, M. *Nano Lett.* **2010**, *10*, 4549.

(28)   Quinto, C. A.; Mohindra, P.; Tong, S.; Bao, G. *Nanoscale* **2015**, *7*, 12728.

Chapter V

Conclusion and Future Perspective

5.1 Conclusions

After a thorough inspection of literature, we have found out that the pore cavities in mesoporous silica particles have not been utilized for loading of drugs by carrying out appropriate functionalization. We realized the importance of a specific functionalization which is useful to adsorb drug molecules independent of their functional groups. We also reasoned that the functionalization should improve the loading capacity of the drug on to the carrier and the stability of carrier in the aqueous medium should be higher to have higher systemic circulation times as well as shelf life. For the latter part the carrier should be appropriately functionalized on the outer surface as well. Furthermore, the outer surface modification also has to be optimal so that it does not affect the drug loading/releasing profiles.

So keeping these requirements in mind:

1. We attempted to design a carrier based on mesoporous silica nanoparticles (MSN) which is tailored for adsorbing hydrophobic drugs. This has been achieved by selectively functionalizing inner pore surface of these MSN particles by hydrophobic functionality. The outer surface of these carriers was functionalized with a polar group, which helps to give dispersion stability to the carrier in the aqueous medium. The hydrophobic inner surface helps to load higher amounts of hydrophobic drug.

2. Further we tried to understand the effect of the outer surface functionality in drug loading. We did this by observing how varying the size of outer surface ligands can affect the uptake of drugs loaded in a mesoporous system. We also tried to understand the role of these functional groups in release process. We also demonstrated two different drug loading methods and compared their advantages and shortcomings.

3. Finally, we incorporated a diagnostic element, a magnetic core in these amphifunctional mesoporous silica shell. We demonstrated the usefulness of this multifunctional system for drug delivery as well as MRI contrast agent.

In chapter II, amphi-functional mesoporous silica nanoparticles were synthesized by stepwise chemical modification approach. The amphifunctional MSN was created by hydrophobic functionality in pores by TMS groups and hydrophillic functionality on the outer surface in the form of azide groups. The presence of hydrophobic pockets created by trimethylsilyl groups inside the pores has been indirectly demonstrated by NR encapsulation. The wider applicability of this strategy is proven with various dyes (cationic and anionic). This amphi-

functional silica material was shown to selectively adsorb and remove a dye from binary mixtures. The separation was predominantly based upon the hydrophobic-hydrophobic interactions between adsorbate and adsorbent. Thus, in this chapter we have successfully demonstrated the importance and affect of appropriate surface functionalization. This material and strategy has been used later in this thesis to build the advanced theranostic system.

In chapter III we have optimized our stepwise functionalized approach to minimize a step of grafting of azide group of silica. In the new protocol the co-condensation apporach has been employed to functionalize silica with azide groups in one pot. This approach seems to be more efficient than the one presented in the previous chapter. The outer surface of the silica is then modified with different functional groups such as PA, TEG and PEG with varying chain length of ethylene oxide moieties. These groups were functionlized by using azide-alkyne click reaction with surface azide groups present on MSN. Here, we also evaluated a two methods of loading of cargo. It was found that; path A where the cargo is loaded after all fucntionalizations has resulted in far less loading (almost by 10 times in all samples) as compared to the other apporach (path B) where the cargo is loaded first followed by outer surface functionalizations. The role of outer surface groups in the process of uptake has also been evaluated. It is quite clear from trends that the chain length of outer surface group do affect the uptake process.. This effect was attributed to "molecular gating" by bulky groups present on the surface. Finally, we conclude from the observations that a trade off between dispersibilty of MSN and blocking of access to the pores is critical for choice of appropriate surface functional group. It is also important here to note that the partition of a particular cargo molecule is also a driving factor. We believe that these findings will open up new avenues for the designing of porous material, with appropriate pore/surface functionalizations, based drug delivery systems in future.

In chapter IV we have successfully demonstrated the incorporation of magnetically active core in silica shell. The silica shell is designed to have porosity so that our stepwise surface modification protocol can be extended to this system as well. The azide groups were grafted by co-condensation method in the process in similar way as mentioned in previous chapter. This $SPION@SiO_2@N_3$ material can be easily functionalized with HMDS as we have proposed in the scheme 4.2 for further modification. The synthesized material has core-shell morphology with porous shell as observed in TEM. The material has been tested for its ability for applications as MRI contrast agent. $SPION@SiO_2@N_3$ shows MRI contrasting

ability by T2 or spin-spin relaxation mechanism. These particles were also tested for their uptake into HeLa cell line which was visualized by TEM imaging.

5.2 Future perspective

With these observations we believe that the surface modification strategies will receive more consideration while designing a drug delivery vehicle. Our proposed strategy is not limited to the mentioned functional groups and can be extended to variety of silane as well as other functional platforms. Also the stepwise modification strategy is not limited to MSN material. As we have shown for some examples it can be readily generalized for other systems such as SBA-15 and KCC. We also believe that this strategy can be taken beyond silica materials and applied to other mesoporous materials as well. For example, porous carbonaceous materials, covalent organic frameworks (COF), and metal organic frameworks (MOF) has been recent additions to the family of porous materials. With certain modifications this selective functionalization strategy can be applied to these materials as well and thus holds great potential to enhance the performances of these materials. Our insights on drug loading methodology and effect of outer surface groups can surely help as guiding principles in future drug delivery designs. Here, we would like to underline the fact that not only the nature of functional groups but its sequence of incorporation in overall design should be considered with utmost importance. Finally we have demonstrated the incorporation of magnetic core in this functionalized silica shell. Having a super paramagnetic core can surely help with T2 contrast. This can also act for multipurpose tool such as, magnetic localization as well as hyperthermia. With proper design and functionalization it is possible to utilize every bit of the materials potential.

List of Publications

1. **Shinde, P**.; Gupta, S. S.; Singh, B.; Polshettiwar, V.; Prasad, B. V., Amphi-functional mesoporous silica nanoparticles for dye separation. *J. Mater. Chem. A* **2017**, 5, 14914.

2. Yenchalwar, S. G.; Rondiya, S. R.; **Shinde, P. N**.; Jadkar, S. R.; Shelke, M. V., Optical antenna effect on SiNWs/CuS photodiodes. *physica status solidi (a)* **2017,** 214, (5).

3. Madhuri, P. L.; Prasad, S. K.; **Pravin, S**.; Prasad, B. L. V., Large reduction in the magnitude and thermal variation of Frank elastic constants in a gold nanorod/nematic composite. *Journal of Physics D: Applied Physics* **2016,** 49, (42), 425304.

4. Ganai, A. K.; **Shinde, P**.; Dhar, B. B.; Gupta, S. S.; Prasad, B. L. V., Development of a multifunctional catalyst for a "relay" reaction. *RSC Adv.* **2013,** 3, (7), 2186-2191.